NANYANG TECHNOLOGICAL UNIVERSITY

FABRICATION OF TITANIUM/TITANIUM ALLOY COMPONENTS BY POWDER INJECTION MOULDING

ONG ZIYAN AMANDA

SCHOOL OF MECHANICAL & AEROSPACE ENGINEERING

2014

FABRICATION OF TITANIUM/TITANIUM ALLOY COMPONENTS BY POWDER INJECTION MOULDING

ONG ZIYAN AMANDA

School of Mechanical & Aerospace Engineering

A thesis submitted to the Nanyang Technological University
in partial fulfillment of the requirements for the degree of
Master of Engineering

2014

ABSTRACT

Titanium (Ti) excellent mechanical and physical properties made it an attractive metal for engineering applications. However, its high material cost and difficulty to machine and bulk form limit its expansion to a vast number of applications. Powder injection moulding (PIM) for titanium material was proposed as it is a near net or net shape forming process, hence, reduces material wastages and manufacturing cost. However, Ti components produced by PIM usually have less superior mechanical properties than their cast or wrought counterparts due to interstitial contamination. Therefore, in this research work, the fabrication of high strength Ti components by PIM is studied. ASTM B265 Grade 3 CP-Ti and Grade 5 Ti-6Al-4V are the targeted standard for this research work.

The first phase of the research focused on PIM of CP-Ti tensile components. Tensile tests showed components sintered at 1240 ^{o}C, 1260 ^{o}C and 1280 ^{o}C in argon have met the ultimate tensile strength (UTS) for Grade 3 CP-Ti (> 450 MPa) but still lacked in elongation. The sintered components have elongations less than 10 %, which were lower than the targeted value of 18 %. Their microstructures revealed high level of porosities and relative densities were measured to be only 95 %. This was attributed by argon gas entrapment and also non-uniform shrinkage of the components during sintering. XRD spectra of the sintered components showed oxides peaks, indicating contamination.

The second phase of the research involved the fabrication of Ti-6Al-4V tensile components. The processing parameters used in the fabrication of CP-Ti were improvised and implemented to the Ti-6Al-4V fabrication process. 2^{4-1} fractional DOE study was also conducted to study the effects of the sintering parameters on the UTS and elongation of Ti-6Al-4V. The sintering parameters examined were sintering temperature (1200 ^{o}C, 1300 ^{o}C), dwell time (1 h, 3 h), ramp rate (1 ^{o}C/minute, 10 ^{o}C/minute) and cooling rate (1 ^{o}C/minute, 10 ^{o}C/minute). Results

showed all four sintering parameters have significant influence on the UTS while, only dwell time and ramp rate have significant influence on the elongation.

In the DOE study, some of the sintered Ti-6Al-4V components with certain parameters have met the Grade 5 Ti-6Al-4V standard for UTS (> 895 MPa) and elongation (> 10%). The relative densities for most of the sintered components obtained from the DOE study were above 96 %. Only one had relative density of 94 % due to incomplete sintering. Lower cooling rate favored thicker α plate thickness and larger α colony size. β prior grains were also identified in some of the components, mainly in those sintered at higher temperature and longer dwell time. The microstructures and the relatively density of the sintered components were also found to have influence on the UTS and elongation. In general, sintered components with smaller α plate thickness or α colony size has better UTS and elongation. UTS and elongation were also observed to increase with increasing relative density.

ACKNOWLEDGEMENT

Firstly, the authoress would like to thank her supervisor at the Nanyang Technological University, Associate Professor Loh Ngiap Hiang, for giving her the opportunity to work on this research topic and also her supervision and guidance for this work. She is also grateful to her SIMTech supervisor, Dr Li Tao, for his supervision and providing valuable technical advices.

The authoress would also like to thank the Management at Singapore Institute of Manufacturing Technology (SIMTech) for allowing her to use their resources for her research work. Thanks are also due to the staffs and ex-colleagues of Forming Technology Group (FTG), especially Ms. Seet Wei Leu, for taking time off their busy schedule to guide her in some of the laboratory works.

Lastly, the authoress would like to express her gratitude to her family and friends for their encouragements and support during her course of study.

TABLE OF CONTENTS

PAGE

LIST OF FIGURES

PAGE

LIST OF TABLES

PAGE

LIST OF ABBREVIATIONS

Abbreviation	Definition
Al	Aluminium
ANOVA	Analysis of Variance
Ar	Argon
ASTM	American Society for Testing and Materials
BCC	Body Center Cubic
C	Carbon
CIM	Ceramic Injection Moulding
CP-Ti	Commercially Pure Titanium
CW	Carnauba Wax
DOE	Design of Experiment
DSC	Differential Scanning Calorimetry
EDS	Electron Dispersive Spectrometer
ELI	Extra Low Interstitial
Fe	Iron
H	Hydrogen
HCP	Hexagonal Close Packed
HDH	Hydride-dehydride
IPA	Isopropyl Alcohol
l	Effect
MIM	Metal Injection Moulding
Mo	Molybdenum
N	Nitrogen
Nb	Niobium
O	Oxygen
P/M	Powder Metallurgy
PIM	Powder Injection Moulding
PP	Polypropylene
PW	Paraffin Wax
SA	Stearic Acid

Abbreviation	Definition
SEI	Secondary Electron Image
SEM	Secondary Electron Microscope
Sn	Tin
Std Dev	Standard Deviation
Ta	Tantalum
TD	Theoretical Density
TGA	Thermogravimetric Analysis
Ti	Titanium
UTS	Ultimate Tensile Strength
V	Vanadium
XRD	X-ray Diffraction
YS	Yield Strength

CHAPTER 1 INTRODUCTION

1.1 Background

Powder injection moulding (PIM) is a deviation of plastic injection moulding technology. In this technology, metallic or ceramic particulates are used to form the desired components, instead of polymer resins. PIM process involving the use of metallic or ceramic powders is termed metal injection moulding (MIM) or ceramic injection moulding (CIM), respectively.

Unlike conventional powder metallurgy (P/M) processes like powder compaction, slip casting and tape casting, PIM offers the possibility of fabricating high density components with intricate and complex geometries and good surface finishing. In addition, moulded components produced by PIM have uniform density hence, eliminating the effects of non-uniform shrinkage when subjected to high sintering temperature. Most importantly, PIM is a net shape or near net shape process. Therefore, little or no secondary processing is required and also there is less material wastage.

PIM process involves four basic steps: 1) mixing, 2) injection moulding, 3) debinding and 4) sintering. Figure 1.1 illustrates the four basic steps of the PIM process [1].

The first step in PIM is mixing, where the feedstock is produced. In this step, the metallic or ceramic powders are mixed with a suitable binder in a predefined condition to form a homogeneous mixture. The mixture is then granulated into pellets for injection moulding.

In the second step, the granulated pellets are fed into the injection moulding machine where they are injected under heat and pressure into the mould cavity. As-moulded components are also known as green components.

The third step in PIM is debinding, where the binder are removed from the green components by chemical or/and thermal method. This step removes the binder in the green component leaving behind a series of pores and powders in the component. Components which have been debound are known as brown components.

Lastly, the brown components will be subjected to a final stage of thermal treatment known as sintering. In this process, the components are heated in a multiple step thermal profile at temperatures below the melting point of the material. Here the powder particulate will fuse and bond together to form a dense sintered component suitable for the desired application.

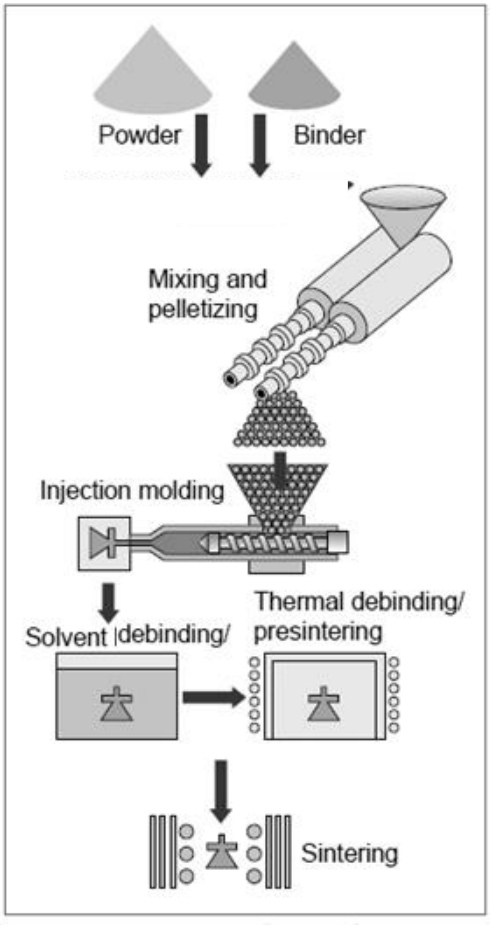

Figure 1.1 Four basic steps in PIM process [1].

1.2 Research Motivation

Due to the advantages of PIM, this technology has been applied to materials which are difficult to form using traditional forming processes (i.e. casting, forging, machining, etc) and in areas for high value applications. One of the interests in the engineering field is the fabrication of titanium (Ti) components.

Ti has attracted much attention for several decades because of its unique properties such as high strength to weight ratio, good toughness, outstanding corrosion and oxidation resistance properties and excellent bio-compatibility [2,3,4] In addition, Ti properties can be altered through alloying and manipulating its microstructures to suit the needs for various applications [5]. For example, commercially pure Ti (CP-Ti), which is softer in nature, can be alloyed with elements such as iron (Fe), aluminium (Al) and vanadium (V) to form stronger and light weight alloys for sports, aerospace, energy, military and bio-medical applications.

However, the cost of Ti material is high and this puts a hinder to the expansion of this material to a vast number of applications. Drivers for the high cost of Ti are its difficulty in extraction from ore, processing and fabrications [6]. Table 1.1 shows the cost of Ti relative to competing materials like steel and Al. The table indicates that the cost of Ti ore doubles that of Al per pound and cost ten times more than steel per pound. In addition, the disparity in their costs widens in the processing and fabrication steps [1].

Table 1.1 Pricing of Ti in comparison to competing metals [1].

	Material ($ / Pound)		
	Steel	**Aluminium (Al)**	**Titanium (Ti)**
Ore	0.02	0.1	0.22 (Rutile)
Metal	0.1	0.1	5.44
Ingot	0.15	1.15	9.07
Sheet	0.30 – 0.60	1.00 – 5.00	15.00 – 50.00

*Contract prices. The high cost of titanium compared to aluminium and steel is a result of (a) high extraction cost and (b) high processing costs. The latter relating to the relatively low processing temperatures used for titanium and the conditioning (surface regions contaminated at the processing temperatures and surface cracks, both of which must be removed) required prior to further fabrication.

Two areas have been identified to lower the cost of Ti components: 1) reduce cost of raw material and 2) reduce manufacturing cost. While the price of raw material contributes a substantial portion to the cost of Ti components, the major cost contributor is from the fabrication of these components. Whittaker et al's paper [7], indicated that almost 50 % of the cost of fabricating a 25 mm Ti alloy plate came from the product forming stage, while the raw material only contributed 39 %. The breakdown of the cost of fabricating a 25 mm Ti alloy plate is illustrated in Figure 1.2. Therefore, net or near net shape forming process has been identified to reduce the fabrication cost of Ti component as it reduces the number of secondary processes required and also material wastages.

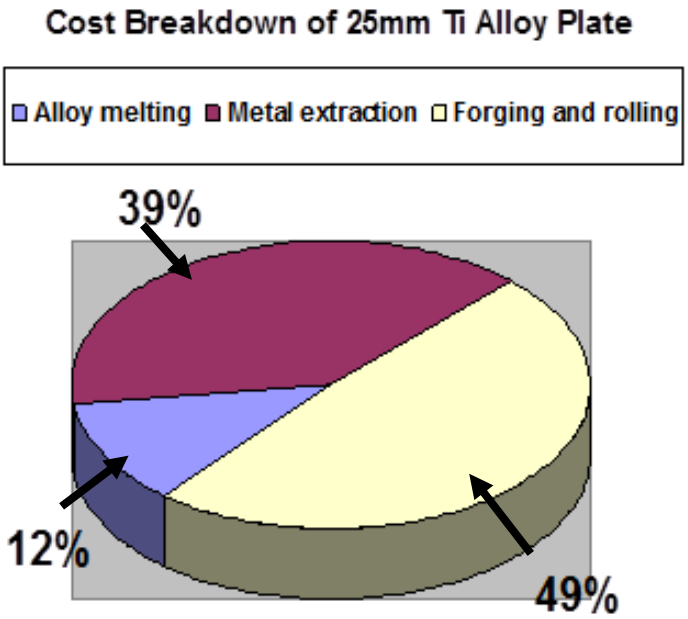

Figure 1.2 Cost breakdown of 25 mm Ti plate [7].

One of such process which has been identified as net or near net shape forming is PIM. PIM allows fabrication of intricate and complex high performance material components. In addition, PIM is also able to fabricate components with more homogeneous microstructures [8]. With PIM, high material wastage associated with the machining of Ti and difficulty in bulk forming of Ti can be overcome, therefore, making PIM one of the preferred methods for Ti component fabrication. Unfortunately, Ti components manufactured by PIM have less superior properties

than those produced by forging or casting. This makes them unsuitable for engineering applications which require superior mechanical properties and high reliability. This is due to Ti high affinity with interstitial elements like oxygen (O), carbon (C) and nitrogen (N), which are detrimental to their mechanical properties and performance. Thus, PIM Ti components have been applied to non-load bearing applications or cosmetic components like golf clubs, watch brackets and rims, gears and dental brackets. However, applications in load-bearing components are limited. In this research the challenges faced in the fabrication of high strength Ti components by PIM will be addressed for possible loading bearing applications.

1.3 Objective

The objective of this research study is to set up the fabrication process for high strength Ti alloy components by PIM, with the aim to achieve mechanical properties of at least Grade 5 for Ti-6Al-4V. This research also focused on the effects of sintering parameters on the mechanical properties and microstructural development by using design of experiment (DOE).

1.4 Scope of Research

In the first phase of the research, the fabrication of CP-Ti tensile components via PIM was studied. This involved selection of suitable processing parameters, such as feedstock composition and sintering parameters, so as to achieve high strength Ti components. The density, porosity, microstructures and the elemental or compositional changes of the sintered Ti tensile components fabricated under the different processing parameters were examined and compared. In addition, experimental work was also conducted to measure the mechanical properties and benchmark to existing standards. This research also included characterisation work conducted on the raw materials (powders and binder). The density, particle size and morphology and shrinkage behaviour were examined on the raw powders while thermal analysis was conducted on the binder for the selection of moulding and debinding profile.

The second phase of the research focused on the fabrication of Ti-6Al-4V component. The processing parameters used in the fabrication of CP-Ti were improvised and implemented to the Ti-6Al-4V fabrication process. In addition, design of experiment (DOE) on the sintering process was conducted to study the effects of the different sintering parameters on the mechanical properties of Ti-6Al-4V tensile components. The mechanical properties measured were the ultimate tensile strength (UTS) and the elongation. The microstructures of the sintered Ti-6Al-4V tensile components and their physical properties such as porosity and density were also examined. In this research, the influence of the sintering parameters on the microstructures, mechanical properties and physical properties of the components were compared and discussed in Chapter four.

1.5 Research Methodology

The flow chart of the research methodology is shown in Figure 1.3. As mentioned, this research study was split into two phases. The first phase involved the study of PIM process on CP-Ti, while Ti-6Al-4V was studied in the second phase. This was because the initial focus of this research work was on PIM of Ti alloy. However, due to the unavailability of the vacuum sintering furnace and the Ti alloy powders, the work was first conducted using CP-Ti. Results from the study on CP-Ti were used to establish the processing parameters for the PIM study on Ti-6Al-4V and also identified areas which required improvements.

One area of work for Ti-6Al-4V which was different from CP-Ti was the implementation of design of experiment (DOE) studies on the sintering process. The objective of the research work is to fabricate high strength PIM Ti-6Al-4V tensile components. This can be achieved by controlling the microstructures of the component through the sintering process. Sintering is a complex process which involves several parameters. Therefore, DOE was applied to investigate the effects of sintering parameters on the UTS and the elongation of sintered Ti-6Al-4V components.

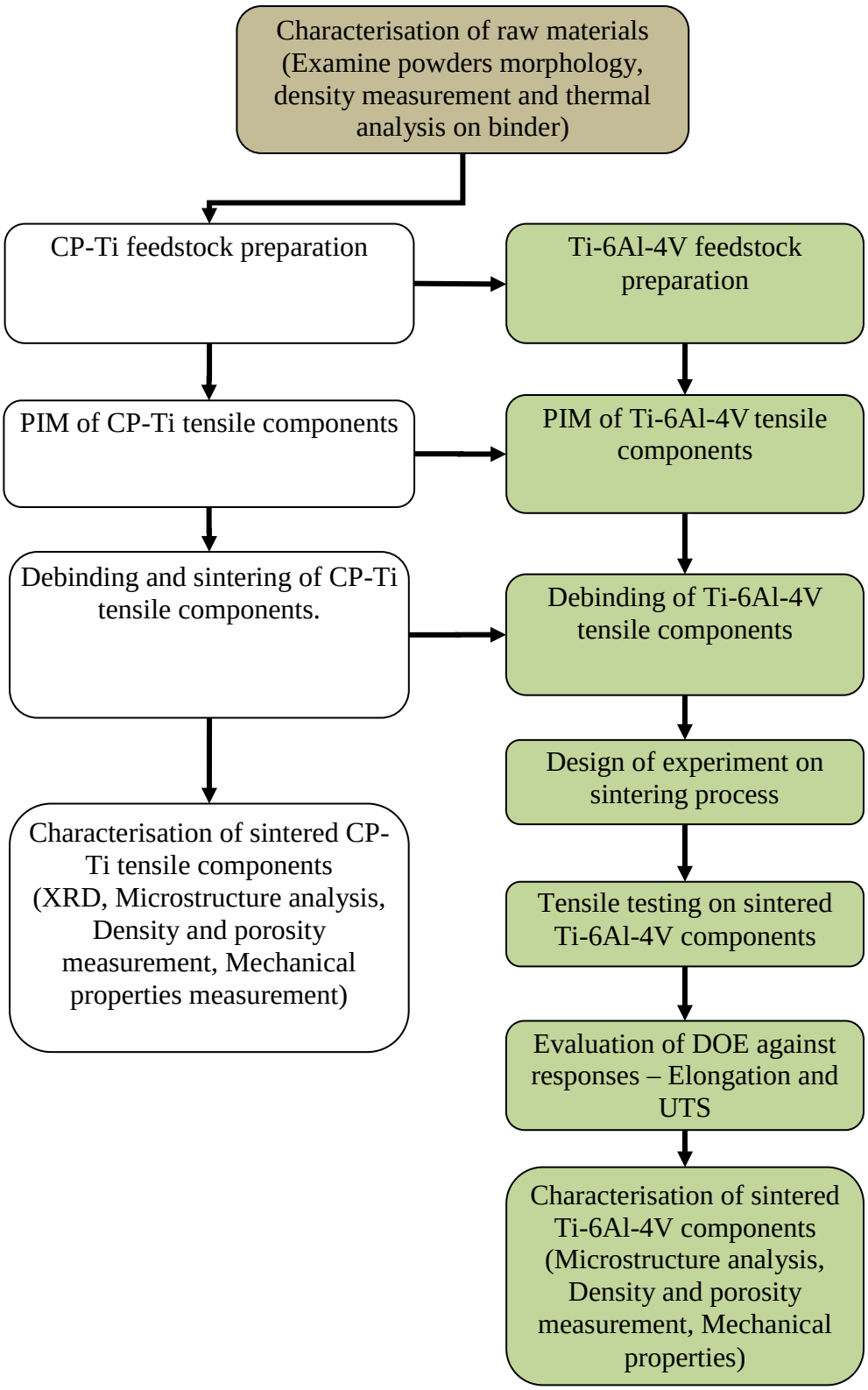

Figure 1.3 Flow chart of research methodology.

CHAPTER 2 LITERATURE REVIEW

2.1 Overview of Powder Injection Moulding

Traditionally, injection moulding process has only been applied to the fabrication of plastic components. However, the popularity and spurs of plastic injection moulding and the desire to form components with more superior properties has led to the development of powder injection moulding (PIM). PIM is a near net-shape or net shape forming process, which allows the fabrication of metallic and ceramic components, which have properties lacking in plastic (e.g. better strength, stiffness, thermal properties and electrical properties). The existence of PIM can be dated back to the late 1920s, where it was used to produce ceramic spark plugs [9]. The property and shape limitations of conventional P/M processes also aid in accelerating the growth of PIM, into areas of advanced materials and engineering processes. To date PIM has been applied to materials such as steel, copper, superalloys and advanced ceramics. As the name suggests, the starting material for PIM is powder or in particulate form. The powders are then mixed with a selected binder to form the feedstock for injection moulding.

There are five key features to PIM: 1) low production costs, 2) shape complexity, 3) tight tolerances (within 0.3 % of the targeted dimension), 4) material flexibility and 5) high final properties [10]. Among the five features listed, material flexibility was one of the major attraction points for PIM. This is because PIM allows the fabrication of any metallic or ceramic material as long as they can be made into powders or particulates form. The powders are mixed with the selected binder to form the feedstock for injection moulding. The binder acts as a media for transporting the powders into the mould cavity when pressurised. Since the forming process of PIM do not involved the use of high temperature, oxidation of metallic material is minimised. In addition, this also allows the fabrication of high temperature ceramic materials.

In addition to the four basic steps of PIM mentioned in Section 1.1, other important criteria for PIM include powder and binder selection. Details of the selection and the processing steps of PIM are presented in the following sections.

2.1.1 Powder Selection

Selecting the right type of powders (shape and size) is critical for PIM. Important attributes for the powders in PIM includes: 1) particle size and its distribution, 2) particle shape, 3) surface area, 4) interparticle friction (measured by packing and flow), 5) internal particle structure and 6) chemical gradients, surface films and admixed materials [10].

Generally, PIM favors the usage of powders with particle size range between 0.5 μm to 20 μm and average particle size, D_{50}, between 4 μm to 8 μm are preferred [10]. Powders with small particle sizes are preferred as they induce higher sintering rate and densification. This is because the driving force for sintering is to eliminate the surface energy. Smaller particles which have higher specific surface area tend to have more surface energy, hence, are able to be sintered more quickly [11].

The shape of the powders is also important for the success of PIM as it indicates the total area available for sintering and binder adsorption [12]. Usually for PIM, spherical shaped powders are preferred as they have better flow ability thus, are easier to mix and give higher packing densities (60 to 64 %) as compared to irregular shaped, short cylinder shaped and filament-typed particles [10]. Though irregular shaped powders result in high viscosity feedstock and lower packing density, they have better component-shape retention during binder removal. Hence, sometimes mixtures of both spherical and irregular shaped powders are used to achieve a compromise between packing density and component-shape retention. Figure 2.1 illustrates some of the possible particle shapes and suggested qualitative descriptors [11]. The shape of the powders is determined by their fabrication

methods. Comparisons between some of the common powder fabrication methods are shown Table 2.1.

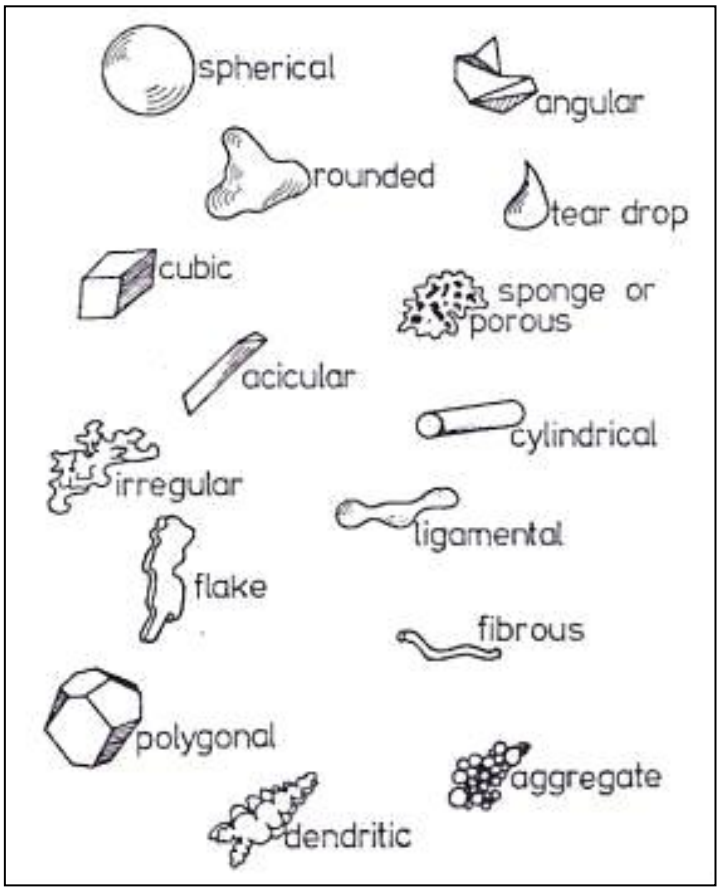

Figure 2.1 Qualitative descriptor for particles [11].

Table 2.1 Common powder fabrication methods for PIM [10].

Type	Size range (μm)	Shape	Material	Cost
Gas atomised	5 - 40	Spherical	Metal	High
Water atomised	6 - 40	Rounded, Ligamental	Metal	Moderate
Milling	1 - 40	Angular, Irregular	Brittle metal or ceramics	Moderate
Fine Grinding	0.1 - 2	Irregular	Ceramics	Moderate

2.1.2 Binder Selection and Solid Loading

After a suitable powder has been selected, the next step is to select an appropriate binder and solid loading for the feedstock. Solid loading, Φ, is defined as the volumetric ratio of powder to binder used. Normally, a solid loading of 60 % is used for PIM.

Moulding difficulties will be encountered if only powder is used for PIM. This is due to difficulty in transporting the powders from the barrel into the mould cavity. Therefore, a media is required to transport these powders into the cavity during the injection moulding process. For that purpose, binder are mixed with the powders and granulated to form a feedstock. Other purpose of binder is to wet the powder surfaces so as to aid mixing and moulding, inhibit powder agglomeration and improve the viscosity of the feedstock [10,12]. Multi-component binder is usually used in PIM. The binder consists mainly of polymers, waxes and additives. Polymers are added to bind the powder particles and provide green strength for the handling of green components. Waxes lower the viscosity and improve wetting. Lastly, additives provide wetting between the powders and the polymeric binder and also lubrication for tool release. Usually a volume percentage of 40 % of binder is used in PIM. Having excessive binder content (low solid loading) is undesirable as they reduced the density of the component. This also results in non-homogeneities in the moulded components and risk collapsing or slumping of the components during the debinding process [10]. Figure 2.2 shows the schematics on the possible outcomes of the feedstock under different variation of binder percentage [10]. Figure 2.2 (a) shows that when excessive binders are used, the green density of the PIM component is reduced as the powders are not packed as closely as it should be. On the other hand, voids are form in a mixture with excess powder or insufficient binder. Therefore, a balance in the powder to binder ratio is required so that there is point contact between the particles. This is illustrated in Figure 2.2 (b).

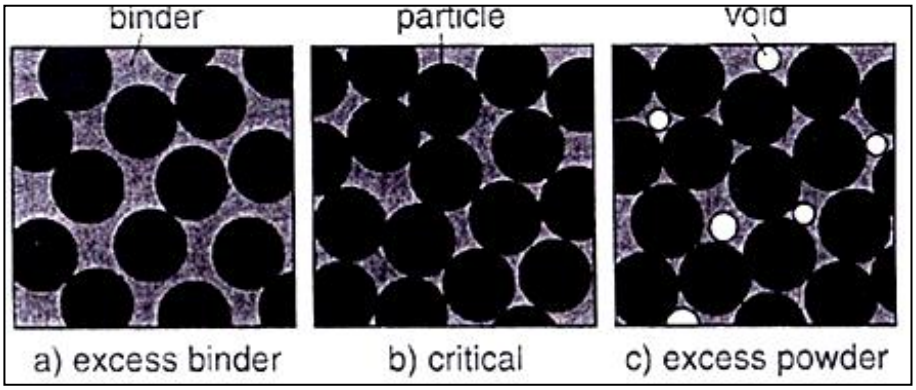

Figure 2.2 Outcomes of the feedstock under different binder quantity [10].

There are at least five types of binder used in PIM. They are categorised as 1) thermoplastic compounds, 2) thermosetting compounds, 3) water-based systems, 4) gelation systems and 5) inorganics [10]. Table 2.2 lists some examples of PIM binder formulations in these categories [10].

Table 2.2 Commonly used PIM binder formulations [10].

	Binder Composition
1	70 % paraffin wax, 20 % microcrystalline wax, 10 % methyl ethyl ketone
2	67 % polypropylene, 22 % microcrystalline wax, 11 % stearic acid
3	33 % paraffin wax, 33 % polypropylene, 33 % beewax, 1 % stearic acid
4	69 % paraffin wax, 20 % polypropylene, 10 % carnauba wax, 1 % stearic acid
5	45 % polystyrene, 455 vegetable oil, 5 % polyethylene, 5 % stearic acid
6	65 % epoxy resin, 25 % paraffin wax, 10 % butyl stearate
7	75 % peanut oil, 25 % polyethylene
8	50 % carnauba wax, 50 % polyethylene
9	55 % paraffin wax, 35 % polyethylene, 10 % stearic acid
10	58 % polystyrene, 30 % mineral oil, 12 % vegetable oil

2.1.3 Feedstock Preparation

Feedstock mixing utilises the concept of shearing the binder and powders under heat to obtain a homogeneous mixture. The shearing action helps to break up the powder agglomerates and coats the binder onto the surfaces of the powders. It is essential to break up the powder agglomerates to eliminate enclosed pores and large irregular shaped components as they act as obstacles and increase flow resistance of the feedstock [13,14].

Factors that affects the homogeneity of the feedstock includes processing variables like mixing speed, time, temperature, geometry of mixing blades, raw material feed rate, and material variables such as particle shape, size, solid loading, binder system and viscosity [14].

The mixing temperature is determined by the melting point of the binder used. It is usually set in accordance to the binder with the highest melting point. Too high of a mixing temperature is undesirable as it degrades the binder and result in powder separation due to low binder viscosity. In the mixing procedure, binder is usually added first to form a homogenous melt mixture. This is followed by the progressive addition of the powders. Powders are added in batches so as to ensure homogeneity during the mixing process. When a good mix between the powders and the binder has been achieved, vacuum is applied to the mixing process to eliminate air bubbles entrapment. After a homogeneous powder-binder mixture is obtained, the mixture is granulated into smaller pellets suitable for moulding. The mixing time and speed are dependent on the type of powders used. Small and irregular powders will require longer mixing time to achieve homogeneity.

It is important to achieve a homogenous feedstock as this will affect the uniformity of the component properties. Therefore, assessing the homogeneity of the feedstock is important for the subsequent moulding process. They can be examined with the following methods:

1. feedstock density measurement,
2. binder burn out test and
3. viscosity measurement via capillary rheometry

Equipment such as the twin screw extruder, single screw extruder, plunger extruder, twin cam mixer, z-blade mixer and double planetary mixer are some commonly used mixing devices for feedstock fabrication. Among them, the twin screw extruder was believed to be the most efficient and effective in producing homogeneous feedstock as it combines high shear with short dwelling time at elevated temperature [10].

2.1.4 Injection Moulding

Injection moulding is the second stage of PIM process. In this stage, the feedstocks are fed into the machine, where they will be melted and pressurised into the mould cavity to form the desired green component. Figure 2.3 shows the typical moulding cycle of PIM [15].

As illustrated in Figure 2.3, the cycle starts with the closing of the mould. Molten feedstock is then injected into the cavity according to the injection parameters set and pressurised to compensate for thermal contraction. This is followed by the cooling of the component after the gate freezes while the injection unit retracts and the screw plasticises for the next shot. The component is then ejected from the mould cavity and the machine prepares for the next shot. In PIM process, the injection moulding step is considered one of the more crucial step as the final outcome or properties of the components is very much influenced by the quality of

the green components. Important parameters for injection moulding include melt and mould temperatures, injection speed, injection pressure, holding pressure, cooling time and dosage. Table 2.3 shows some of the common defects in PIM.

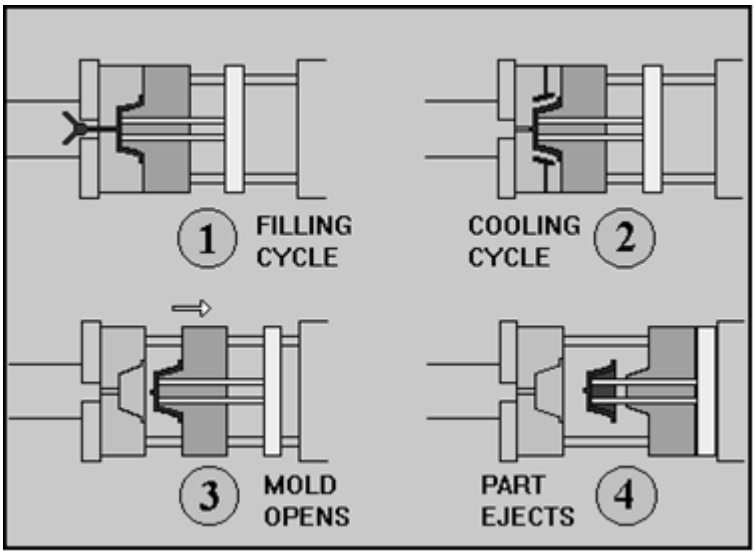

Figure 2.3 Schematics of moulding cycle [15].

Table 2.3 Common defects in PIM.

Defects	Causes
Short shot (Incomplete filling of cavity.)	• Insufficient dosage • Insufficient injection speed • Insufficient injection pressure • Melt or mould temperature too low
Flashing (Complete filling of the cavity with excess material along the parting line or die wall.)	• Pressure too high • Clamp force too low • Over packing
Sink Mark (Depression on the surface of green component)	• Insufficient injection pressure • Insufficient packing • Non-uniform cooling rate
Weldline	• Melt or mould temperature too low • Insufficient injection speed • Inadequate air vents
Voids	• Metering speed too fast and inadequate back pressure • Inadequate air vents • Jetting due to too fast of injection speed

2.1.5 Debinding

The third stage in PIM is debinding. In this stage, the binder in the green components is extracted by chemical and/or thermal methods. Extraction of binder by chemical and thermal method is known as solvent debinding and thermal debinding, respectively.

Solvent debinding involves the extraction of at least one of the binders in the green component. This creates a series of open and interconnected pore structure to allow the remaining binder in the component to be burnt out during the thermal debinding stage. There are three different solvent debinding methods: 1) solvent immersion, 2) supercritical extraction and 3) solvent vapor condensation. Table 2.4 summarises the advantages and disadvantages of each solvent debinding method [10].

Table 2.4 Description of the different solvent debinding processes [10].

Method	Description	Advantages	Disadvantages
Solvent immersion	Components immersed in solvent for a period of time for the dissolution of the binder.	Components remain rigid chemical reaction. Opens pore channels for subsequent degradation of binder.	Solvent hazard Environmental concerns due to involvement of chemicals. Requires chemicals to be dried off before thermal debinding or sintering.
Supercritical extraction	Heat and pressurise solvent above its critical point to dissolve the binder into fluid.	No phase change. Minimise defect formation.	Requires precise temperature and pressure control. Slow process.
Solvent Vapor Condensation	Solvent are vapourised and binder are removed via the absorption of the condensate.	Low component temperature minimises defects and distortion, with replenished surface solvent aiding rapid debinding.	Chemical, environment and health concerns due to involvement of chemicals. Requires chemicals to be dried off before heating.

The second stage of debinding is thermal debinding. In this step, the remaining polymeric binder is removed via thermal treatment. At this stage, the removal of binder occurs in either by liquid flow through the liquid network or by gas flow through the vapour network.

As mentioned by German et al. [10], in the initial stage of thermal debinding, binder removal via gas flow is higher than liquid flow due to abundance of binder residing near the surfaces. The debinding rate at that point is dependent on the binder degradation rate. Subsequently, as the distance between the binder and surface increases, the rate of binder removal by liquid flow decreases. Therefore, this leads to a surface free of binder. If the feedstock is not homogenous, there will be a possibility of cracks occurring at this point. This is because the small pores at the surface region have more attraction for the liquid binder than the larger pores, thus, this will cause the large pores to split. With increasing distance between the binder residing area and the component's surface, removal via liquid flow eventually becomes the limiting factor. Lastly, binder removal will occur within the component itself. The path for binder removal is summarised in Figure 2.4, where a fully saturated initial pore condition is assumed [10]. Saturation is defined as the degree of which the pores are filled by a liquid.

The temperature and atmosphere for thermal debinding depend on the type of binder and the material used. Metallic powders which are prone to oxidation, are usually thermal debound in inert atmosphere such as argon (Ar), nitrogen (N_2) or reactive atmosphere like hydrogen (H_2). As the binder consists of multiple components, a multi-step thermal profile is usually used for binder removal to prevent defects (i.e. blistering, internal cracks, voids and collapsing of parts) during the process. Multi-step thermal profile is also preferred for debinding larger and complex components. Components which have been thermal debound are known as brown components. Figure 2.5 shows the schematic of the possible defects arising during thermal debinding [16]. These defects are also applicable to the sintering stage.

Sometimes an alternative debinding method known as catalytic debinding is also employed in binder removal. Catalytic debinding is a process where the binder is depolymerised and removed by heat treatment in an atmosphere containing catalyst.

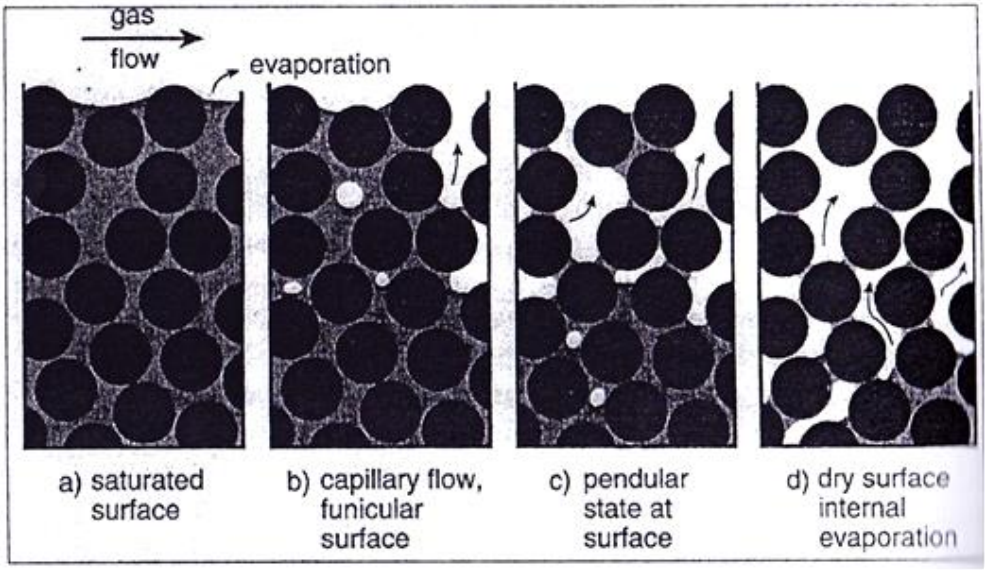

Figure 2.4 Paths for binder removal during thermal debinding [10].

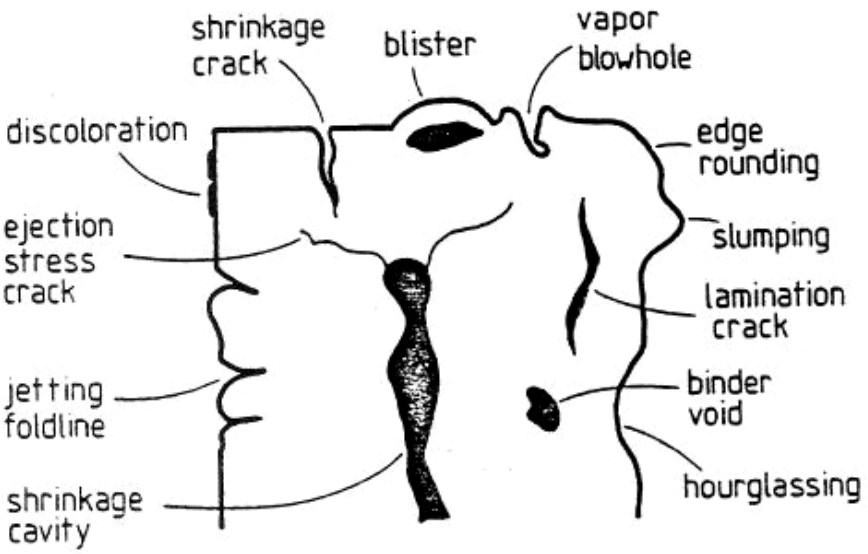

Figure 2.5 Possible defects arising during debinding and sintering [16].

2.1.6 Sintering

The last step of the PIM process is sintering. Sintering is a process where thermal energy is applied to either metallic or ceramic powders components to fabricate density-controlled components [17]. It is usually conducted below the material's melting temperature to prevent shape distortion. Similar to thermal debinding, the sintering atmosphere is also dependent on the material of the powder. Sintered components not only have significantly higher density but also better strength, hardness and mechanical properties than the green components.

Sintering can be classified into two categories: 1) solid state sintering and 2) liquid phase sintering. In solid state sintering, the powder component remained solid during the entire sintering process, while liquid phase sintering involved the presence of a liquid phase in the component during sintering. The type of sintering process to be used depends on the material of the powder and the desired microstructure of the component. Generally, sintering occurs by the fusion of the powder particles via atomic diffusion. Figure 2.6 shows the schematics of different diffusion processes taking place during sintering [10].

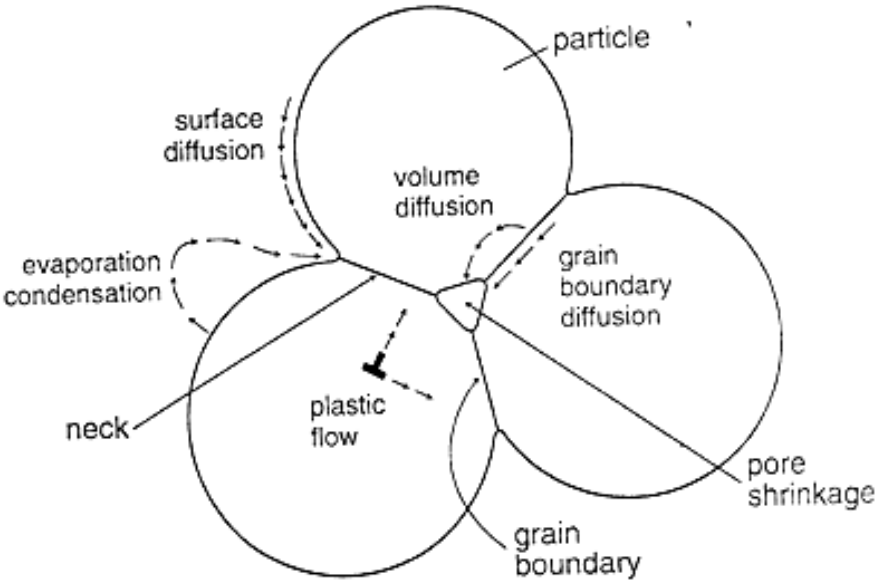

Figure 2.6 Atomic diffusions and mechanisms during sintering [10].

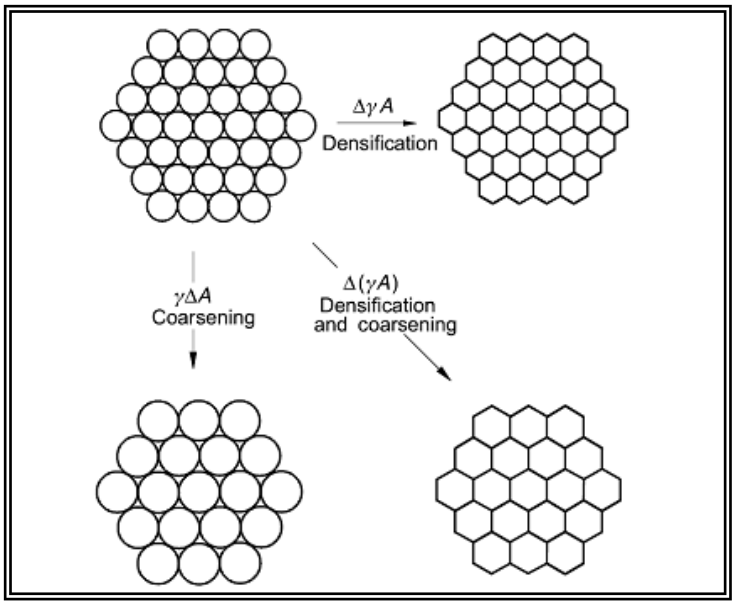

Figure 2.7 Densification and coarsening of the powder particles [17].

As shown in Figure 2.8, the sintering process occurs in three stages [11]. Before sintering, the component consists of a bunch of loosely packed powders. At the initial stage of sintering, necking starts to occur on the particles. The pores at this stage of sintering are open, interconnected and irregularly shaped. With increasing temperature in the intermediate stage of sintering, further neck growth occurs and becomes large enough to interfere with each other and overlap [11]. The pores starts to shrink and formation of isolated pores occurs at this point. In addition, grain growth is also observed at this stage of sintering. Lastly, in the final stage of sintering, the pores are closed and become spherically shaped, giving the component a relatively dense structure. Grain growth continues at an accelerating rate as there are fewer pores to impede grain boundary motion [11].

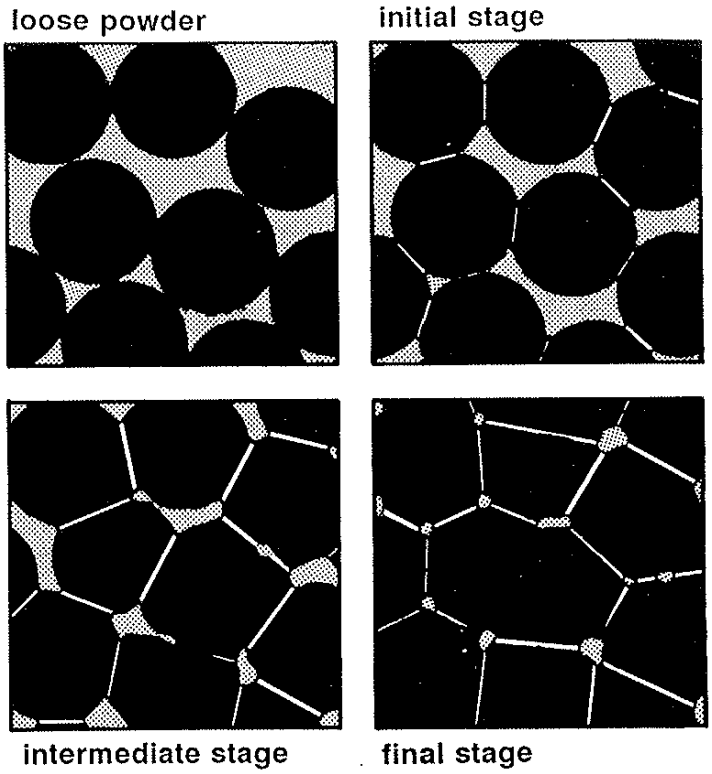

Figure 2.8 Three stages of sintering [11].

2.2 Powder Injection Moulding of Titanium

PIM has been successfully applied to several metallic powders like stainless steel, Al and copper as they are relatively easy to handle [18]. However, the case differs for Ti. This is because Ti is a reactive material, which readily reacts with O, C and N. Therefore, the major challenge in PIM of Ti is controlling Ti absorption of impurities during the entire processing, which is detrimental to the final density, mechanical properties and even surface finishing of the Ti components.

Owing to the above reason, it could be why majority of PIM Ti components are mostly commericalised in non-load bearing sectors. PIM Ti components have been used in moderate to low stress applications like watch cases, sports equipment, mobile phones, automotive interior components, surgical hand tools, dental brackets and cosmetics cases [6]. Companies like Mimest SpA (Italy) have successfully fabricated PIM Ti components for photographic tripods, trigger for guns and small lightweight gears for racing bicycles [19]. An article featuring

Osaka Yakin Kogyo Co., Ltd also commented that PIM of Ti will see strong growth in Japan with watch and medical devices sectors being the primary consumers [20]. However, the applications of PIM Ti components can be further extended to engineering or structural applications due to their excellent properties mentioned earlier. Currently, TiJet Medizintechnik GmbH (Germany) is one of the few PIM commercial companies which have successfully produced and commercialised PIM Ti products for medical implants [21]. Figure 2.10 shows PIM Ti aortic-valve-prosthesis fabricated by TiJet Medizintechnik GmbH [22].

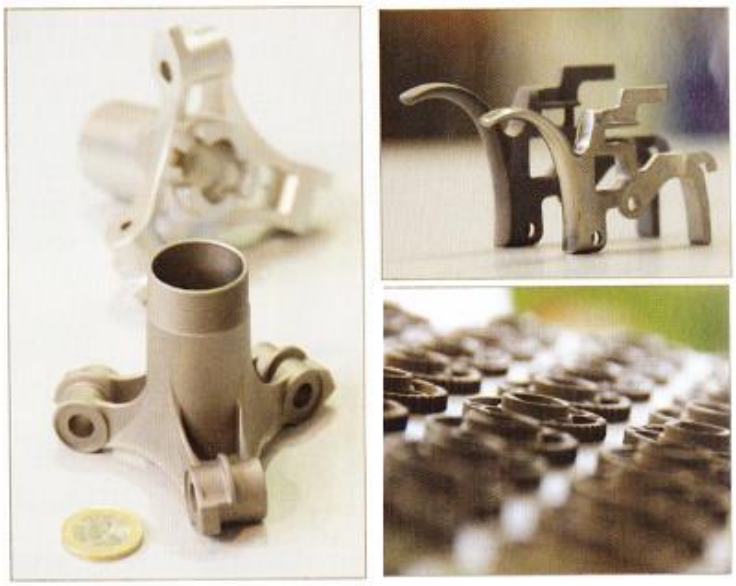

Figure 2.9 PIM Ti components fabricated by Mimest SpA [19].

Figure 2.10 PIM Ti Aortic-valve-prosthesis [22].

2.3 Challenges in Powder Injection Moulding of Titanium

The main challenge in fabricating Ti components by PIM process is maintaining the desirable inherent mechanical properties of Ti after the manufacturing process. The mechanical properties of PIM Ti components are dependent on: 1) the interstitial elements Ti absorbs during fabrication and 2) its microstructure.

It is vital to control the absorption of interstitials like oxygen (O), carbon (C), nitrogen (N) and hydrogen (H) due to Ti high reactivity. These interstitials affect the mechanical properties and relative density of Ti. High levels interstitial can increase the elastic modulus and yield strength of Ti but drastically reduce its ductility [3]. Although N has the most significant effect on the mechanical properties, it is usually not found in high concentrations in dense Ti. Extra caution need to be taken when exposing Ti to O. This is because Ti has high affinity and solubility for O. The O restricts twinning and prismatic slip hence, lowing Ti ductility and impact resistance.

The second factor which affects Ti mechanical properties is its microstructure. This includes the porosity, grain morphology and phase composition of the sintered component. The challenge here is how to optimise these features to achieve the desirable mechanical properties for the intended applications.

As explained earlier, PIM consists of several processing steps: 1) powder selection, 2) binder selection, 3) feedstock preparation, 4) injection moulding, 5) debinding and 6) sintering. Powder and binder selection, debinding and sintering steps were considered to be the more crucial stages as they have significant influence on the final impurities and properties of the sintered Ti components. The effects which each of these factors have on Ti processing will be explained in the following sections:

2.3.1 Powder Selection

There are three key attributes for powders in PIM: 1) particle size distribution, 2) particle shape and 3) O and C levels.

As mentioned earlier, in PIM powders with small particle size, between 0.5 to 20 μm with D_{50} between 4 to 8 μm are ideal for PIM. Unfortunately, such particle size range is not easily achievable for Ti powders as they are difficult to produce due to cost and hazards issues (explosive). In addition, smaller particle size also induced higher exposure to impurity contaminations due to larger surface area for reaction. Smaller particle size powders adsorb O contributed by the binder more significantly than the larger ones due to their larger surface area. However, this effect is less significant in the sintering stage due to faster densification and hence, reduction of surface area as compared to their larger counterparts [3], as indicated in Figure 2.11.

The starting purity of the powders is also important as the final level of O and C in the Ti component is dependent on initial powder purity. In PIM of Ti, low levels of O and C are highly desirable. As Ti has high affinity with impurities, the difficulty is obtaining Ti powders that have these attributes.

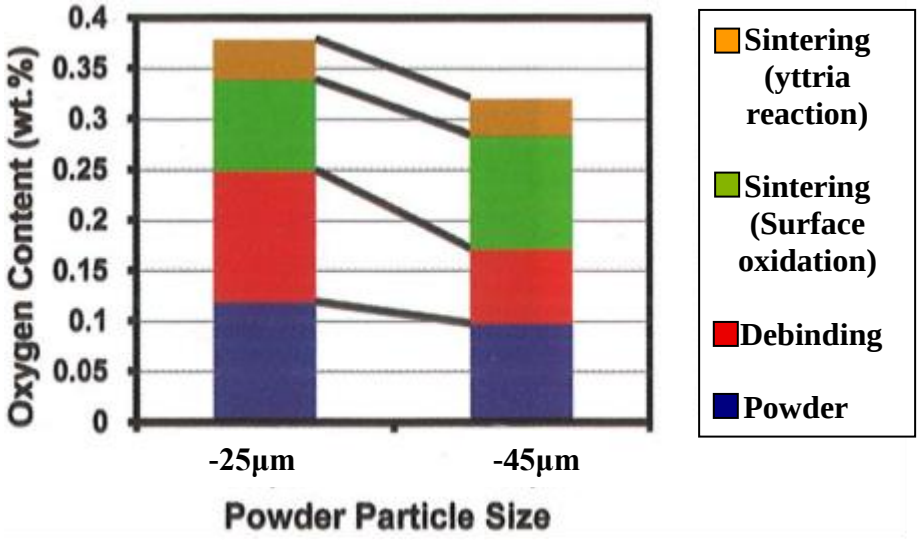

Figure 2.11 O content in different powder sizes at each fabrication stages [3].

Currently, most of the Ti powders used are gas atomised. Spherical shaped gas atomised powders are easy to mould and provide higher solid loadings, but it causes the components to be prone to distortion in debinding as compared to angularly shaped powders. To overcome this issue, alternative powder fabrication method has also been employed to fabricate finer angular Ti powders. This process is known as hydride-dehydride (HDH) process. In HDH, large TiH_2 pieces are crushed, milled and screened into fine angular-shaped powders [23]. The powders are then heated in vacuum to obtain the Ti powders. Though HDH Ti powder is finer in particle size, it's O and C level exceeds that of powder produced by gas atomisation. Moreover the angularly shaped particles do not have good flowability during injection moulding.

A combination of both gas atomisation and HDH Ti powders have been used to achieve a balance in solid loading, feedstock flowability and shape retention during debinding. However, higher interstitial contents in HDH Ti powders increased the overall O level in the feedstock, which is not desirable if the products are to be used for advanced engineering components [6]. Study conducted by Kusaka et al. [24] also showed that the O content in the PIM Ti component increased with increasing percentage of HDH powders mixed with gas atomised Ti powders. Table 2.5 shows the characteristics of the Ti powders produced by the different methods.

Table 2.5 Characteristics of Ti powders produced by different methods [6].

Powder type	Media size (μm)	Tap density, (% of pycnometer)	Oxygen (wt. %)	Carbon (wt. %)
Sponge fines	38	48	0.35	0.05
Hydride-dehydride	38	38	0.25	0.04
Titanium hydride	35	40	0.20	0.02
Reactive	30	47	0.30	0.10
Gas atomised	32	60	0.15	0.03
Plasma atomised	60	62	0.15	0.04
Rotating electrode	130	72	0.15	0.02

2.3.2 Binder Selection

The mechanical (e.g. ductility and tensile strength) and physical properties are highly dependent on the amount of interstitial elements absorbed by Ti during processing. A major contributor of these interstitial is the binder as most of them are hydrocarbons, which is a rich source of O and C. Therefore, one of the key factors in controlling the impurities level in PIM Ti component is to select an appropriate binder. The binder used for the PIM of Ti shall contribute minimal impurities during processing.

Some of the criteria for binder for PIM of Ti include:

- Low decomposition temperature (preferably below 260 ^{o}C as the decomposition temperature of polymers coincides with the reactive temperature of Ti).
- Chemically stable [7].

Most of the binder developed for PIM mainly consists of mixtures of polyethylene or polypropylene, synthetic or natural wax and stearic acid as feedstocks based on these formulations are easy to mould [25]. However, the mechanical properties of Ti components fabricated with these traditional binder tend to be poor and unable to match the properties of wrought Ti [8,26,27]. Improvement works have been conducted on these binder but results showed little improvement on the mechanical properties, especially on the elongation [8,27].

The naphthalene based binder has also been experimented but components did not exhibit excellent mechanical properties [28]. Moreover, long term usage of naphthalene also has adverse effect on human health and environment. Intensive research has been going on for the binder formation. Table 2.6 presents some of the binders which are compatible with Ti-6Al-4V.

Commercial companies who have reportedly achieved mechanical properties comparable to wrought and cast Ti alloys, kept their binder as trade secrets. TiJet Medizintechnik GmbH, a German MIM company which specialized in PIM Ti components, has reported outstanding ductile characteristics in their Ti components. Table 2.7 shows the mechanical properties and also the impurities levels of their products in comparison to wrought and cast Ti.

Although, some of the binders have either achieved the targeted O level or elongation, improvement in formulating the desirable binder for the PIM of Ti components is still required. Moreover, there is also limited information or disclosure on the binder composition used. The ultimate goal in selecting a good binder for Ti is to have one that contributes minimal impurities during the processing steps.

Table 2.6 Compatible binder with Ti-6Al-4V.

Binder	O Content (wt %)	Elongation (%)	Reference
polyethylene glycol, polymethylmethacrylate and stearic acid (water based binder)	*0.20	*12.5	[4]
Polypropylene, ethyl vinyl acetate, paraffin wax, carnauba wax, dioctyl phthalate	0.24	12	[29]
Polyethylene, paraffin wax, stearic acid	0.28	7.81	
Polypropylene, polymethy methacrylate, paraffin wax, stearic acid	0.25 – 0.28	14	
Polypropylene, paraffin wax, carnauba wax, etc	0.2	-	
Naphthalene, stearic acid, ethylene, vinyl acetate	0.17	14.6	
Undisclosed	0.19	-	
Undisclosed	0.20	15	

**Average reading of 6 components.*

Table 2.7 Mechanical properties and contaminants in Ti from various sources [21].

Material	0.2 %-Yield Strength (MPa)	Tensile Strength (MPa)	Elongation (%)	O %	C %	N %
Ti_6Al_4V ELI, MIM (TiJet)	700	800	15	0.20	0.05	0.018
Ti_6Al_7Nb, MIM (TiJet)	660	760	12.5	0.23	0.04	0.0015
Pure Ti, MIM (TiJet)	420	500	20	0.21	0.07	0.03
Ti_6Al_4V ELI per ASTM F136 (Wrought)	795	860	10	0.13	0.08	0.05
Ti_6Al_4V per F1472 (Wrought)	780	860	10	0.20	0.05	0.08
Ti_6Al_4V per ASTM 1108, Ti_6Al_4V (casting)	758	860	8	-	-	-

2.3.3 Debinding

The debinding stage is one of the more critical steps in PIM of Ti, as this is where the extraction of the binder takes place, therefore, exposing Ti impurities such as C and O. Debinding of PIM components is usually conducted in two stages: 1) solvent debinding and 2) thermal debinding.

The process of solvent debinding involves soaking of PIM green components in solvents under low heat (50 to 80 ^{o}C) for up to 10 hours. Generally, solvent debinding does not cause Ti to absorb impurities easily due to the involvement of low processing temperatures. In most PIM Ti components, solvent debinding is conducted in solvents like heptane [26,30,31] or mixture of heptane and ethanol [8,27].

The bulk of the C and O contamination risks come from the thermal debinding process. This is because the decomposition temperatures of the binder are close to the reactive temperature of Ti. Hence, in order to minimise the absorption of these interstitial elements, it is desirable for this process to be carried out under low temperature and in environments where the fumes or residues of the binder can be effectively removed. Important parameters for thermal debinding are temperature, atmosphere and time.

Current methods of thermal debinding include, debinding in Ar atmosphere, vacuum atmosphere or sweepgas concept (debinding conducted in both Ar and vacuum condition). Among these methods, vacuum and sweepgas debinding are preferred over Ar as they are more efficient in removing moisture and other residues resulting from the decomposition of the binder. Vacuum debinding involves the burning off of the binder in a high vacuum environment. The sweepgas concept is a combination of Ar and vacuum debinding. Ar gas will sweep through the debinding furnace, removing moisture and impurities, while a vacuum pump is connected to the outlet drawing out the "used" Ar. Ar debinding is not preferred as Ti debound in Ar exhibited higher levels of C and O level as compared to vacuum and sweepgas concept [27]. The reason for this was believed to be due to the O and moisture content in the Ar gas. Therefore, the use of high purity Ar and installation of filters or moisture traps is highly recommended if Ar debinding is to be employed.

Besides the debinding atmosphere, debinding temperature also influences the amount of C and O being absorbed by Ti. Figure 2.12 shows that O level increased drastically with increasing debinding temperature while C level decreased and remained relatively stable when components were debound at temperatures 600 ^{o}C and above [8]. This finding was also supported by a study conducted by Baril et al. [3] and Lefebvre et al. [32], as shown in Figure 2.13.

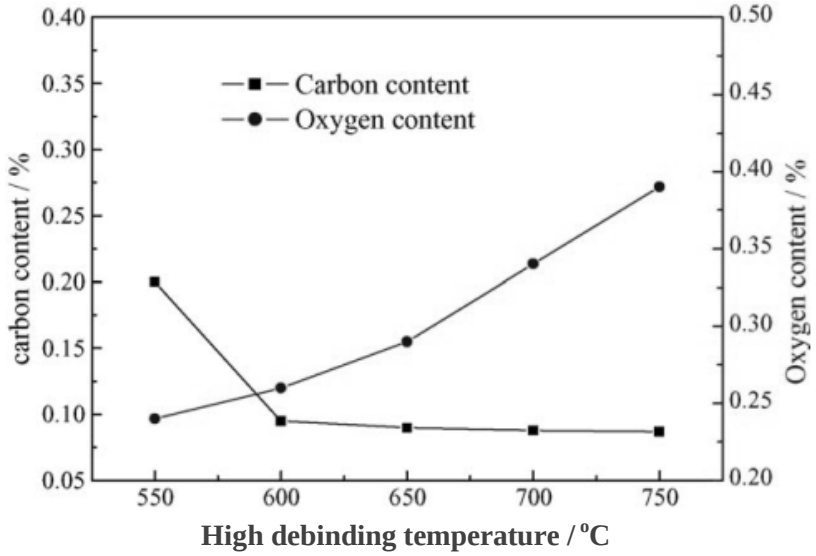

Figure 2.12 Effects of temperature on O and C content in Ti-6Al-4V [8].

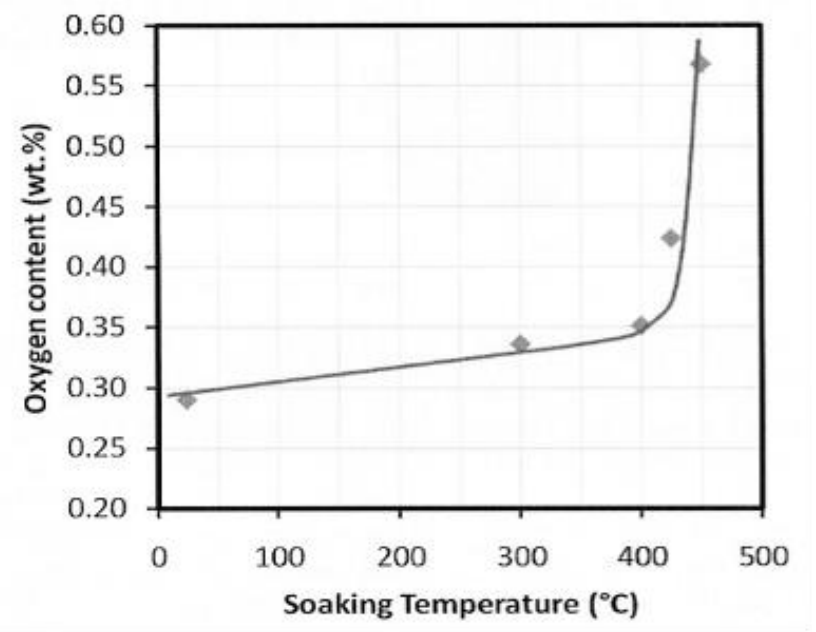

Figure 2.13 O in Ti foam at different temperatures in Ar with 20 vol% of O [3, 32].

Study also found that sample batch size is important for debinding processes with temperature above 400 °C. Larger sample batch size is preferred as there is more Ti volume to absorb the atmospheric impurities, hence, reducing the amount of impurities taken up per Ti component [3]. Therefore, it was recommended that sacrificial Ti be added during debinding for this purpose. This method can also be applied to the sintering of Ti components.

There has not been a standard method for the debinding of Ti as its processing parameters are dependent on the type of binder used. However, the final aim of debinding is to carry out the debinding process at as low temperature as possible to reduce the risk of impurity contamination. A review paper written by R.M German et al. [6] recommended that the best method for debinding of Ti with wax-polymer binder is to first solvent debind then sweepgas thermal debind to 450 ^{o}C.

2.3.4 Sintering

Like debinding, sintering also plays a major role in influencing the final properties of Ti. Important factors for sintering include temperature, atmosphere, dwell time and substrate material [6].

Higher sintering temperatures usually favor higher sintering density and lower porosities (mostly in isolated forms). However, this comes with a tradeoff of larger grain size which degrades the mechanical properties. Zhang et al. [33] reported that by designing an appropriate multiple-step sintering profile, sintering conducted under lower temperature and shorter time can also achieve parts with high density. Results from his studies are tabulated in Table 2.8. Other studies have shown that the peak temperature for Ti sintering ranges from 1100 – 1450 ^{o}C [6]. It was also recommended that the sintering of PIM Ti components to be conducted at temperature below 1200 ^{o}C due to the significant O absorption at higher temperatures [3,34]. This is illustrated in Figure 2.14, where a drastic increased in the O content in Ti powders, particularly for smaller powder size, when the temperature goes beyond 1200 ^{o}C.

Table 2.8 Influence of sintering conditions on densities of MIM Ti-6Al-4V [33].

Sample	Sintering Condition	Sintered Density (% TD)
1	1250 ^{o}C 3 hours	98.6
2	1280 ^{o}C 3 hours	98.8
3	Multiple-step cycle to 1250 ^{o}C 3 hours	99.4
4	Multiple-step cycle to 1280 ^{o}C 3 hours	99.5

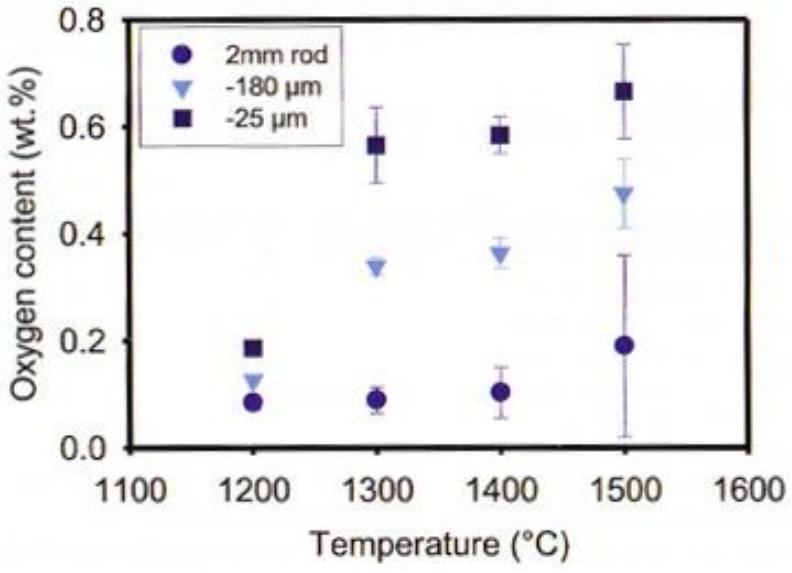

Figure 2.14 O in Ti powders and rod at different temperatures for 1 h in vacuum [3,32].

The ideal condition for sintering of PIM Ti components is under high vacuum condition. In the past, other researchers encountered difficulties in achieving the desired vacuum level for sintering. However, with improvements on the furnaces and vacuum pumps, this issue is no longer an obstacle in producing Ti components. It was also commented that sintering in Ar is detrimental to a high sintered density as it will be trapped in the pores because of its insolubility [6]. The effects on sintering Ti powder in Ar and vacuum condition have also been studied and results from Heaney et al. [35] study coincide with the finding on Ar sintering

A longer dwell time was also observed to promote higher levels of impurities in Ti. As shown in Figure 2.5, it was found that longer dwell time increased the O content drastically in the component [8].

The choice of substrate material for sintering is also important. It was commented that graphite and alumina substrate are not acceptable as they react with Ti under high temperature. Zirconia and yttria sintering substrates were found to be more compatible [6].

Generally, issues pertaining to equipment and sintering substrates have been resolved due to the availability of good quality vacuum furnaces, installations and also inexpensive substrates. The challenge in producing PIM Ti components is on the sintering profiles. A suitable sintering profile is required to achieve maximum tensile strength, elongation, density and to minimise impurities for PIM Ti components.

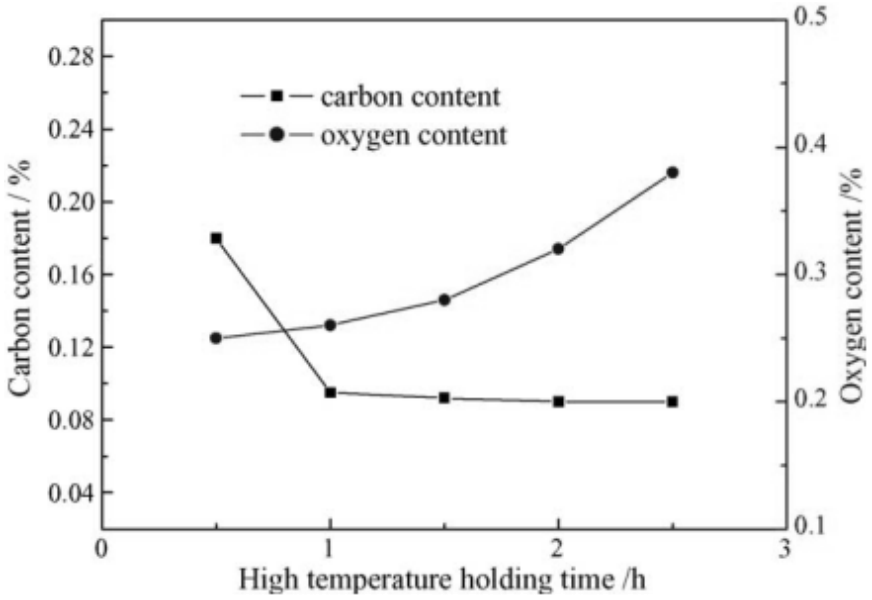

Figure 2.15 O and C content with dwell time [8].

2.4 Classification of Titanium and its Alloys

Ti and its alloys can be classified into three main groups: 1) α alloys, 2) α+β alloys and 3) β alloys. The phase at which Ti and its alloys exist at room temperature is dependent on the type and amount of alloying elements (α or β phase stabilisers) in it [36]. These stabilisers will either decrease or increase the α/β transformation temperature of 882 ^{o}C for titanium [38]. Figure 2.16 shows the classification of Ti against the concentration of β phase stabilisers alloyed in them. The typical microstructures for each alloy classes are also presented in Figure 2.17.

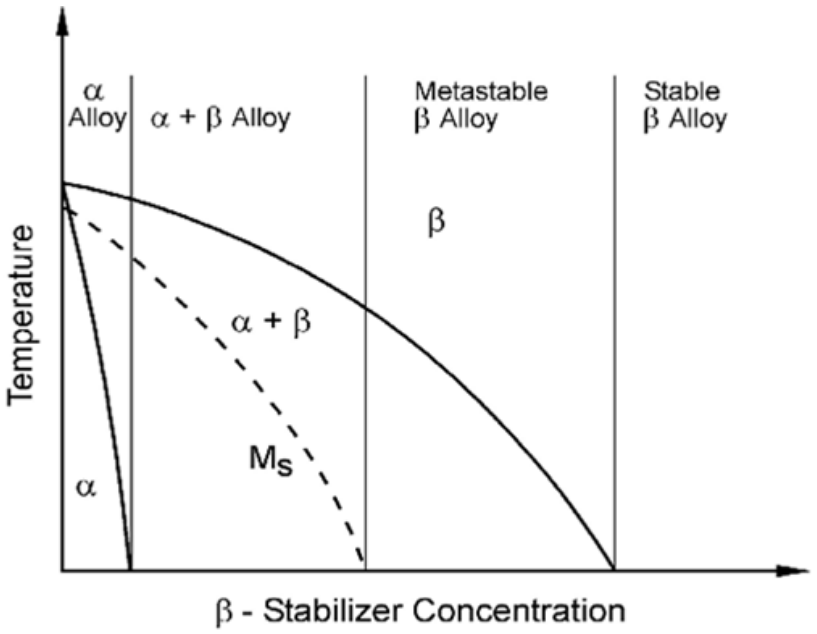

Figure 2.16 Pseudo-binary section through a β isomorphous phase diagram [38].

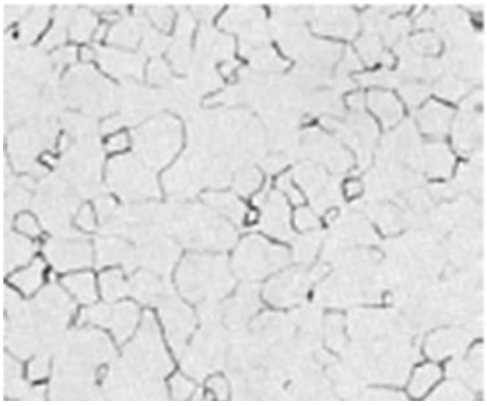

α alloy: Equiaxed α in unalloyed Ti after 1 h at 699°C.

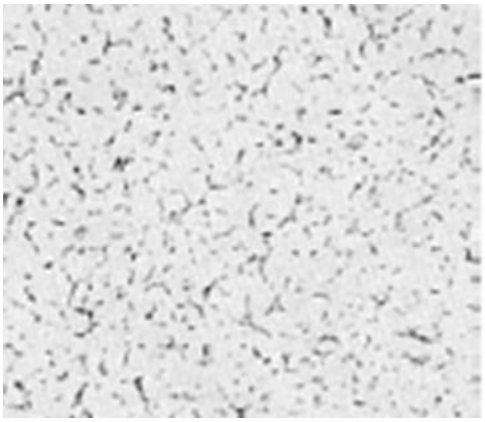

α+β alloy: Equiaxed α+β

α+β alloy: Acicular α+β alloy in Ti-6Al-4V

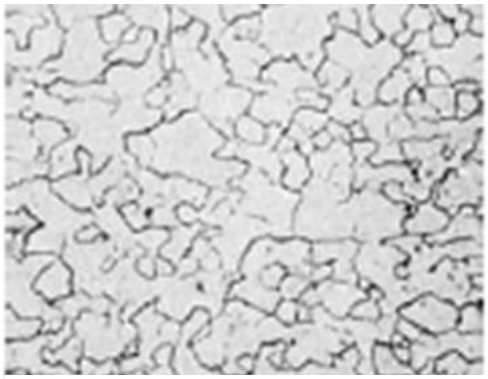

β alloy: Equiaxed β in $TiV_{13}Cr_{11}Al_3$

Figure 2.17 Typical microstructures of α, α+β and β alloys [37].

2.4.1 α alloys

α alloys are Ti or Ti alloys with α stabilizers such as aluminium (Al) and tin (Sn) [36,38]. This group of alloys contains high volume of α phase and takes the form of hexagonal close-packed (hcp) structure at room temperature. α alloys generally have better weldability and resistant to creep at high temperature as compared to α+β alloys and β alloys [37]. However, they lose out in terms of strength and toughness to their α+β alloys and β alloys counter parts.

2.4.2 α+β alloys

This group of alloys contains both α and β stabilizers elements. Therefore, α+β alloys contain a mixture of α and β phases at room temperature. The existence of two phases in the α+β alloys allow them be used in a wide range of applications as their properties can be modified by controlling the amount α and β phase formed and also their microstructures through appropriate heat treatments.

α+β alloys generally have good fabricability, high strength at room temperature and moderate strength at elevated temperature [36,39]. Images of some of the microstructures of α+β alloys are shown in Figure 2.18 and Figure 2.19. The microstructures of the α+β alloys can be divided into three groups [40]:

1) Fully lamellar – Microstructures achieved by heat treating the α+β alloys above the β recrystallization temperature, followed by cooling from the β phase field. The thickness of the α lamella and size of the α colonies are depended on the cooling rate

2) Bi-modal – Microstructures with a combination of equiaxed α grains dispersed in the β matrix.

3) Fully equiaxed – microstructure consists of a combination of α grain with β phase between them. Such microstructure can be achieved by slow cooling rate from the bimodal recrystallization annealing temperature.

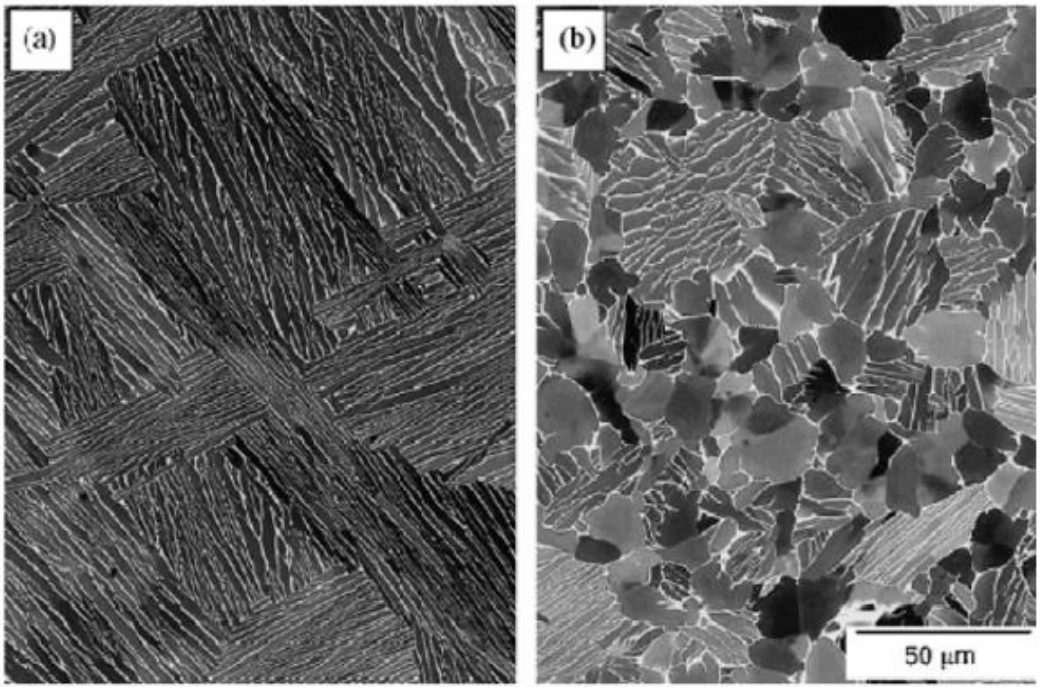

Figure 2.18 (a) Fully laminar and (b) Equiaxed microstructures [40].

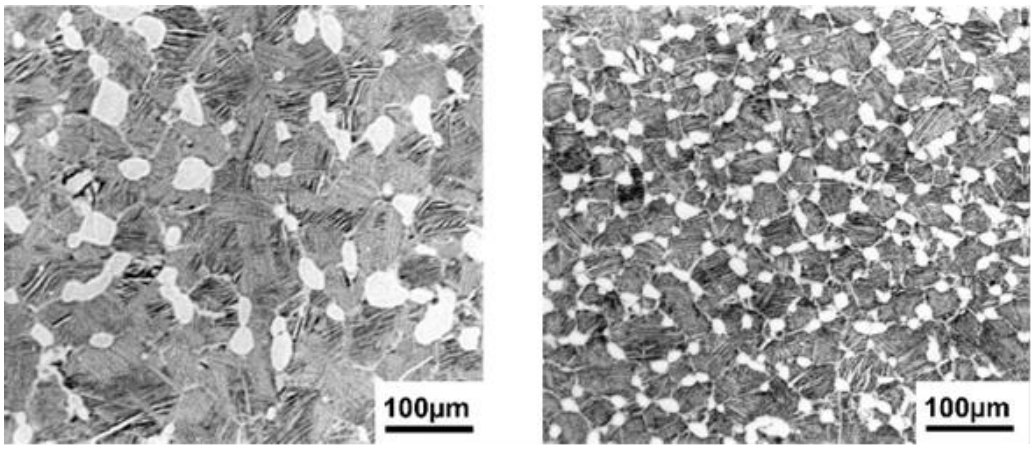

Figure 2.19 Bi-modal microstructures [38].

2.4.3 β alloys

β alloys are rich in β stabilizers like Vanadium (V), Niobium (Nb), Tantalum (Ta) and Molybdenum (Mo) and their matrix consist of large percentage of β phase. β alloys are metastable and can allow partial transformation to α phase with the appropriate heat treatment [37].

Solution treated β alloys generally have good ductility, toughness and formability but low basic strength. They are not suitable for elevated temperature applications without stabilization or over aging treatment due to the precipitation of α phase under high temperature. However, α phase precipitation promotes fracture toughness in β alloys, which can be better than aged α +β alloys of comparable yield strength [37].

CHAPTER 3 EXPERIMENTAL WORK

This chapter discussed the characterisation work conducted on the experimental materials (powders and binder). In addition, the experimental procedures for four basic steps of PIM (mixing, moulding, debinding and sintering) will also be reported.

3.1 Materials Characterisation

3.1.1 Chemical Composition of CP-Ti and Ti-6Al-4V Powders

Gas atomised CP-Ti (Grade 2) and Ti-6Al-4V (Grade 5) powders with particle size <45 μm were purchased from TLS Technik GmbH & Co., Germany. The powders' chemical compositions, obtained from the supplier's material data sheet, are shown in Table 3.1.

Table 3.1 Chemical composition of CP-Ti and Ti-6Al-4V powder.

CP-Ti

Elements	%
Ti	Balance
C	0.020
Fe	0.065
O	0.170
N	0.020
H	0.003

Ti-6Al-4V

Elements	%
Ti	Balance
Al	6.00
V	4.00
C	0.02
Fe	0.16
O	0.14
N	0.02
H	0.001
Y	<0.01
Zn	<0.002
Mg	<0.002

3.1.2 Morphology of Ti and Ti alloy Powders

The morphology and elemental composition of the powders were examined with EVO 50 XVP secondary electron microscope (SEM) and Oxford Instruments DCL 7672 electron dispersive spectrometer (EDS). Figure 3.1 and Figure 3.2 show the morphology of both powders. The secondary electron images (SEI) show that both powders are spherically shaped, which is a characteristic of gas atomised powders. EDS results, analysed using the Oxford Instruments INCA 4.08 software, showed only Ti peaks for CP-Ti powders, while Ti, Al and V peaks were detected for Ti-6Al-4V powders. These results coincide with the general composition of the powder, thus, indicating that the powders are generally pure with no significant contamination. Note that EDS is only a qualitative analysis and elements which exist in minute amount will not be detected.

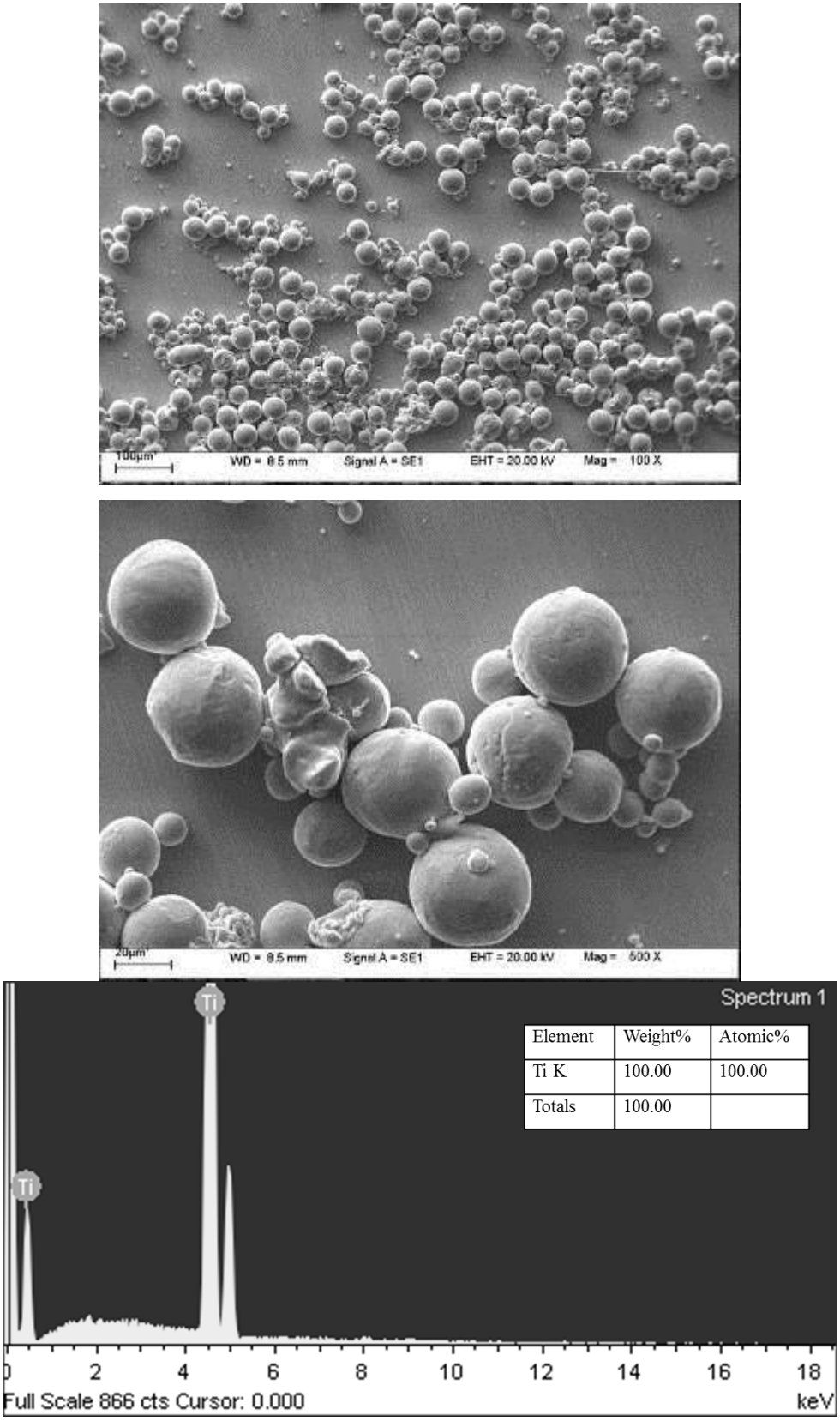

Figure 3.1 SEIs and EDS data of gas atomised CP-Ti.

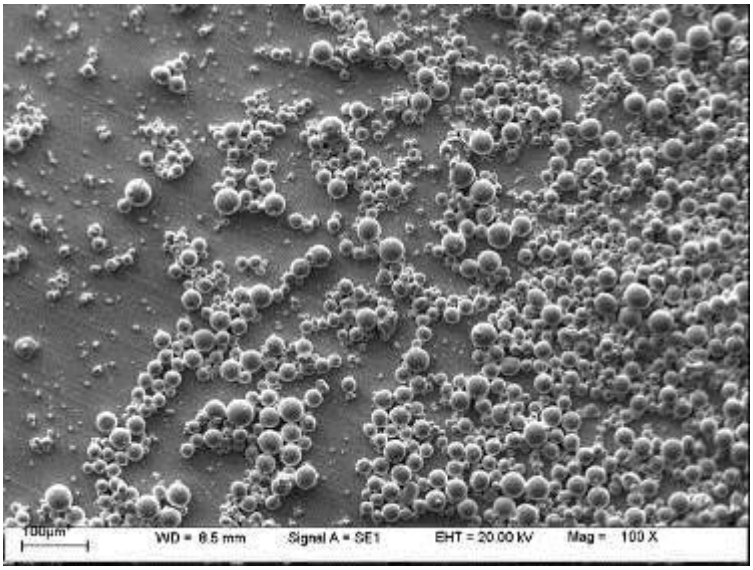

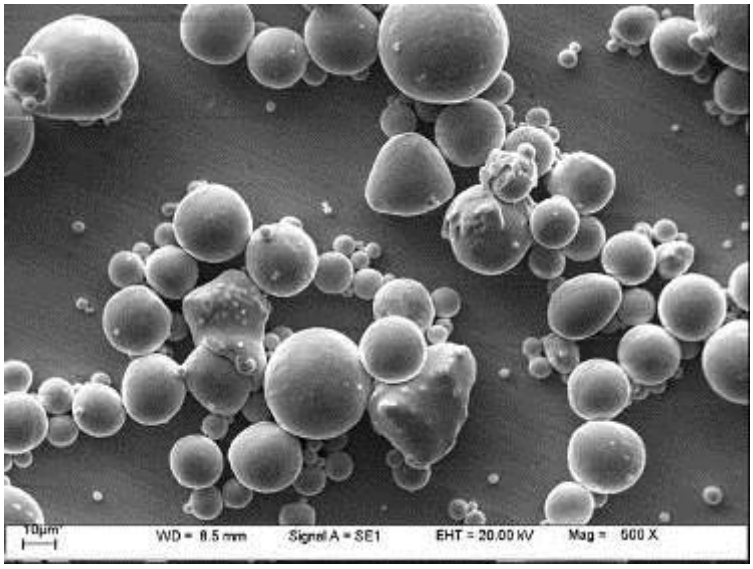

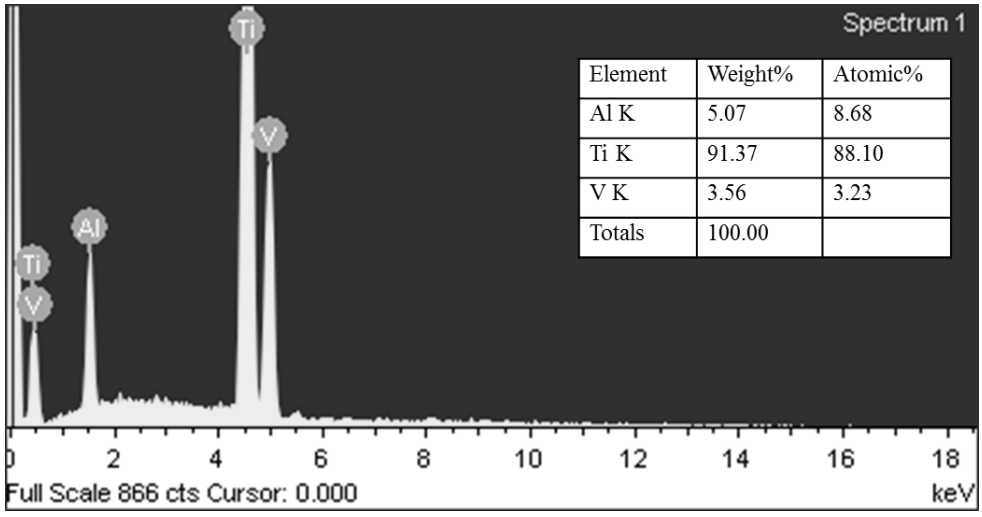

Element	Weight%	Atomic%
Al K	5.07	8.68
Ti K	91.37	88.10
V K	3.56	3.23
Totals	100.00	

Figure 3.2 SEIs and EDS data of gas atomised Ti-6Al-4V powders.

3.1.3 Particle Size Analysis of CP-Ti and Ti-6Al-4V Powders

The particle size of CP-Ti and Ti-6Al-4V powders were measured using a Fritsch Size Analsysette 22 particle size analyser via laser diffraction method. The laser diffraction method uses the properties of the laser's diffraction patterns to measure the size of the particles based on Fraunhofer diffraction theory [41]. The theory states that the particle size is directly proportional to the intensity of the light scattered by it [41]. In this experiment, the Ti powders were first dispersed in water using ultrasonic methods before it was fed into the analysis chamber for measurements.

Based on the measured results, CP-Ti has an average particle size, D_{50}, of 27.50 µm, while Ti-6Al-4V has a D_{50} of 24.70 µm. These values coincide with the SEI of the powders, which shows that the CP-Ti particles in general are slightly larger than the Ti-6Al-4V particles. Results of the particle size measurement are displayed in Figure 3.3.

Besides the morphology of the particles and their sizes, the powder density is also important. This value will be used as a reference with regards to the density of the sintered components. The relative density of the sintered component is calculated by dividing the density of the sintered component with the powder density. Relative density gives an indication on how dense the sintered component is with respect to the powder density. The powder densities of CP-Ti and Ti-6Al-4V measured by Micrometrics AccuPyc 1330 pycnometer are displayed in Table 3.2.

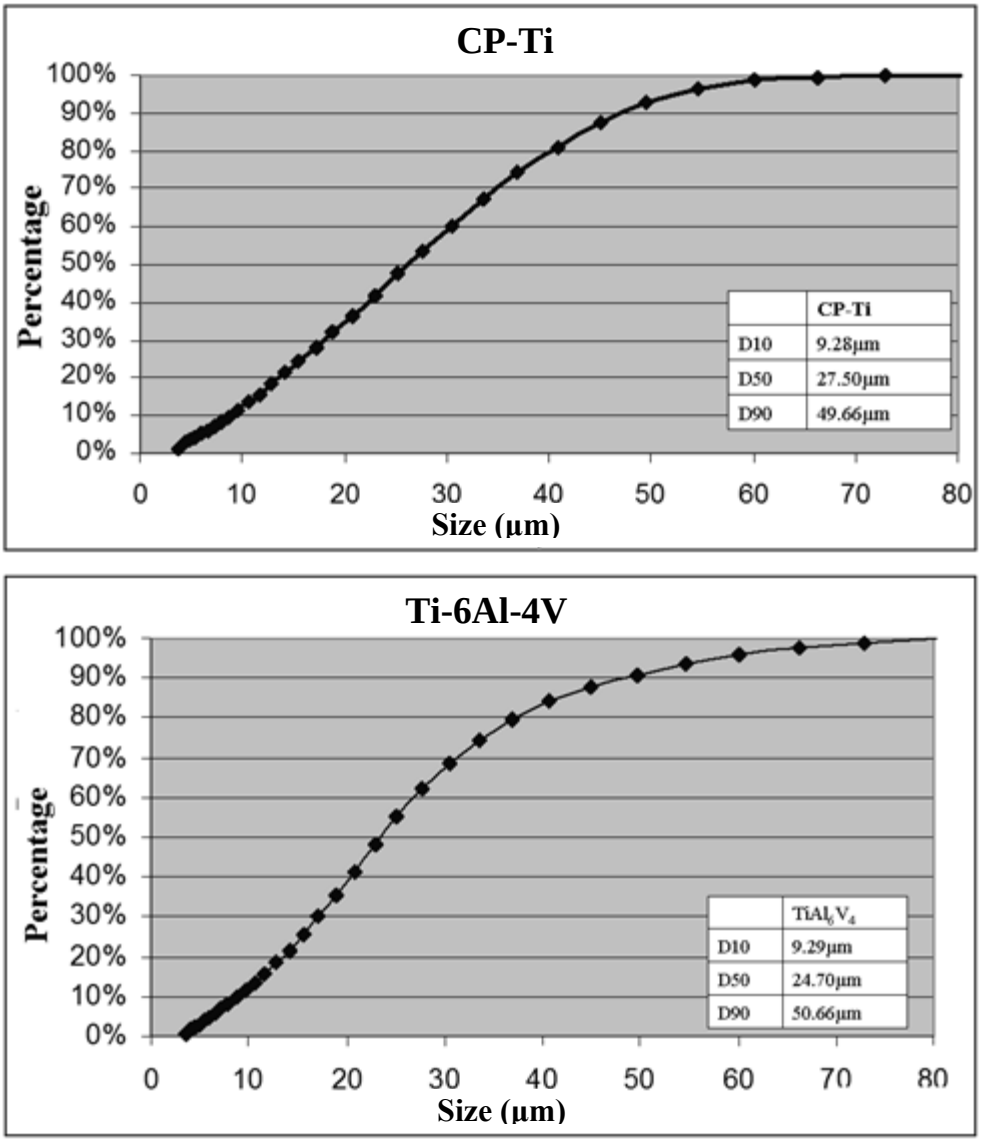

Figure 3.3 Particle size analysis of CP-Ti and Ti-6Al-4V.

Table 3.2 Densities of powders measured by pycnometer.

Powder	Measured Density (g/cm^3)
CP-Ti	4.47
Ti-6Al-4V	4.39

3.1.3 Binder

Binder are essential in PIM as they aid in the flow of the powders during the injection moulding process and provide sufficient green strength for the handling of green components. Based on past experiences, in this research, four binder components were used as the binder for CP-Ti and Ti-6Al-4V. The binder components used in this research are polypropylene (PP), paraffin wax (PW), carnauba wax (CW) and stearic acid (SA). Table 3.3 describes the function for each of the components.

Table 3.3 Functions for each binder component.

Component	Function
PP	• Aids in binding of the powder particles. • Acts as the backbone polymer which provides strength for handling of the green component.
PW	• Reduces viscosity of the feedstock. • Aids in the flow of the powders during injection.
SA	• Acts as wetting agent to reduce contact angle between the powder-binder interfaces.
CW	• Improve the hardness of the green component.

Thermogravimetric analysis (TGA) and differential scanning calorimetry (DSC) were conducted to study the thermal behaviour of these binder components. TGA results will aid in plotting a suitable temperature profile for debinding, while DSC data provides an indicative temperature for feedstock mixing and the moulding temperature.

TA instrument TGA Q500 V6.7 was used to conduct the TGA experiments. For this study, each binder was heated to a temperature of 900 ^{o}C at a ramp rate of 5 ^{o}C per minute in N_2 atmosphere. Due to the limitation of the equipment, the tests were unable to be conducted in the Ar environment. The graphical representations of the TGA results for the four binder components are shown in Figure 3.4.

As seen in Figure 3.4, all of the binder components, except CW, decomposed and burnt off completely before 500 ^{o}C. Table 3.4 summaries the onset temperature, temperature at peak of derivative, temperature at which binder were burnt off completely and weight percentage of residue after the tests. Table 3.4 shows that PW and SA burnt off completely at approximately 323 ^{o}C and 339 ^{o}C, respectively. PP decomposed completely under a higher temperature of 461 ^{o}C. However, a residual weight of 2.145 % remained for CW even with further heating to 900 ^{o}C in N_2. Hence, this pose possible C, O and N contamination when Ti reacts with the CW residue during sintering, affecting the mechanical properties and interstitial level of Ti. However, for this phase of the experiment no changes will be made to the binder composition, thus, CW was incorporated into the feedstock.

Table 3.4 Summary of TGA results for the binder.

Binder	**Onset Temperature (^{o}C)**	**Temperature at Peak of Derivative (^{o}C)**	**Temperature for Complete Burnt off (^{o}C)**	**Remaining Weight at 900 ^{o}C (%)**
PP	390.71	429.88	461.16	0
PW	216.27	281.58	322.95	0
CW	322.93	392.56	Incomplete	2.145
SA	184.58	239.21	339.09	0

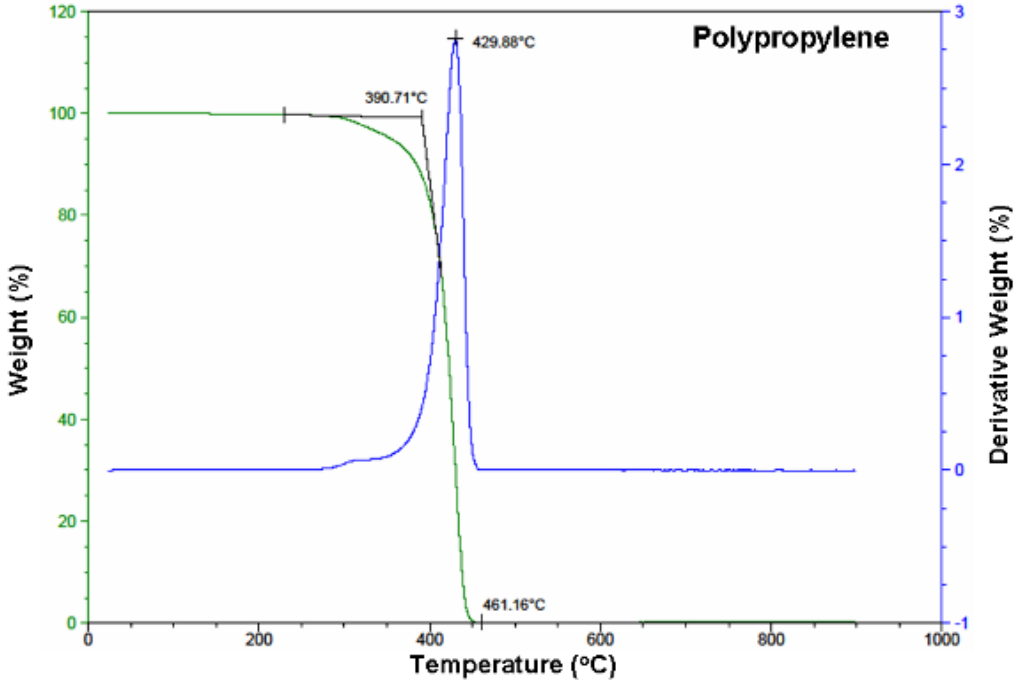
Polypropylene
429.88°C
390.71°C
461.16°C
Weight (%)
Derivative Weight (%)
Temperature (°C)
0
20
40
60
80
100
120
200
400
600
800
1000
-1
1
2
3

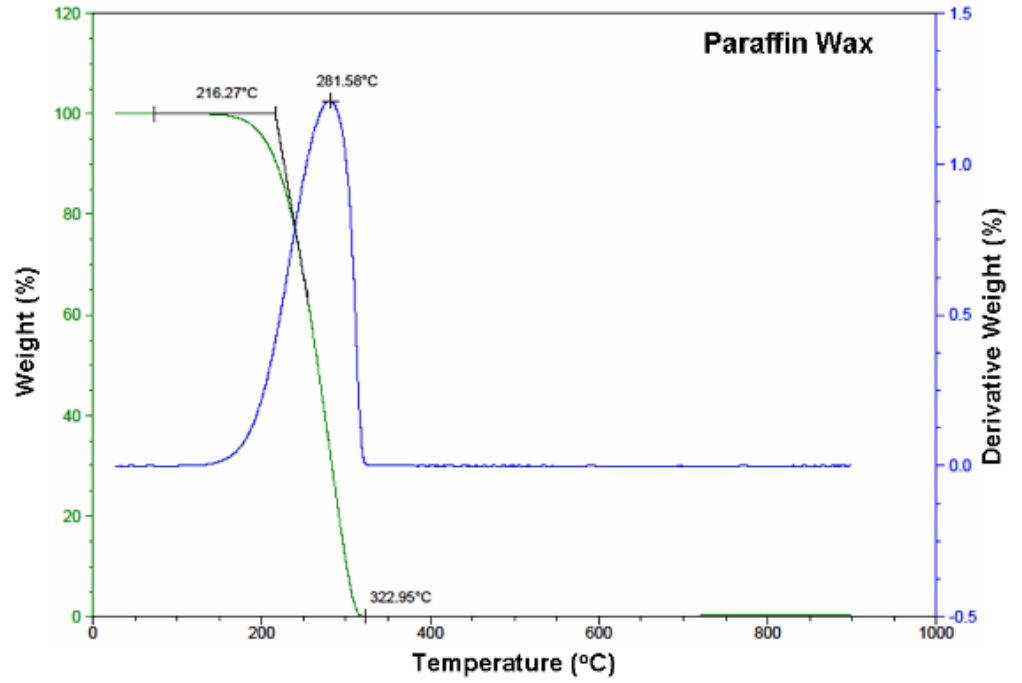
Paraffin Wax
216.27°C
281.58°C
322.95°C
Weight (%)
Derivative Weight (%)
Temperature (°C)
0
20
40
60
80
100
120
200
400
600
800
1000
-0.5
0.0
0.5
1.0
1.5

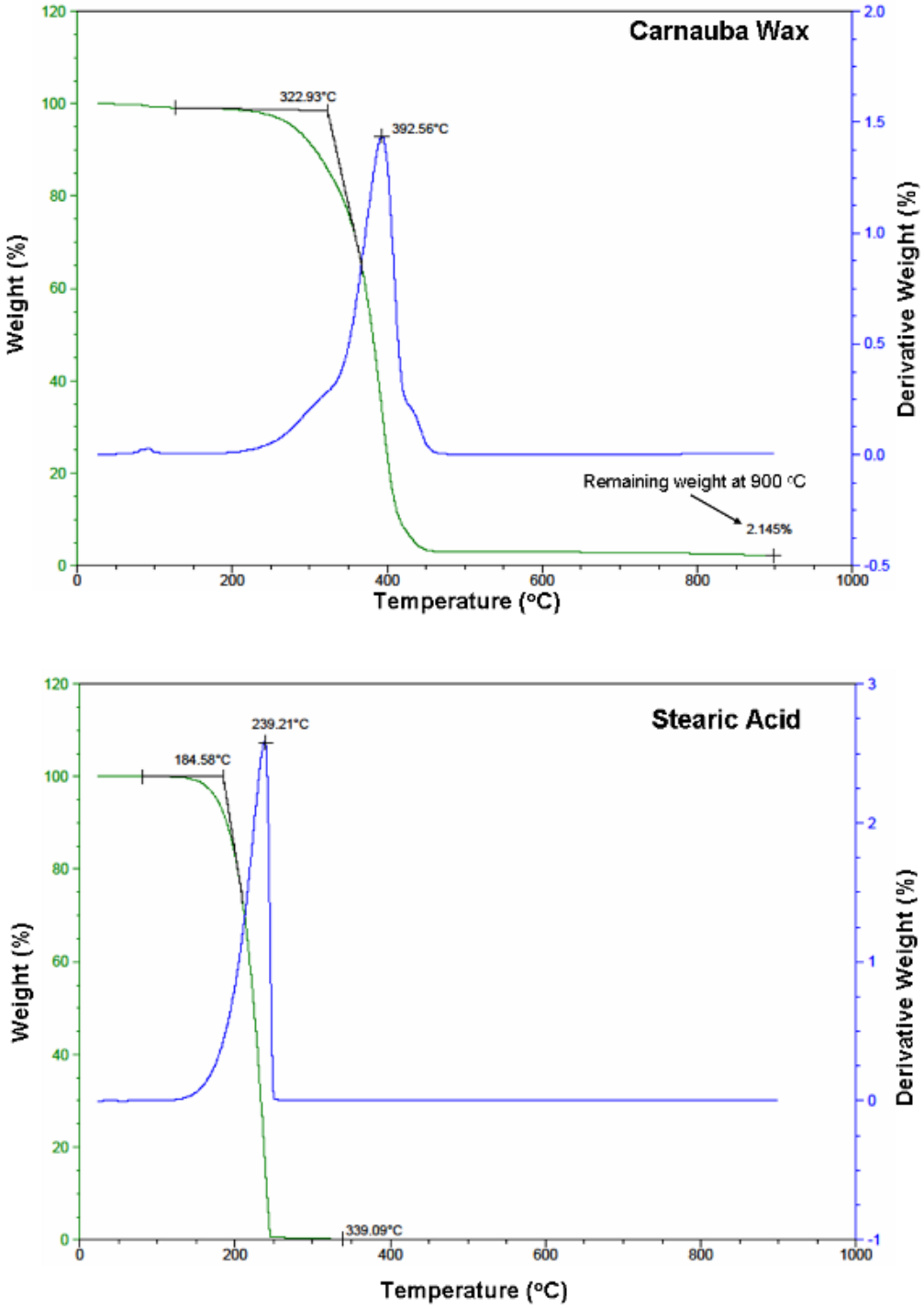

Figure 3.4 Decomposition onset temperature and weight loss of the binders.

DSC analysis was conducted to examine the melting and recrystallisation temperatures for each binder. The tests were conducted using TA instrument DSC Q500 V24.4. The components were crimped in Al pans and heated to temperatures below their degradation temperature at 5 ^{o}C per minute in N_2 atmosphere. Again due to the limitations of the equipment, tests were unable to be conducted in Ar environment. Figure 3.5 displays the DSC results for each of the binder components. The DSC results show that among the four binder components, PP has the highest melting point of approximately 144 ^{o}C. Hence, the mixing temperature for Ti feedstock needs to be at least 144 ^{o}C in order to completely melt all the components to obtain a homogeneous mixture. Two distinct melting and recrystallization points also were observed in the DSC curve of CW as it is a compounded substance, predominately made up of aliphatic esters, di-esters of 4-hydroxycinnamic acid, ω-hydroxycarboxylic acid and fatty acid alcohols [42].

Table 3.5 Binders melting and recrystallisation temperature.

Binder	Recrystallisation Temperature (^{o}C)	Melting Temperature (^{o}C)
PP	84.16 & 107.02	144.04
PW	54.20	55.19
CW	42.31, 71.76 & 76.93	76.80 & 81.84
SA	49.65	54.73

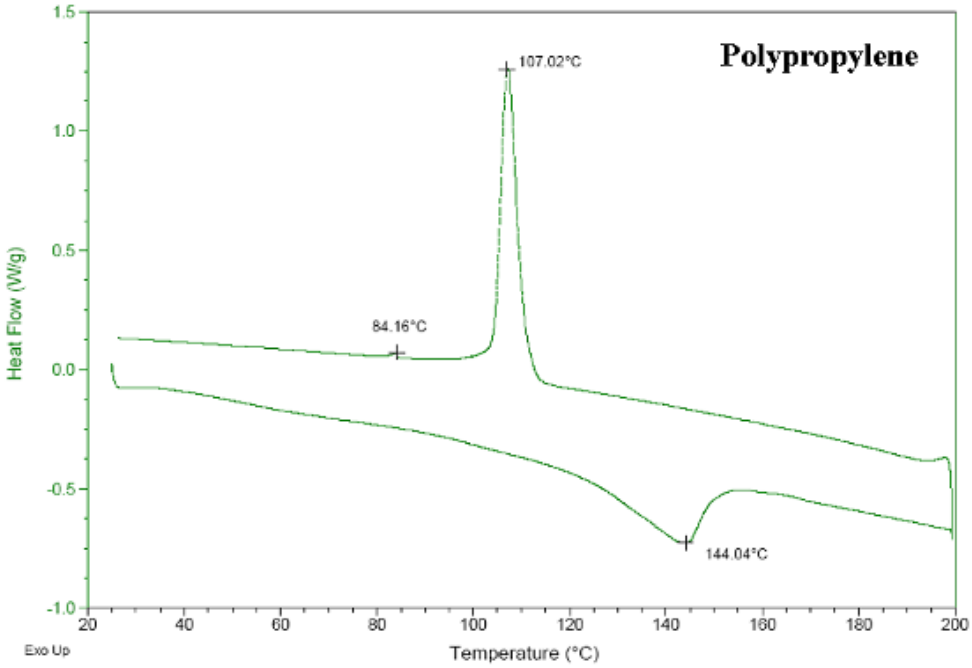
Polypropylene
107.02°C
84.16°C
144.04°C
Heat Flow (W/g)
Temperature (°C)
Exo Up

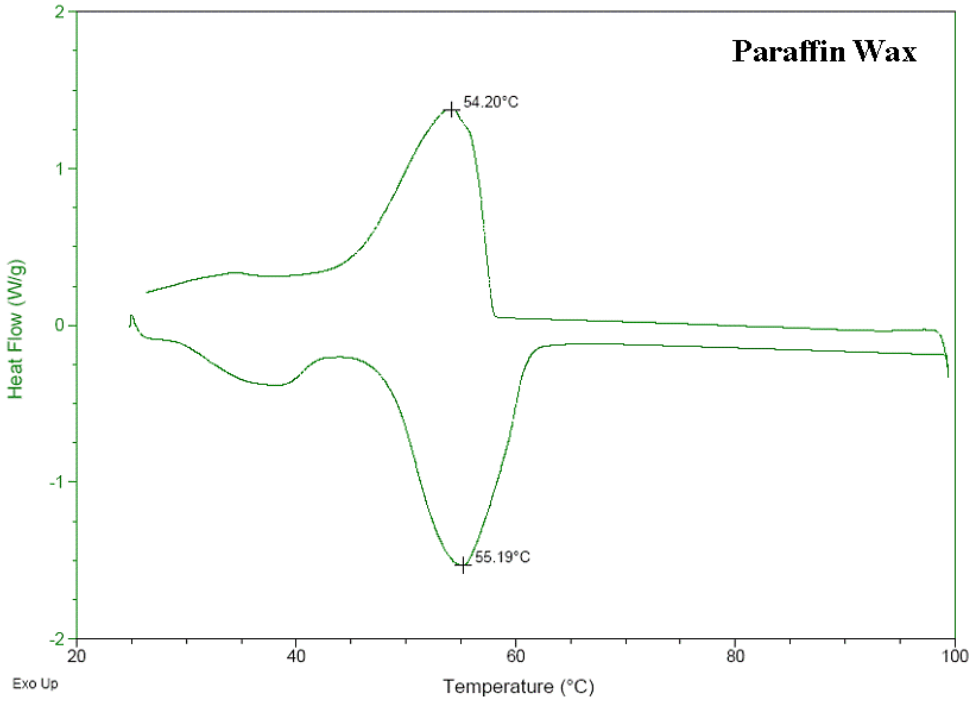
Paraffin Wax
54.20°C
55.19°C
Heat Flow (W/g)
Temperature (°C)
Exo Up

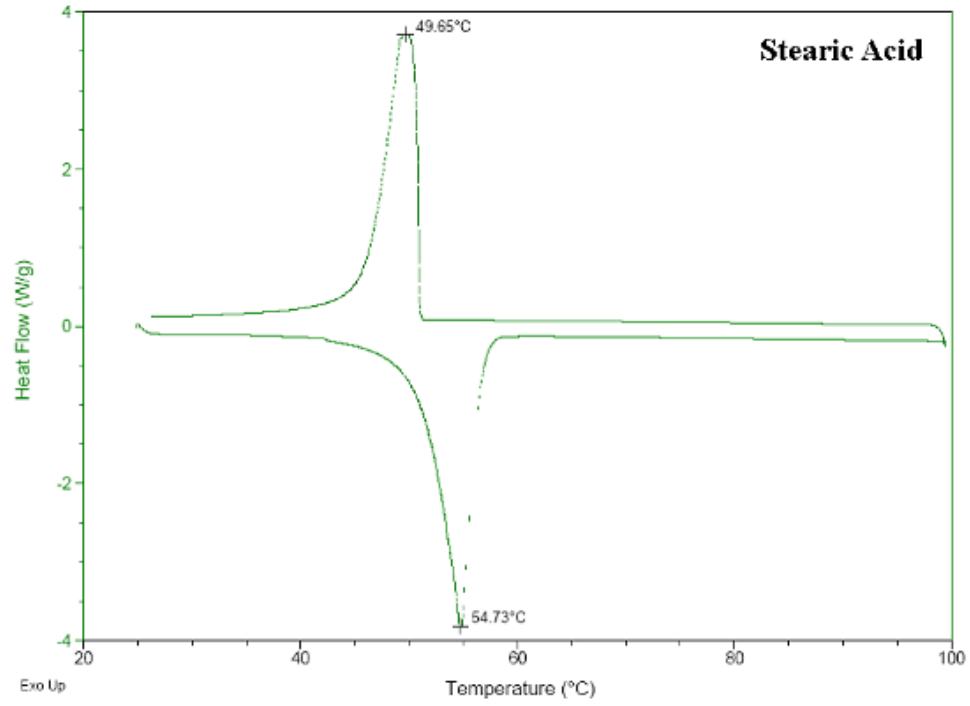

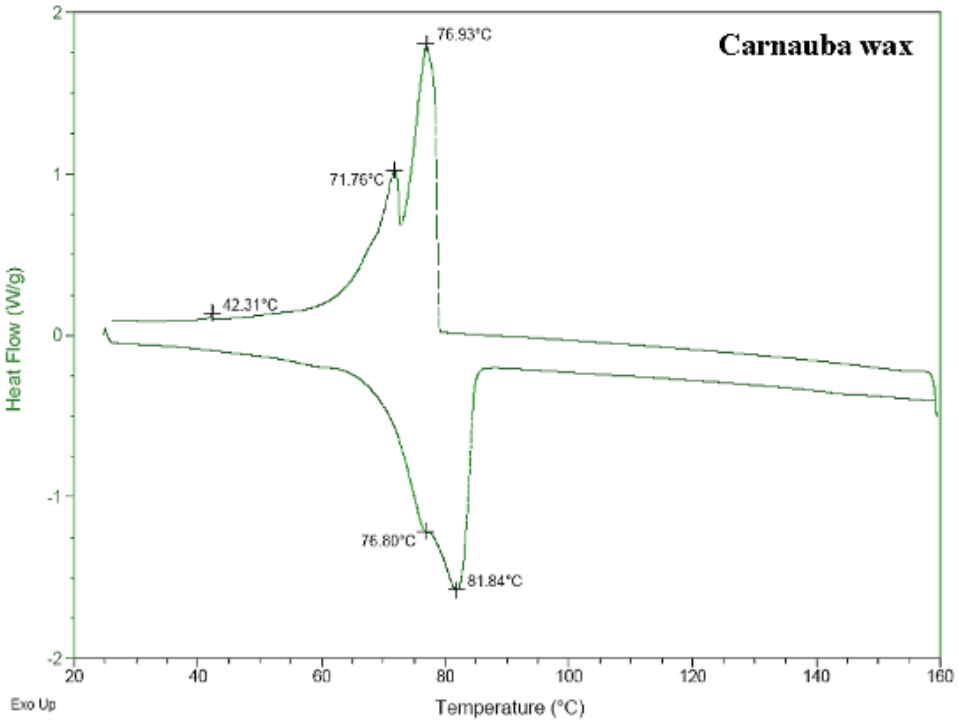

Figure 3.5 DSC results for binder components.

3.2 Fabrication of CP-Ti Tensile Components

In this section, the fabrication process of CP-Ti tensile components via the four basic steps in PIM: 1) feedstock preparation, 2) moulding, 3) debinding and 4) sintering, is discussed.

3.2.1 Mixing: Feedstock Preparation

The CP-Ti feedstocks were prepared using the Ross double planetary mixer. Mixing was performed in a steel mixing chamber, with circulating oil heated at 165 ^{o}C. The CP-Ti powders and binder were mixed for 1.5 hours with a mixing speed of 25 rpm in an Ar purged environment followed by another hour in vacuum environment. Ar purged environment was used at the initial stage of mixing to prevent or minimise O attachment to the Ti powders during the mixing process, while the vacuum at the final stage prevents air entrapment in the feedstock. The rotation of the mixer's blades was alternated to ensure homogeneity of the mixture.

Table 3.6 displays the solid loading and composition of CP-Ti feedstock that have been mixed. In this study the solid loading of 66 % was selected for CP-Ti feedstock. The selection of solid loading was based on previous work experiences in metal feedstock preparation. Due to the confidentiality issues, the percentages of the binder components used will not be revealed in this report.

Table 3.6 Composition, solid loading and density of CP-Ti feedstock.

Binder	PP, PW, SA, CW
Solid Loading (%)	66.0
Average measured density (g/cm^3)	3.27

3.2.2 Injection Moulding

In this study, the feedstock was moulded into tensile components. The dimension of the mould cavity is shown in Figure 3.6. The moulding was conducted using Arburg (Germany) 220S 15 ton single barrel powder injection moulding machine (see Figure 3.7). The dimensions of the green components are shown in Figure 3.8. The progressive filling of the CP-Ti feedstock in the mould cavity is presented in Figure 3.9.

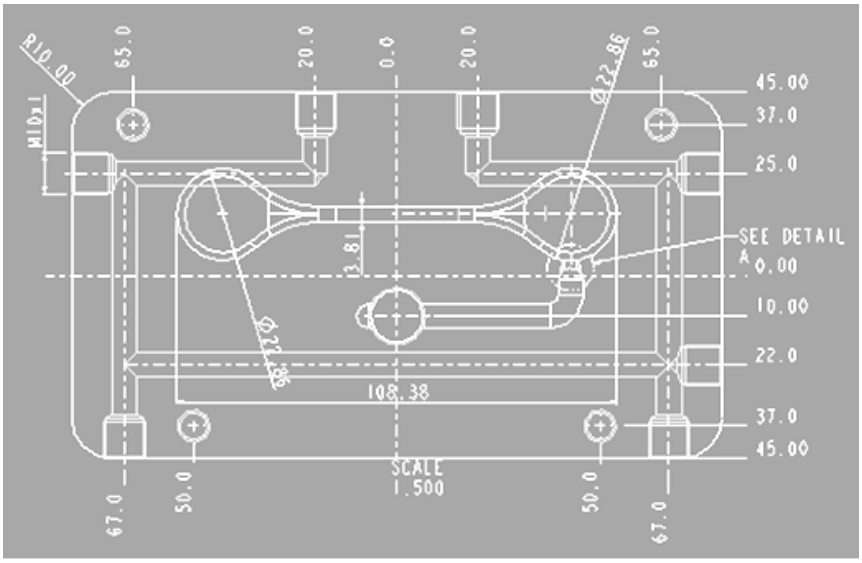

Figure 3.6 Dimension of mould. Units are in mm.

Figure 3.7 Arburg 220S 15 ton PIM machine.

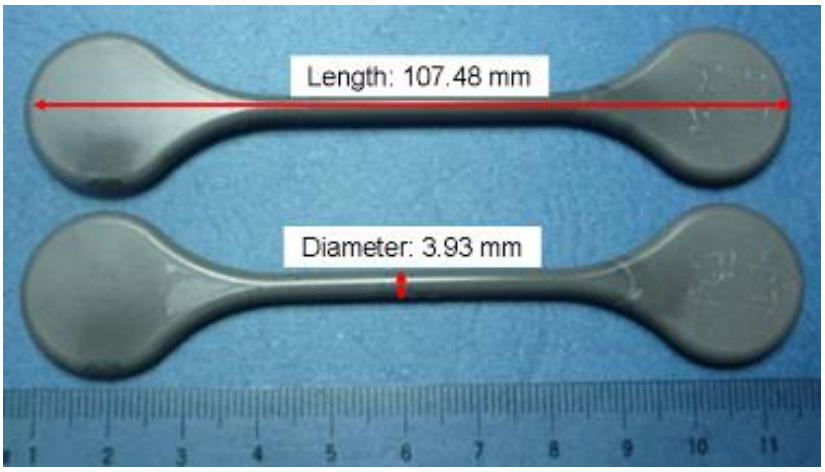

Figure 3.8 CP-Ti tensile components in green stage.

Figure 3.9 Progressive filling of cavity during injection moulding.

The injection moulding parameters used for the moulding of CP-Ti tensile component is shown in Table 3.7. From the table, it can be seen that an incremental moulding temperature profile was used. Incremental temperature profile prevents the degradation of the binder in the injection barrel. In addition, the shearing action from the injection screw also increases the temperature of the feedstock during the moulding process. Therefore, the temperatures at regions away from the nozzle in the injection barrel are usually kept below the binder melting point. A higher temperature was set at the nozzle as this is to ensure that the feedstock is maintained at a molten phase and also fluid enough to flow and fill the mould cavity completely during the injection moulding process. In this research, the nozzle temperature was set at 141 ^{o}C, which was based on the DSC studies

conducted on the binder. From Table 3.5, PP, which is the major component in the binder, has a melting point of 144 ^{o}C. Therefore, the nozzle temperature was maintained at a temperature close to the melting point of PP. Initial trials with lower and higher temperature were not successfully as lower temperature reduced the flowability of the feedstock, while a higher temperature resulted in "drooling". Drooling is undesirable as it results in material loss. Hence, the amount of material injected into the mould cavity is lower than the set dosage. This may cause moulding defects such as short shot and sink marks in the green component. Drooling also results in material to be deposited on the nozzle head, which damages the nozzle head in the long run.

The mould temperature was set at 45 ^{o}C, where most binder would have recrystallised. Initial mould temperature was set around 50 to 60 ^{o}C, however, breakage of the green components occurred during ejection. Therefore, the mould temperature was reduced to enhance the cooling rate so that the green components gained sufficient green strength before being ejected from the mould cavity. The breakage of the green components was also thought to be due to insufficient powder packing, hence, resulting in weaker green strength. However, the problem persisted even with the increase in packing and holding pressure. This issue was eventually resolved by increasing the cooling time. Additional cooling was provided by using the air gun to cool the green component before ejection. After each change was made to the moulding parameters, the cross-sections of the green components were inspected under the magnifying glass for defects such as cracks or porosities. Moulding of the remaining green components only proceed when no cracks or porosities can be visually identified in the cross-sectioned of the green component after several injection moulding cycles.

Slight flashing was also observed on the parting line region of the green component due to higher injection pressure used. A higher injection pressure is desired as it provides sufficient powder packing and also improves the green density, but care should be taken as an overly high injection pressure will result in cracks and breakage of the green components.

Table 3.7 Moulding Parameters for CP-Ti.

Melt temperature (ºC)	141/139/135/131
Mold temperature (ºC)	48
Injection pressure (bar)	250/300/300
Injection speed (ccm/s)	12/15/15
Holding pressure (bar)	130
Cooling time (s)	60

3.2.3 Debinding and Sintering

The green components were subjected to a two stage debinding processes: 1) solvent debinding and 2) thermal debinding.

In solvent debinding, the green components were soaked in isopropyl alcohol (IPA) for 24 hours in a Memmert waterbath with temperature controlled at 70 ^{o}C. This step removes the PW component, leaving behind a series of open and interconnected pores for the removal of the remaining binder components in the thermal debinding stage. Based on amount of PW component used in the binder, a weight loss of more than 4 wt. % is required to ensure that sufficient porosity or internal channels have been created to facilitate the release vapours from the remaining binder components during thermal debinding. In this study, a weight loss of 4.2 wt. % was achieved using the above solvent debinding parameters. Therefore, the solvent debinding parameters selected were suitable as it has sufficiently removed the desired quantity of binders from the green components. The solvent debound components are shown in Figure 3.10.

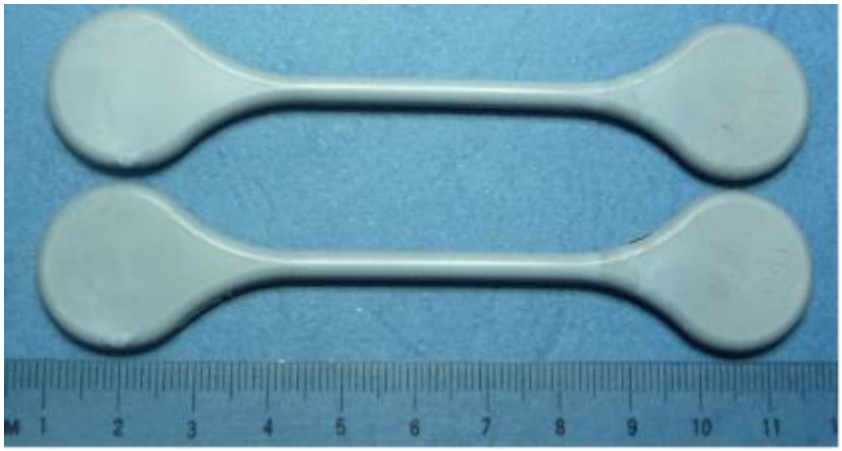

Figure 3.10 CP-Ti tensile components after solvent debinding.

The components were then thermal debound in Ar (99.995 % purity) at 600 ^{o}C with a dwell time of 1 hour. Thermal debinding was conducted in the CM Furnaces Inc. (serial no. 970264) horizontal tube furnace. The profile for thermal debinding is shown in Figure 3.11. As shown in Figure 3.11, a multiple set debinding profile was selected for the thermal debinding process. This profile was design based on the decomposition temperatures of the binders, as examined from the TGA studies in Section 3.1.3. In this profile, lower ramp rates and longer dwell time were used at temperature below 500 ^{o}C. This is to ensure that the binder components are sufficiently removed from the components, as the binder residues contribute interstitial elements such as O, N and C, which degrade the physical and mechanical properties of Ti. In addition, Ti has lower affinity with these interstitial elements at temperatures below 500 ^{o}C, therefore, reducing the risk of interstitial contamination.

With the complete removal of the binders, the brown components will have little or no strength for handling. Therefore, debinding temperature was increased to 600 ^{o}C for the pre-sintering of the components to ensure sufficient strength for handling. A higher ramp rate (3 ^{o}C / minute) and shorter dwell time (1 hour) were used for this section of the debinding process. This is because Ti tends to react and absorbs impurities at temperature above 500 ^{o}C, therefore, higher ramp rate and shorter dwell time minimises the exposure time to impurities at high temperature. This was discussed in Section 2.3.3, where research work was conducted by Guo et al. [8],

found that increasing the debinding temperature led to higher C content in Ti. A constant flow of high purity Ar gas was kept throughout the thermal debinding process for the removal of the vaporised binders and also to keep the environment in an inert condition under high temperature. This minimises interstitial contamination between Ti and O, C and N.

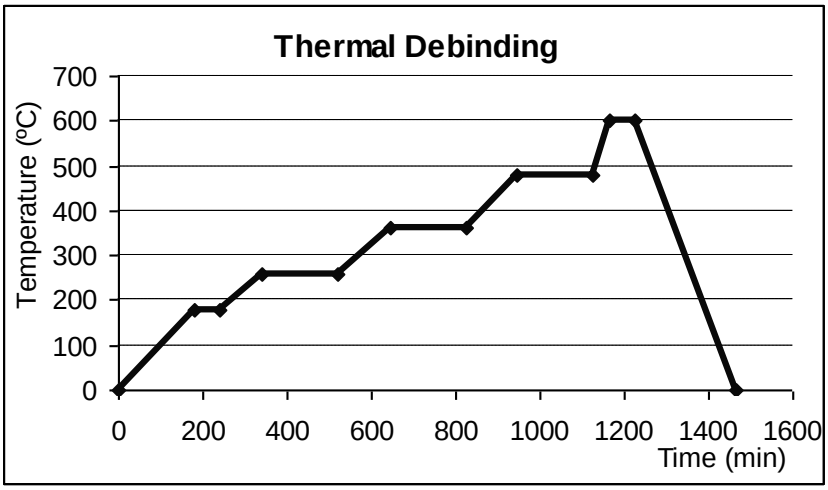

Temp (^{o}C)	180	260	360	480	600	30
Ramp (^{o}C/min)	1	0.8	0.8	1	3	Furnace cool (Ar)
Dwell (min)	60	180	180	180	60	-

Figure 3.11 Thermal debinding CP-Ti and Ti-6Al-4V tensile green components.

The thermal debound components are shown in Figure 3.12. As shown Figure 3.12, the components were able retain their shape and no visible cracks or other defects were observed after thermal debinding. However, slight discolouration was observed at in the ends of the clamping area, towards the gas discharge direction. No discolouration was observed on the clamping area towards the gas entry direction and at the gauge area of the tensile bar. This phenomenon was suspected to be due to Ti absorbing the impurities, either from the gas or vaporised binder, during thermal debinding. The solution is to debind the Ti brown components together with porous Ti brown components. The porous Ti brown component

"sacrifices" itself by acting as a sponge to absorb the impurities generated during thermal debinding. This part of the work will be conducted in the future experimental work.

Figure 3.12 Tensile components after solvent and thermal debinding.

The debound CP-Ti components were later sintered using the CM Furnaces Inc. horizontal tube furnace. The components were sintered at 1240 ^{o}C, 1260 ^{o}C and 1280 ^{o}C in Ar (99.995 % purity) environment with a dwell time of three hours. Ar gas was used to create a protective environment so as to minimise the risk of interstitial contamination in Ti under high temperature condition. The sintering profile for CP-Ti is shown in Figure 3.13. The sintering temperatures were selected based on literature studies. Ideally the sintering of Ti should be done in vacuum environment. However, due to the unavailability of a suitable vacuum sintering furnace at the point of time when the experiment was conducted, vacuum sintering could not be performed on CP-Ti components.

Multiple-step sintering profiles were also employed in the sintering of CP-Ti tensile components. From the sintering profile, a 30 minutes holding step was added at 600 ^{o}C to remove the remaining binder residue (if any) in the component. Another 30 minutes dwell stage was added at 1050 ^{o}C in the profile. The purpose for this is to ensure the complete phase transformation of Ti-6Al-4V to β phase and also to burn off any other volatile contaminants remaining in the component.

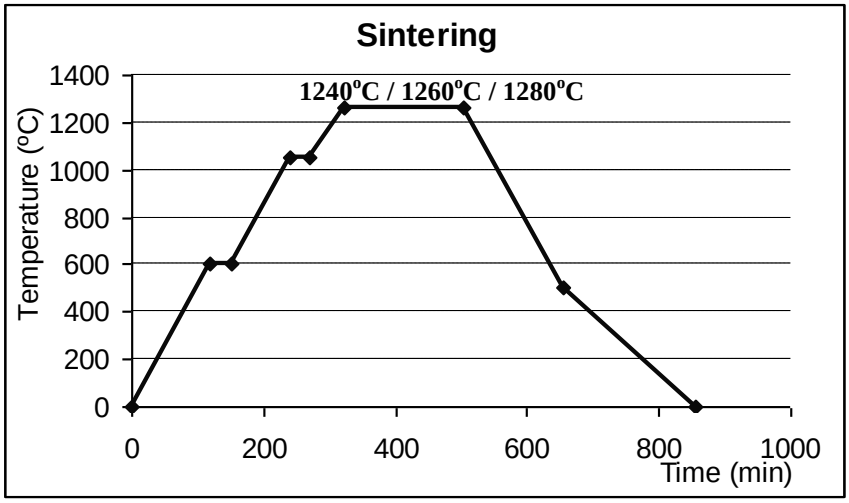

Temp (°C)	600	1050	1240/1260 /1280	500	30
Ramp (°C/min)	5	5	4	3	Furnace cool (Ar)
Dwell (min)	30	30	180	-	-

Figure 3.13 Sintering profile for CP-Ti tensile components.

3.3 Material Shrinkage on CP-Ti

Dilatometer studies were conducted on the CP-Ti components in accordance to the three sintering conditions. Dilatometer studies provide the shrinkage behavior of the material under each sintering condition, which is crucial for the tooling design. In addition, dilatometer studies also indicate the stage where shrinkage of the components occurs most rapidly during sintering. Hence, modification can be made to the sintering profile to prevent slumping, warping or cracks in the component during sintering. In this experiment, the dilatometer studies were conducted on a Setaram Instrumentation dilatometer. The profile used for the study is similar to the sintering profile shown in Figure 3.13. Due to the requirements of the equipment, the binder in the moulded CP-Ti components needs to be removed prior to conducting the test. Therefore, the CP-Ti components were thermal debound up to a temperature of 600 °C for 1 hour in Ar atmosphere. Results of the dilatometer studies for CP-Ti are displayed in Figure 3.14.

Based on the graphical plots in Figure 3.14, the final shrinkage for CP-Ti sintered at 1240 ^{o}C, 1260 ^{o}C and 1280 ^{o}C are 10.85 %, 11.0 2% and 13.23 %, respectively. The plots also showed that the material starts to shrink rapidly after 800 ^{o}C. Therefore, the ramp rates for temperature beyond 800 ^{o}C should be reduced to prevent cracks or to eliminate pores entrapment in grains.

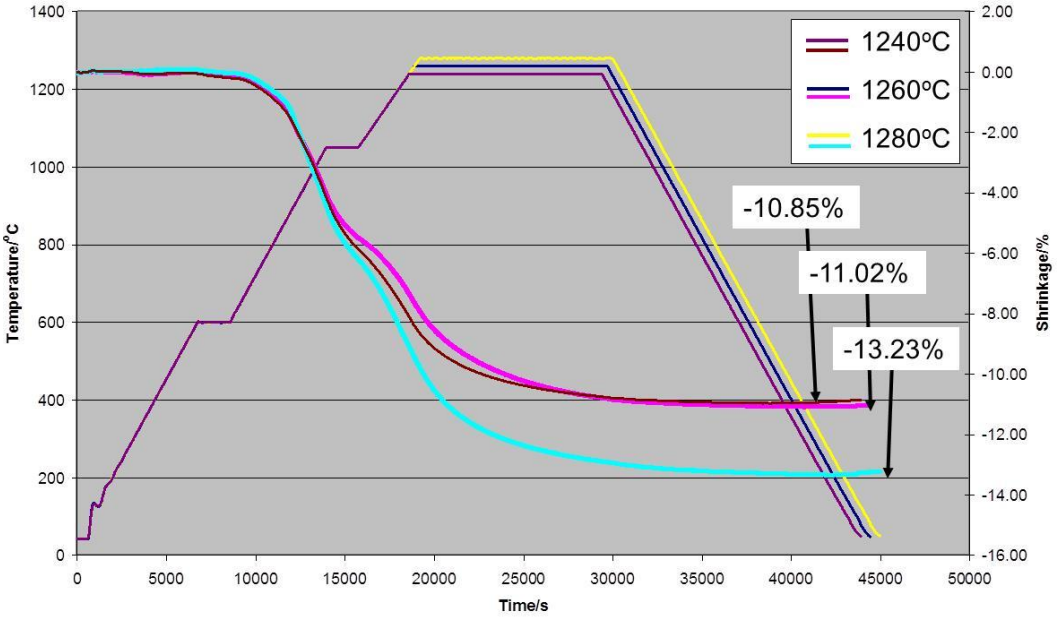

Figure 3.14 Dilatometer studies on CP-Ti at different temperatures in Ar.

3.4 Fabrication of Ti-6Al-4V Tensile Components

The second phase of the research work involved the study of fabricating high strength Ti-6Al-4V components. As mentioned earlier, due to the unavailability of Ti-6Al-4V powders, CP-Ti was used to set up the experimental and fabrication process for Ti-6Al-4V. This section discussed on the fabrication process for Ti-6Al-4V tensile components.

3.4.1 Mixing: Feedstock Preparation

The mixing equipment and parameters used for Ti-6Al-4V feedstock is similar to that of CP-Ti. The only differences were the solid loading and the binder system used. The mixer was also "cleaned" with recycled Ti feedstock, prior to mixing to remove any remaining solid residues. This is to address the contamination issue which was observed in CP-Ti sintered component. Detail of this problem is discussed in Section 4.1.2.

Table 3.8 shows the solid loading for Ti-6Al-4V feedstock. A solid loading of 66 % was initially selected for Ti-6Al-4V. However, after running some trials on the mixing and the injection moulding process, it was found that a higher solid loading can be achieved. The solid loading of Ti-6Al-4V was eventually set at 68 %. Higher solid loading is usually preferred as it gives better sintered density and mechanical properties. It also reduces the amount of binder needed hence, reducing the possibility of C and O contamination from the binder. The binder composition used for Ti-6Al-4V also differed from CP-Ti. In Ti-6Al-4V feedstock, CW component was omitted from the binder composition to reduce the risk of O and C contamination from the binder under high temperature. The presence of O and C risked potential contamination and disintegration to the mechanical properties of Ti. Based on the TGA studies in Section 3.1.3, a debinding temperature of more than 900 ^{o}C is required to completely remove CW. This is not ideal as the reactivity of Ti with O, C and N increases at temperature above 600 ^{o}C.

Table 3.8 Composition, solid loading and density of Ti-6Al-4V feedstock.

Binder	PP, PW, SA
Solid Loading (%)	68.0
Average measured density (g/cm^3)	3.20

3.4.2 Injection Moulding

The Ti-6Al-4V feedstock was also moulded into tensile component using the same mould cavity shown in Figure 3.6. The injection moulding parameters of Ti-6Al-4V tensile components are presented in Table 3.9. Comparing the moulding parameters used for both CP-Ti and Ti-6Al-4V, similar melt and mold temperatures were used for the injection moulding of both materials. However, a higher injection pressure and holding pressure were used for Ti-6Al-4V as it has a higher solid loading. High injection pressure ensures that the hot molten feedstock is able to fill the entire cavity before it begins to solidify, while high holding pressure ensures good packing of the powder particles. This will translate to higher green density and eventually higher sintered density.

Table 3.9 Moulding parameters for Ti-6Al-4V.

Melt temperature (ºC)	141/139/136/132
Mold temperature (ºC)	48
Injection pressure (bar)	200/600/600
Injection speed (ccm/s)	10/13/13
Holding pressure (bar)	350
Cooling time (s)	70

3.4.3 Debinding and Sintering

The solvent and thermal debinding processes used in CP-Ti were applied to the debinding of Ti-6Al-4V components. Sintering of the debound Ti-6Al-4V components were conducted in a high vacuum environment using the Thermal Technology LLC sintering furnace. Sintering of Ti in vacuum environment is preferred over Ar environment as it eliminates Ti exposure to moisture and interstitial elements, which may be present in small amount in high purity inert gases. Sintering of the Ti-6Al-4V components was conducted in vacuum atmosphere as the sintering furnace with the vacuum capabilities was only commissioned in the later stage of the project. The sintering profile for Ti-6Al-4V components are shown in Figure 3.15. Multiple step sintering profile was also used for the sintering of the Ti-6Al-4V components.

The sintering profile for Ti-6Al-4V components was modified for design of experiment (DOE). DOE was applied in the sintering of the Ti-6Al-4V components to investigate the effects of the sintering parameters on the UTS and elongation of Ti-6Al-4V. The parameters involved for this DOE study are: 1) sintering temperature, 2) dwell time, 3) ramp rate and 4) cooling rate. As indicated in Figure 3.15, different values were selected for each of these parameters. These parameters were selected based on past experimental results and literature studies. Based on some of the literature studies, sintering of Ti and Ti alloy was usually performed at temperatures between 1100 to 1450 ^{o}C. Sintering temperatures of 1200 ^{o}C and 1300 ^{o}C and dwell time of 1 hour and 3 hours were selected to ensure the complete sintering of the Ti-6Al-4V components. The ramp and cooling rates of 1 ^{o}C per minute and 10 ^{o}C per minute were selected based on the furnace capability. The outcome of the DOE study is discussed in Chapter four.

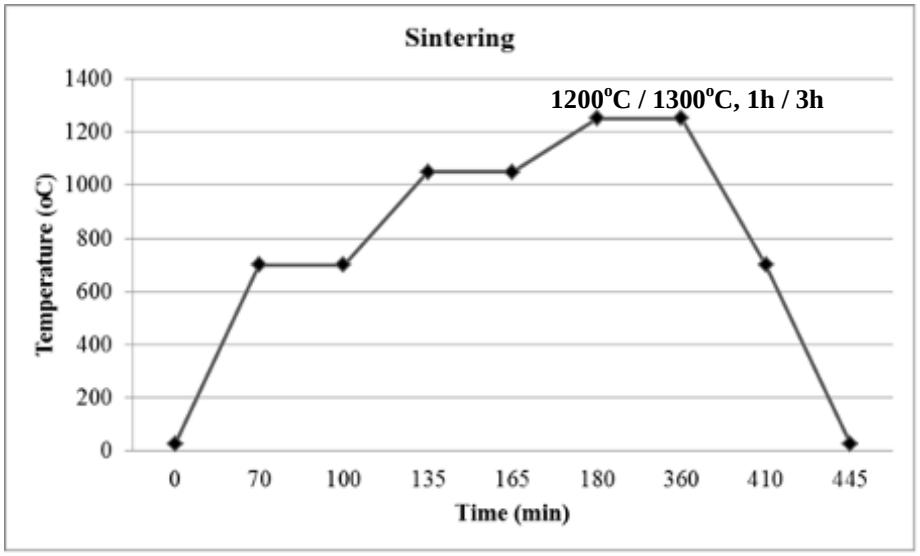

Temp (^{o}C)	700	1050	1200/1300	700	25
Ramp (^{o}C/min)	10	10	1/10	1/10	Furnace cool
Dwell (min)	30	30	60/180	-	-

Figure 3.15 Sintering profile for Ti-6Al-4V tensile components.

3.5 Characterisation of Sintered CP-Ti Components

The sintered components were subjected to various characterisation studies to examine their properties.

Firstly, their densities and porosities were measured by Archimedes' method. This is to assess their sintered density in relation to the sintering temperatures. Archimedes' principle states that when an object is immersed into a fluid, it is buoyed up by an equal force which is equal to the weight of the fluid displaced by the object. Based on this principle, the density and porosity of the test piece can be determined by measuring the sample's dry mass, its apparent mass when immersed and impregnated with a fluid under vacuum and mass in air soaked with liquid. Using the formulae shown below, the sample apparent solid density, ρ_s, and apparent porosity, π_a, can be calculated. The apparent solid density is defined as the ratio of the dry mass of the material to its apparent solid volume, while the apparent porosity is the ratio of the total volume of open pores in the material in relation to its bulk volume [43].

$$\rho_s = [m_1 / (m_1 - m_2)] \times \rho_L \quad (1)$$

$$\pi_a = [(m_3 - m_1) / (m_3 - m_2)] \times 100 \quad (2)$$

where,

m_1 is the dry mass of the sample.

m_2 is the apparent mass of the sample when immersed in fluid.

m_3 is the mass of the sample in air soaked with liquid.

ρ_L is the density of the fluid used.

Secondly, their microstructures were analysed via optical microscopy and SEM. The cross-sections of the sintered components were hot mounted in conductive resin followed by surface preparation work using the different grades of SiC sand papers and also alumina paste until a mirror finished surface is achieved. The surfaces of the components were then etched to reveal the desired microstructures. Microstructure study helps to identify abnormalities in the structure and also to

look at the porosity distribution. In addition, X-ray diffraction (XRD) analysis was also conducted to determine the phases present in the sintered components and how they have changed compared to the raw materials.

Lastly, the tensile properties of the sintered components were measured and compared to evaluate the effects of the processing parameters (i.e. sintering atmosphere and temperature) have on the mechanical properties.

3.6 Design of Experiment for Ti-6Al-4V Tensile Components

Sintering is a complex process as there are many sintering parameters (i.e. sintering environment, sintering temperature, time etc.) which can affect the final properties of component.

Therefore, in the second phase of the research work, DOE was conducted to evaluate the effects of four common sintering parameters on the tensile properties of PIM Ti-6Al-4V components. The four sintering parameters studied were: 1) sintering temperature, 2) dwell time, 3) ramp rate and 4) cooling rate. The sintering environment is vacuum. One factor at a time experiments can be applied to this study but it is tedious and not resource efficient. On the other hand, factorial design reduces the number of experimental runs required and it takes into account interactions between factors [44].

A two-level fractional factorial design was chosen for this study. Full factorial design can be applied to examine all the possible combinations of all the factors involved. However, fractional factorial design reduces the lead time for screening of relevant factors. For instance, in a 2^n design, where n is the number of factors, a total of 16 (2^4) run combinations have to be performed for a four factors experiment. Whereas in fractional design, the number of runs can be reduced to eight (2^{4-1}). Fractional factorial experiments are done under the assumption that

high-order interactions are negligible and observations are normally and independently distributed with the same variance for each factor level [45].

The responses for this DOE are the average UTS and elongation. The average of three UTS and elongation readings are reported here. The tensile properties of the sintered Ti-6Al-4V components were measured using Intron 4450 machine. Details of the DOE were discussed in Chapter Four.

3.7 Characterisation of Sintered Ti-6Al-4V Components

The tensile properties of the sintered Ti-6Al-4V components were measured using the Intron 4450 machine and evaluated against the sintering combinations used in DOE. The densities of the sintered Ti-6Al-4V components were measured using Archimedes' method, while their porosities were determined via image analysis with analySIS Pro software. Lastly, the microstructures of the components were analysed and co-related to the sintering combinations and tensile properties obtained from the DOE study. The results on the characterisation of the sintered components are discussed in Chapter Four.

CHAPTER 4 RESULTS AND DISCUSSIONS

In this chapter, the mechanical and physical properties and microstructures of the sintered CP-Ti and Ti-6Al-4V tensile components were examined and reported. In addition, the outcome of the DOE study on Ti-6Al-4V was also discussed in this chapter. As this research work consists of two phases of study: fabrication of CP-Ti and Ti-6Al-4V tensile components, the discussion was split into two sections to report on the different phases of work conducted. Evaluation and characterisation studies on the sintered CP-Ti and Ti-6Al-4V tensile components were discussed in Section 4.1 and 4.2, respectively.

4.1 Phase One – Characterisation of Sintered CP-Ti Components

4.1.1 Density and Porosity

High relative density and low porosity are preferred as they usually translate to better mechanical properties. The density and porosity of the sintered PIM components are influenced by the feedstock solid loading, material packing during injection moulding, sintering temperature, dwell time and sintering environment. Therefore, careful control of these factors is required to achieve the desired properties.

The PIM CP-Ti components were sintered in Ar environment at 1240 ^{o}C, 1260 ^{o}C and 1280 ^{o}C. The apparent densities and porosities of the sintered tensile components were measured by Archimedes' method and presented in Table 4.1 and Figure 4.1. The definition and calculation of the density and porosity measured by Archimedes' method was discussed in Section 3.5.

Table 4.1 Density and porosity of sintered CP-Ti components.

Sintering Temperature (°C)	Average Apparent Porosity (%)	Average Apparent Solid Density (g/cm^3)	Relative Density (%)
1240	0.53	4.26	95.3
1260	0.42	4.25	95.1
1280	0.58	4.27	95.5

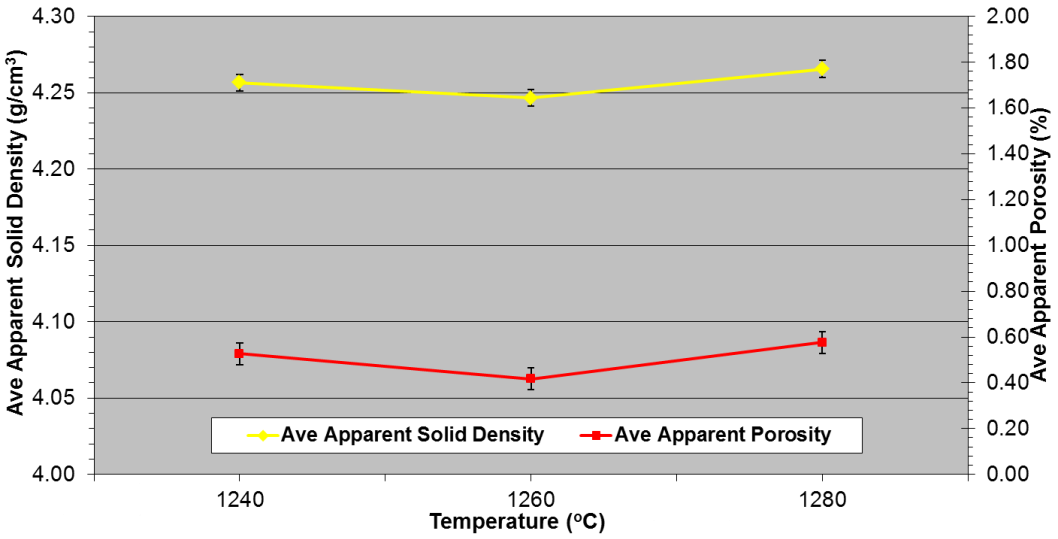

Figure 4.1 Plot of CP-Ti average porosity and density.

A total of three components were measured for each temperature and their averages are reported here. The results indicate that the apparent porosity of CP-Ti decreases when the sintering temperature was raised from 1240 to 1260 °C. This is because higher temperature promotes densification of the powder particles, thus, sealing off most of the open pores in the structure. The apparent porosity increases slightly when the temperature was further increased to 1280 °C. Overall a low percentage of apparent porosity (< 1 %) was observed in all three sintering temperatures. This is an indication that the sintering temperatures selected were sufficient for the densification of the powder particles and sealing off most of the open porosity.

A trend similar to the apparent porosities was observed for the apparent solid densities of the sintered CP-Ti components. Based on the Archimedes' results, it is difficult to deduce which sintering temperature is better as the porosities and densities for CP-Ti components sintered under all three sintering temperatures are relatively similar. Therefore, further evaluation on the components microstructures and minor elements analysis is required to have a more comprehensive and conclusive indication.

The relative densities of the components were also calculated. Relative density is defined as the ratio of the density of the sintered component to the powder density. CP-Ti tensile components sintered under all three sintering temperatures gave a relative density of approximately 95 %. This value is lower than the expected value of 98 %. Hence, further improvements on the material packing and sintering profile is required to increase the relative density of the component. This issue was addressed in the second phase of the research where the solid loading of the Ti-6Al-4V feedstock was increased to 68 % and higher injection moulding and holding pressure were used to improve the powder packing of the green components.

4.1.2 Microstructure Analysis

The microstructures of cross-sections of the sintered CP-Ti components, along the gauge area, were examined with the Olympus GX51 optical microscope and EVO 50 XVP SEM. Figure 4.2 shows the optical images of the unetched sintered CP-Ti components. Spherical and irregular pores of different sizes were observed in the cross-sections of the components as shown in Figure 4.2. The cause of these porosities is likely due to Ar entrapment in the component during sintering. This is because the molecule of Ar is relatively large hence, it cannot be easily dissolved or diffused out during the sintering process.

The porosity in the components cross sections was measured from their optical images at a magnification of 100x using the analySIS Pro software. Measurements conducted by this method enable the measurement of the closed porosities in the components. An average of three readings was taken for each component. Results of their porosity are tabulated in Table 4.2. The results reveal that CP-Ti component sintered at 1260 ^{o}C in Ar has the highest percentage of porosity followed by those sintered at 1240 ^{o}C and 1280 ^{o}C.

In comparison with the porosities measured by Archimedes' method, the porosities measured by optical microscopy are relatively higher. This is because Archimedes' method uses water impregnation for porosity measurement. As water can only be impregnated into the open and interconnected pores, it is unable to measure the closed and isolated pores. On the other hand, optical microscopy enables both open and closed pores to be captured in a single image. The porosities on the image was then measured based on the percentage of area which these pores occupied in the single frame. Therefore, both open and closed pores can be taken into account. Hence, higher porosities were reflected in the latter.

Table 4.2 Average porosity of CP-Ti components measured from optical images.

Sintering Conditions	Average Measured Porosity (%)
1240 ^{o}C 3 hours, Argon	3.66
1260 ^{o}C 3 hours, Argon	4.06
1280 ^{o}C 3 hours, Argon	1.15

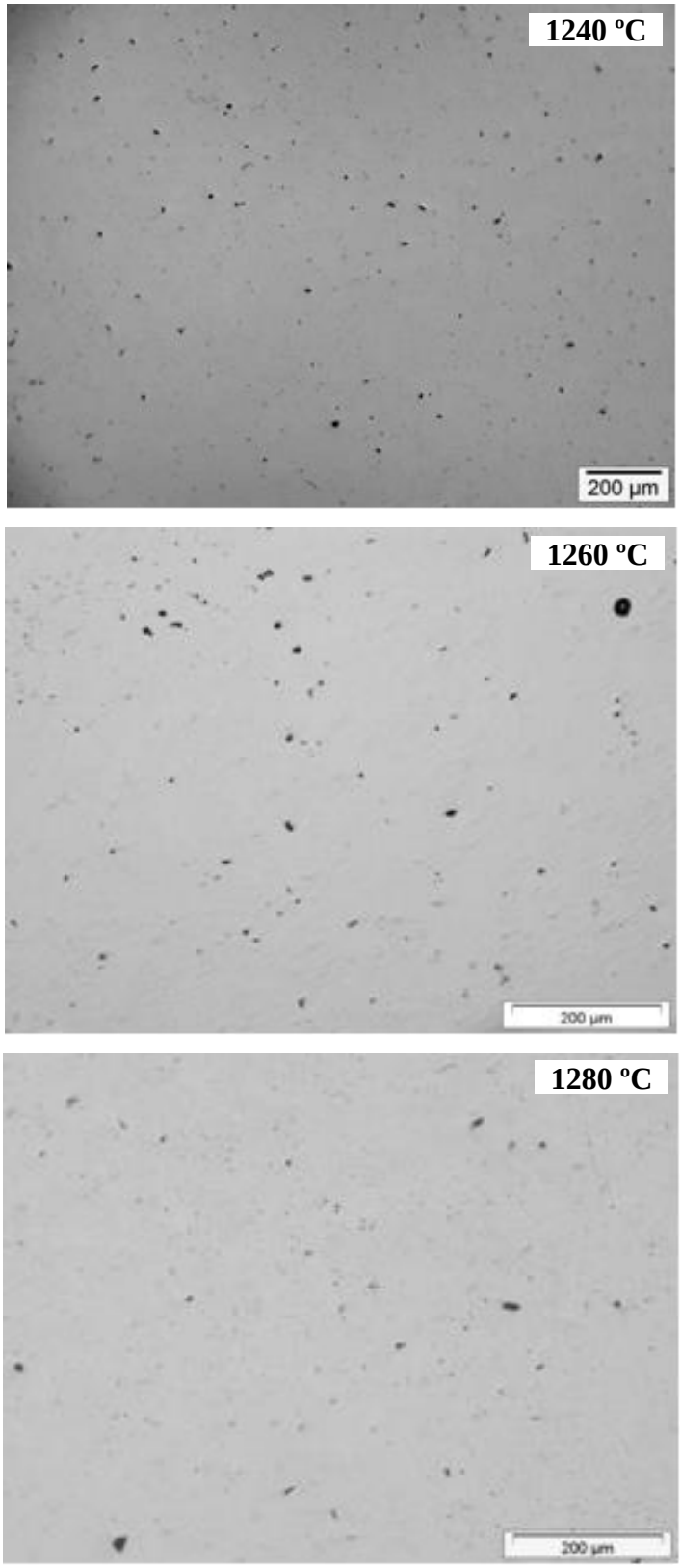

Figure 4.2 Cross-sections of sintered CP-Ti components.

The sintered components were chemically etched to examine the grain structure of the components. The etchant composition is shown in Table 4.3. Chemical etching is a process where chemicals are used to selectively erode the materials on the surface of the polished cross-section to reveal the desired structure or phase in the component cross-section.

Table 4.3 Composition of etchant sintered CP-Ti components.

Distilled Water	100 ml
Hydrogen peroxide (H_2O_2)	5 ml
Hydrogen fluoride acid (HF)	2 ml

Figure 4.3 shows that CP-Ti sintered at 1240 ^{o}C and 1260 ^{o}C have a mixture of elongated and irregularly shaped grains with some measuring about 100 μm. In addition, pores were also observed within the grains. It is undesirable to have pores entrapped within the grains as they reduced densification [10]. Therefore, further improvement on the sintering profile is needed to reduce the number of pores trapped within the grains. The sintering profile and environment were amended in the second phase of the study to address the above issue. DOE was also conducted as part of the process to improve the microstructures and the mechanical properties of Ti alloy components.

Comparing Figure 4.2 and Figure 4.3, an increased in porosity was observed in the cross-sections of the components after etching. There are two possible reasons for such occurrence. Firstly, the etchant may have created more pores in the structure. In the etching process, the etchant tend to attack the weaker region in the structure, which are usually the grain boundaries, scratches, cracks or inclusions. Hence, additional pores may have been resulted due to that. The second reason could be that the pores were already inherent in the structure and were only revealed after etching. Pores noted in the latter explanation are usually a resultant of the sintering process.

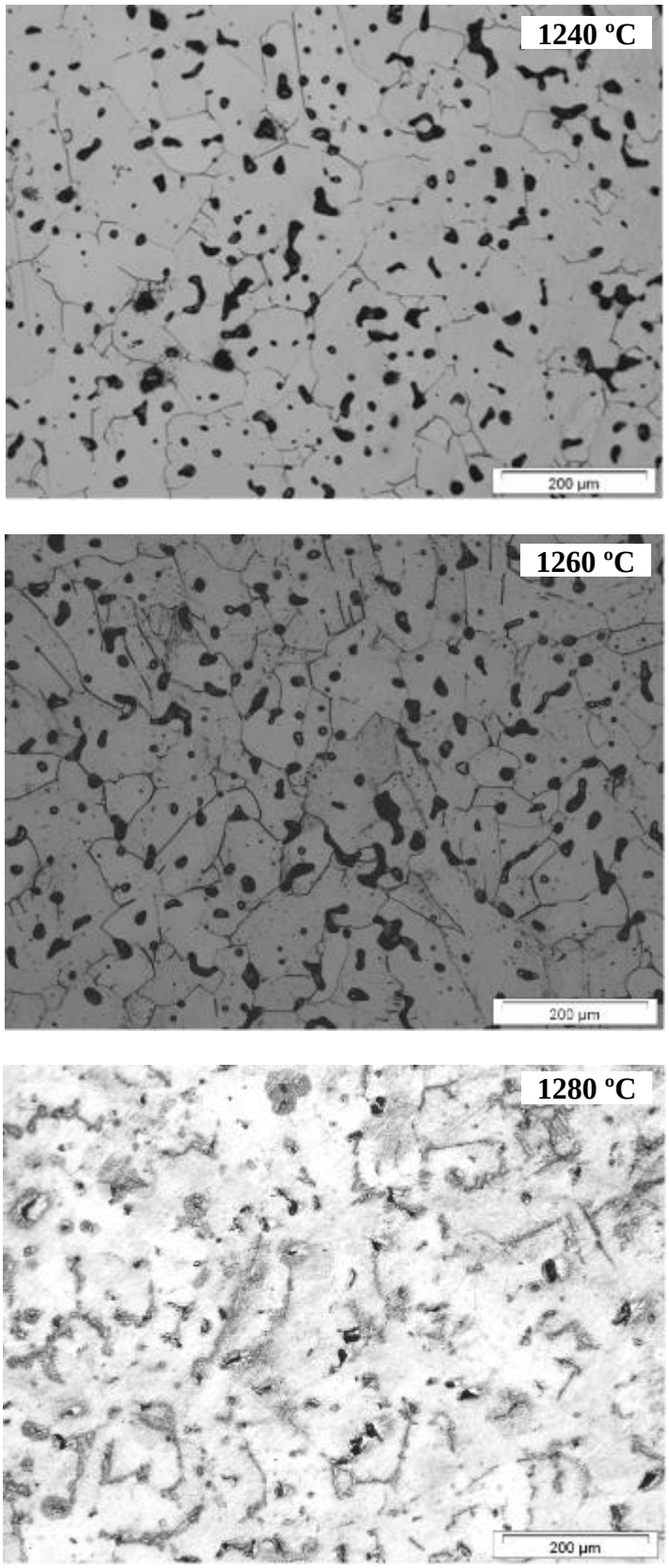

Figure 4.3 Optical images of etched CP-Ti sintered at different temperatures.

The grain structure of CP-Ti sintered at 1280 ^{o}C could not be studied due to incomplete grain exposure. Further etching resulted in burnt marks, indicating over-etching. Even though the same etchant formula and parameters were used, it was ineffective on CP-Ti sintered at 1280 ^{o}C.

Besides optical images, the topographies of the cross-sections were also examined by SEM and are shown in Figure 4.4. Sparingly dispersed needle-liked structures were observed in the SEIs of CP-Ti components sintered under different temperatures. EDS analysis on this structure showed a combination of both Ti and Fe. The amount of Fe detected was higher than the original content in the powder (~0.065%), thus, indicating possible contamination of Fe during the processing stages. The source of contamination was either from the sintering furnaces or from the mixing process, when the Ti powders were in contact with the stainless steel blades and mixing jar.

Both optical images and SEIs of the sintered components showed relatively dense structures of the cross sections. Hence, indicating that the sintering temperatures selected are viable for the sintering of the CP-Ti. However, improvement work is required to reduce or eliminate the Fe-related phases in the structures. The improvement work was implemented in the processing of the Ti-6Al-4V, where the mixer was cleaned down with recycled Ti feedstock prior actual feedstock preparation. The ideal solution is to have a dedicated mixer for Ti feedstock preparation.

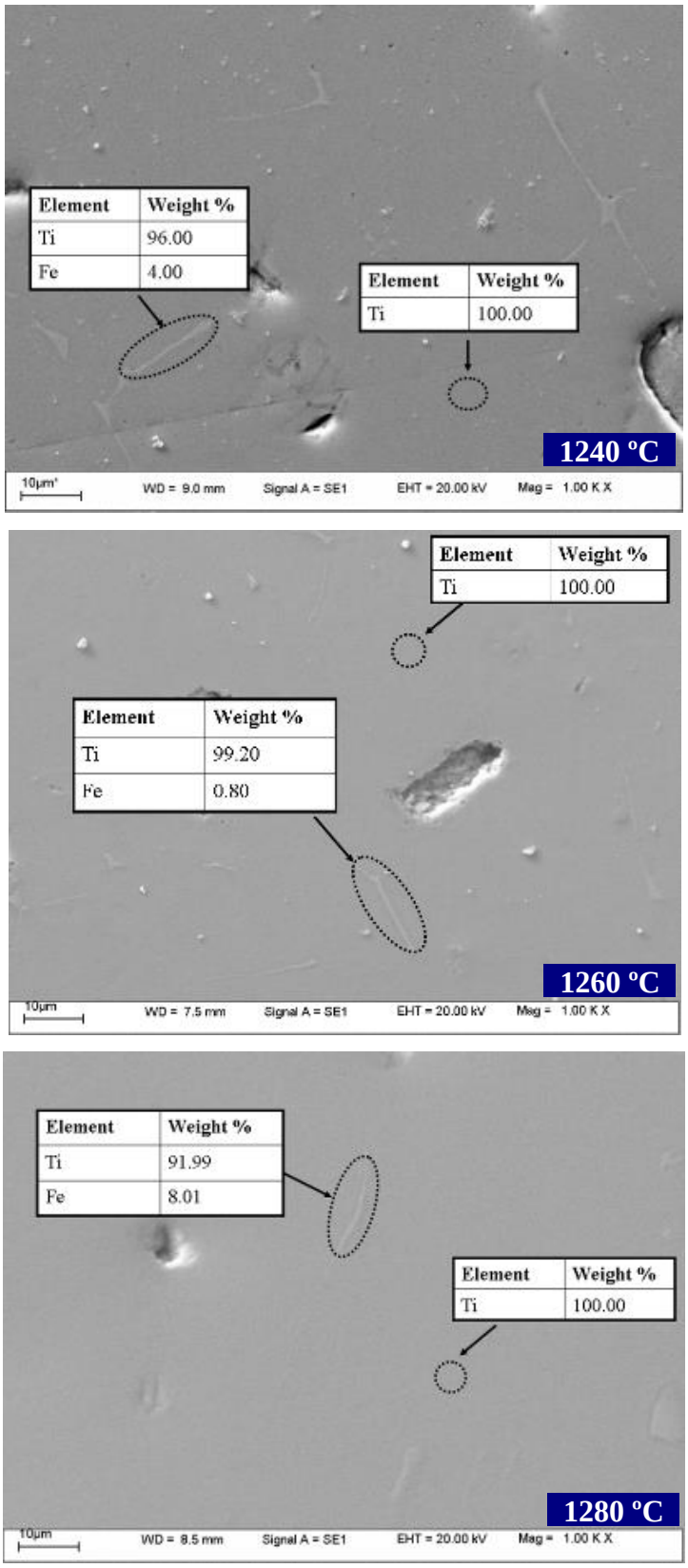

Figure 4.4 SEI of CP-Ti components sintered at different temperatures.

4.1.3 XRD Analysis

In order to examine if any impurities has been introduced during the process, XRD analysis was conducted on CP-Ti powders, green, debound and sintered components. In this experiment, Bruker D8 Discover XRD machine was used to conduct the analysis. The components were scanned from a 2-theta (2θ) range of 20 to 90 degrees. The results are shown in Figure 4.5. For comparison purposes, the scan pattern of CP-Ti powder will be used as a reference.

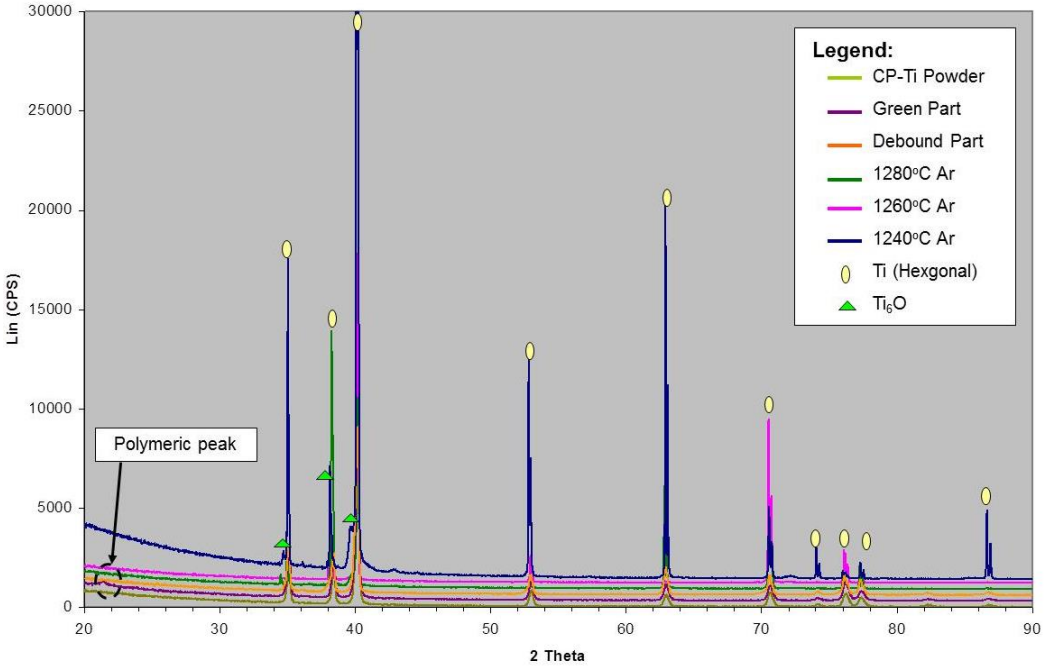

Figure 4.5 XRD spectra of CP-Ti powders, green, debound and sintered components.

As indicated in Figure 4.5, only Ti (hexagonal) signals were detected in the initial CP-Ti powders. This coincides with the EDS data for CP-Ti in Section 3.1.2, which showed only Ti signals. Ti (hexagonal) peaks were also detected for CP-Ti green component except that a small peak was observed at $2\theta = 21.7^{o}$. This peak was probably due to the polymeric binder and wax used in the feedstock as the major polymeric peaks exist mostly at $2\theta < 20^{o}$.

The debound component also gave similar scan patterns as the CP-Ti powders. The peak at $2\theta = 21.7^{o}$, which was initially observed in the scan pattern of the green component, was no longer observed for the debound components. This is because the polymeric binder had been completely removed during the debinding stage, leaving behind Ti powders and possible carbon residues. Thus, this confirmed the earlier deduction that the peak at $2\theta = 21.7^{o}$ is that of the binder.

As for the sintered CP-Ti components, the scan patterns differed slightly from that of CP-Ti the powder. In both the scan patterns of CP-Ti sintered at 1260 ^{o}C and 1280 ^{o}C, minor peaks which were originally observed at $2\theta = 82.5^{o}$ and 87.0^{o} in the powder scan pattern were not detected. A difference in the trend of peak intensities between CP-Ti powder and the sintered components (1240 ^{o}C, 1260 ^{o}C and 1280 ^{o}C) were also observed. This could be because in the CP-Ti powders, the orientations of the grains of the powders are random. However, during sintering, there could be a preferred growth orientation of the grains, hence, resulting in missing peaks and differences in the trend of the peak intensities.

Titanium oxides (Ti_6O) peaks were also detected in CP-Ti components sintered at 1240 ^{o}C and 1280 ^{o}C, indicating O contamination. No oxides peaks were detected in CP-Ti sintered at 1260 ^{o}C. However, this does not omit the possibility that no oxides are present in the component. It could be because the amount in the component is too small to be detected by XRD.

In Section 3.1.2, Fe signals were detected in the sintered CP-Ti components in the EDS analysis. However, the scan patterns of the sintered CP-Ti components did not show any peaks pertaining to Fe related phases. Again, this could probably due to the amount of the Fe related phases in the structure are not large enough to be detected by the XRD. The same reason can be applied to the inability to detect any other oxides or carbides phases in the components. The measurement of O, C or any other minor elements needs to be conducted via chemical methods, which will not be covered in this report due to the unavailability of such facilities in SIMTech.

4.1.4 Tensile Properties

The mechanical properties of PIM Ti components are important especially for engineering applications. In this research, the mechanical properties of CP-Ti components sintered under the three sintering temperatures (1240 ^{o}C, 1260 ^{o}C and 1280 ^{o}C) were tested. In this research work, only tensile properties (UTS and elongation) were examined. Tensile test was performed using an Intron 4450 machine. For each of the three sintering temperatures, a total of five components were used to conduct the tensile tests. The average tensile tests results for CP-Ti are presented in Table 4.4 and Figure 4.6.

Table 4.4 Tensile properties of sintered CP-Ti components.

Sintering Condition	Average UTS (MPa)	Average YS (MPa)	Average % Strain (25mm)
CP-Ti 1240^{o}C Argon	466.37	398.74	8.31
CP-Ti 1260^{o}C Argon	455.47	378.86	10.30
CP-Ti 1280^{o}C Argon	484.57	402.95	9.31

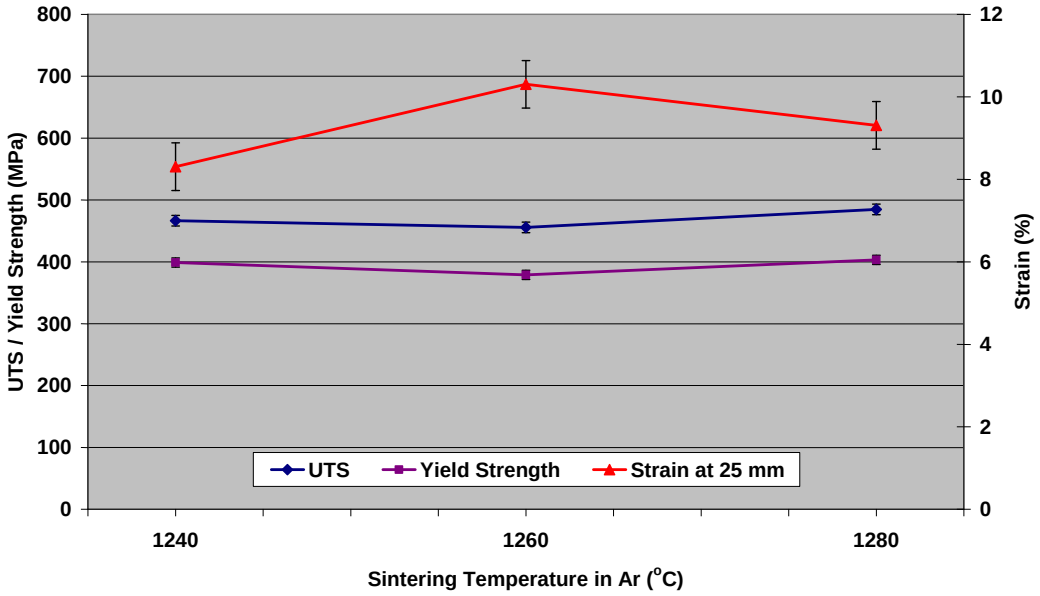

Figure 4.6 Plot of tensile properties of sintered CP-Ti components.

There are currently no standards for PIM of Ti components, therefore, the mechanical properties of these components were benchmarked against wrought Ti (billet/bar, plate, sheet, tube, wire and other forms) and casted Ti. In this research, the tensile properties of CP-Ti are benchmarked against ASTM B265 Grade 3 CP-Ti. The mechanical properties of CP-Ti from Grade 1 to 4 for ASTM B265 are presented in Table 4.5.

Table 4.5 ASTM B265 for unalloyed titanium.

CP-Ti	YS (MPa)	UTS (MPa)	Young's Modulus (GPa) (typical)	Elongation in 50 mm (%)	Chemical Composition (maximum in wt. %)					
					O	N	C	H	Fe	Residual
Grade 1	>170	>240	103	>25	0.18	0.03	0.08	0.015	0.2	0.4
Grade 2	>275	>345	103	>20	0.25	0.03	0.08	0.015	0.3	0.4
Grade 3	>380	>450	103	>18	0.35	0.05	0.08	0.015	0.3	0.4
Grade 4	>485	>550	104	>15	0.40	0.05	0.08	0.015	0.5	0.4

The tensile test results show that CP-Ti sintered at 1280 ^{o}C has the highest ultimate tensile strength (UTS) followed by that sintered at 1240 ^{o}C and 1260 ^{o}C. This is likely due to interstitial strengthening in the lattices of CP-Ti sintered at 1280 ^{o}C and 1240 ^{o}C. The existence of interstitial element is evident in the XRD analysis in Figure 4.5, where oxides peaks were observed in the CP-Ti components sintered at 1280 ^{o}C and 1240 ^{o}C. Whereas, in the XRD analysis of CP-Ti sintered at 1260 ^{o}C, only Ti peaks were detected.

Though CP-Ti sintered at 1260 ^{o}C has the lowest UTS, its elongation was higher than those sintered at 1240 ^{o}C and 1280 ^{o}C. The low elongation for Ti sintered at 1240 ^{o}C and 1280 ^{o}C is again due to the interstitial content. As shown in Figure 4.7, the UTS of Ti increases while its elongation decreases with increasing O interstitial content. Hence, this explains the higher UTS and lower elongation observed for Ti components sintered at 1240 ^{o}C and 1280 ^{o}C.

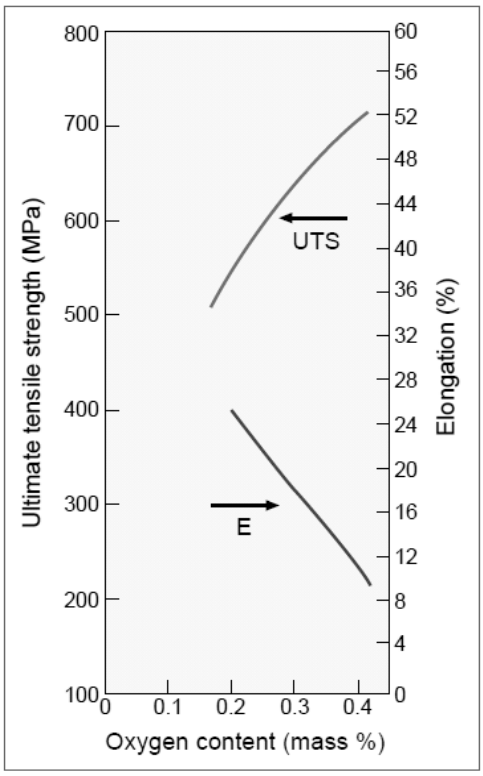

Figure 4.7 Effects of O content on the UTS and elongation on Ti [1].

Variations in the mechanical data were observed in the sintered tensile components. This is likely to be due to the influence of the porosity (pore size, shape and distribution) and also the non-homogeneous shrinkage observed in the sintered tensile components.

Figure 4.8 shows the variation in dimensions between two components from the same sintering batch. During sintering, the debound components were placed on a ceramic sintering plate. After sintering a portion of the ceramic sintering plate was found attached to the contact surface of the CP-Ti component. It was believed that the bonding between the CP-Ti component and the sintering plate was the cause for the non-homogenous shrinkage. This deduction was confirmed from the SEIs of the sintered CP-Ti component shown in Figure 4.9. Traces of ceramic substances were noted on the surface of the CP-Ti component which was in contact with the sintering plate. EDS analysis detected O and Al signals which were believed to be from the sintering plate. The surface which was not in contact with the sintering

plate, as shown in Figure 4.10, did not show any O and Al signals in the EDS spectrum. The reaction between the sintering plate and the CP-Ti component was probably be due to impurities from the sintering plate or the CP-Ti debound components or the material of the sintering substrate is not suitable for the sintering of CP-Ti.

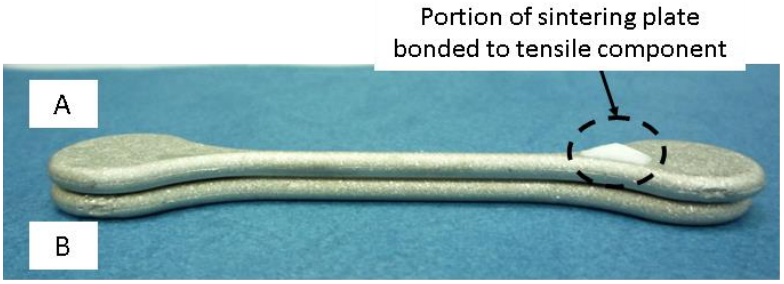

Figure 4.8 Dimensional variations of components from same sintering batch.

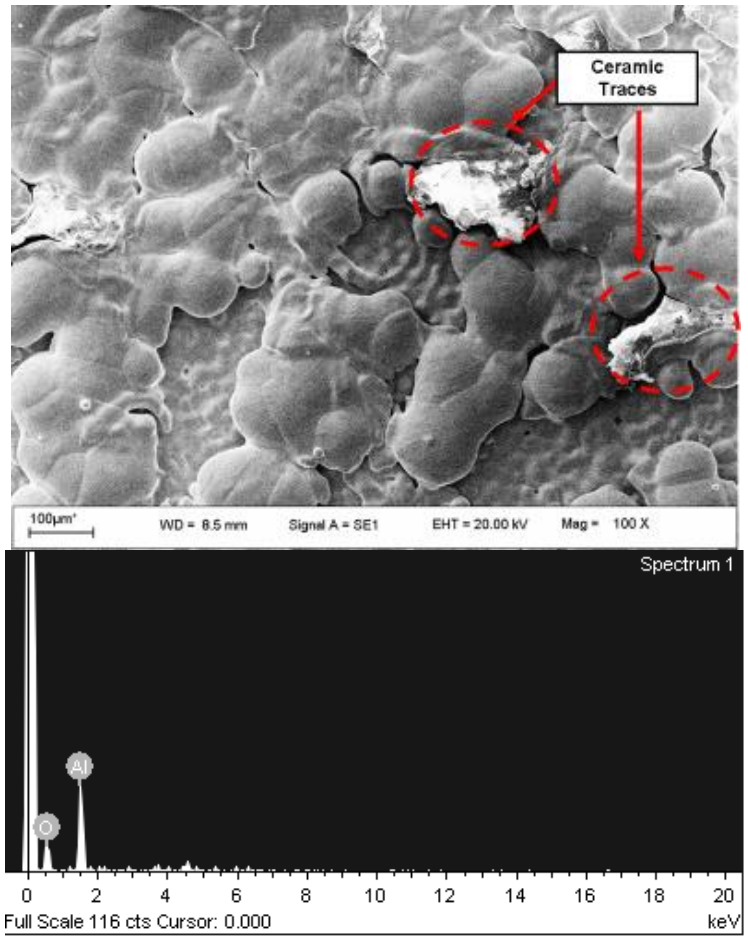

Figure 4.9 SEI and EDS data of contact surface.

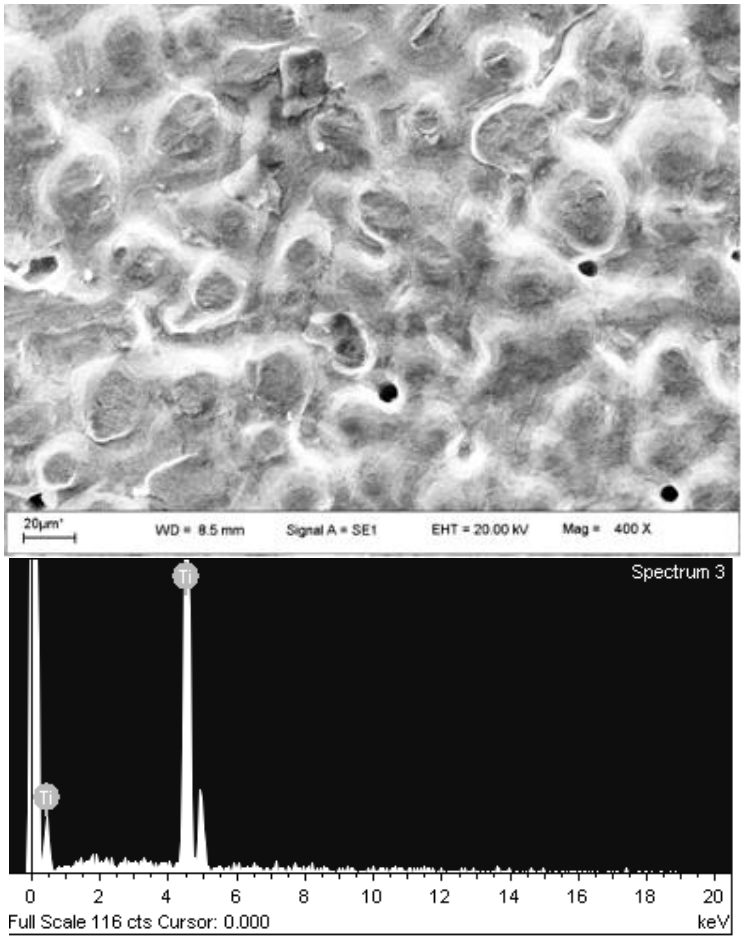

Figure 4.10 SEI and EDS data non-contact surface.

The bonding between the CP-Ti component and the sintering plate during sintering has given rise to constrained sintering. Constrained sintering arises when the shrinkage or densification of the component during sintering is restricted. Constrained sintering results in large variation in the dimensions because of the uncertainty in the position and area of bonding. This is evident in the measurements taken from the two CP-Ti components (shown in Figure 4.8) sintered in the same sintering condition under constrained condition. The measurements are tabulated in Table 4.6. From Table 4.6, a variation of 3.11 % and 2.93 % were observed in the length and diameter, respectively. In general, the dimensional variation of PIM components is to be +/- 0.3 %.

Table 4.6 Dimensions of CP-Ti components from the same sintering batch.

Component	Length (mm)	Diameter (mm)
Sample A	100.24	3.32
Sample B	97.22	3.42
Variation	3.11%	2.93%

Figure 4.11 illustrates the effect of free and constrained sintering on the dimensions (in length and diameter) of the component during sintering. As shown in Figure 4.11, in free sintering, there is no bonding between the component and the sintering plate. Therefore, uniform shrinkage in both the lateral and transverse direction is expected. However, in constrained sintering, the component is partially bonded to the sintering plate, resulting in non-uniform shrinkage. This bonding created an opposing stress, as indicated by the red arrows in the diagram, which restricted shrinkage in the lateral direction. Constrained sintering is not desirable as it leads to high porosity in the sintered component and higher shrinkage in the transverse direction. Therefore, this translates to lower sintered density and poorer mechanical properties.

The final length and thickness of the sintered components from free and constrained sintering are labeled as L1, D1 and L2, D2, respectively. From the figure, the final length of the component from free sintering is smaller than that from constrained sintering. On the other hand, a larger diameter is obtained with free sintering than constrained sintering.

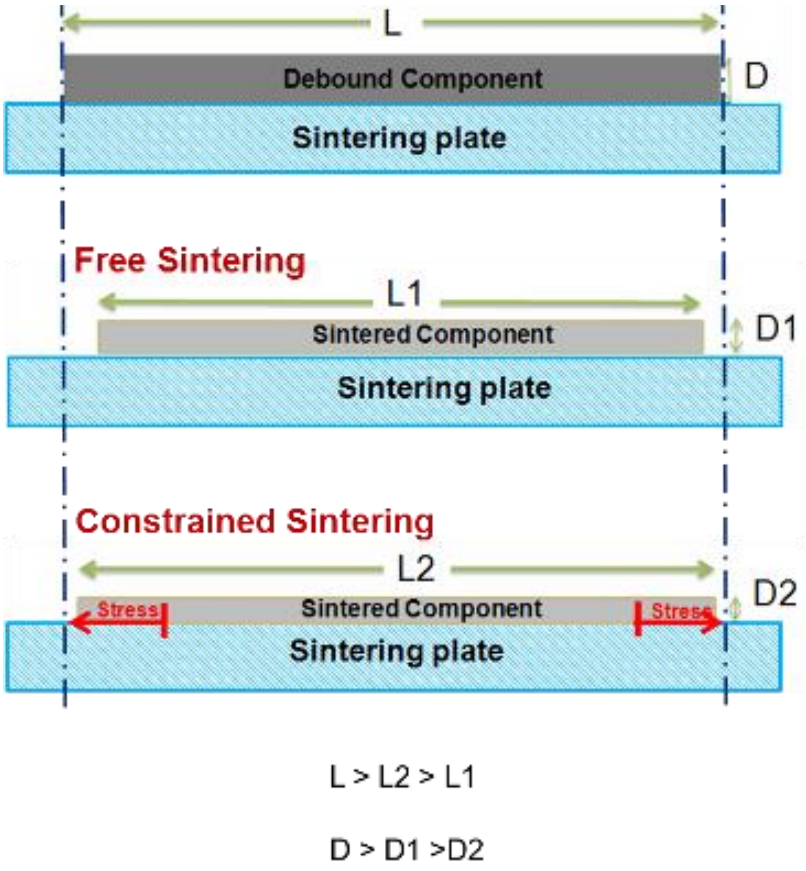

Figure 4.11 Schematics of free and constrained sintering.

Overall, the average UTS for all CP-Ti components sintered under all three sintering temperatures have met the criteria for CP-Ti ASTM grade 3 (see Table 4.5). The yield strength for CP-Ti components sintered at 1240 ^{o}C and 1280 ^{o}C have met the criteria for ASTM grade 3 (>380 MPa). Only CP-Ti components sintered at 1260 ^{o}C, which has yield strength of 378.86 MPa, failed to meet the standard. However, the elongation for all sintered CP-Ti still lacked behind that of ASTM grade 3 (>18 %). It is believed that the elongation, UTS and yield strength can be further improved with the rectification of the bonding between the Ti component and the sintering plate. This bonding problem was subsequently resolved when sintering Ti-6Al-4V components as discussed in Section 4.2.

4.1.5 Material Shrinkage

The shrinkage of the sintered CP-Ti component was calculated by dividing the difference in diameter between the green and sintering component over the diameter of the green component. The diameter of the green and sintered CP-Ti tensile components were measured using the vernier caliper.

The shrinkage of the sintered CP-Ti components measured by vernier caliper were compared to that obtained from the dilatometer measurements on CP-Ti. Table 4.7 shows the shrinkage values measured from the diameters of the CP-Ti components and those obtained from the dilatometer. The average shrinkage reported in the table is the average reading of four components measured for each sintering temperature.

From Table 4.7, it can be observed that there are some differences between the shrinkage values measured from the sintered components and the dilatometer results. This is especially so at the lower sintering temperatures. The differences between the shrinkage values measured from the two methods could be due to several reasons:

- Variation in temperatures between the sintering furnace and the dilatometer.
- Oxidation of CP-Ti during dilatometer tests may have altered the sintering behaviour of the powders, hence, resulting in the differences in the shrinkages. This is evident in Figure 4.12, where a deep blue colour was observed on the surfaces of the component sintered in the dilatometer. The cause for this is likely to be due to the poor sealing of the dilatometry equipment.

Table 4.7 Shrinkage data from the sintered components and dilatometer.

Temperature (^{o}C)	Ave shrinkage of sintered component (%)	Shrinkage from Dilatometer (%)
1240	12.22	10.85
1260	12.39	11.02
1280	12.81	13.23

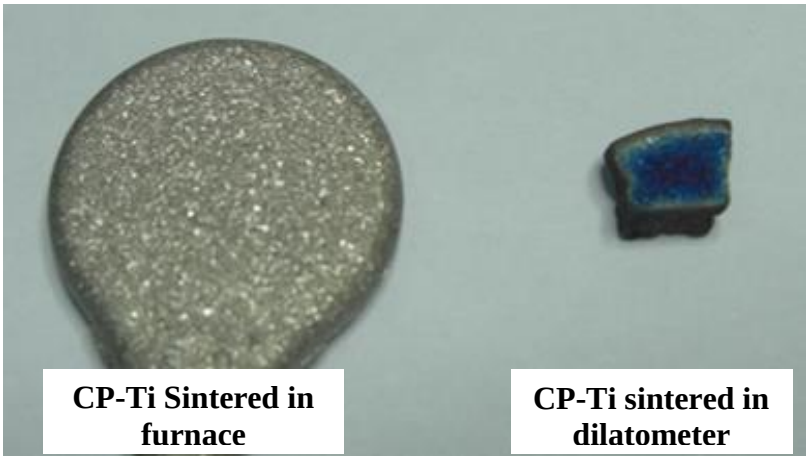

Figure 4.12 Surface finishing of CP-Ti sintered in furnace and dilatometer.

4.2 Phase Two – Characterisation of Sintered Ti-6Al-4V Components

The second phase of the research work focuses on the fabrication of Ti-6Al-4V tensile components. This section discussed on how some of the issues encountered in the first phase of the study (on CP-Ti components) were rectified and implemented in the research on Ti-6Al-4V tensile components. In addition, the results of the design of experiment (DOE) conducted for the sintering process will also be examined and reported in this chapter. Lastly, the influence of the sintering parameters on the microstructures, physical and mechanical properties of the sintered Ti-6Al-4V components is discussed.

4.2.1 Rectification of Sintering Issues

Two issues were encountered during the sintering of CP-T tensile components:

1. The use of Ar gas resulted in large amount of porosity in the sintered components due to gas entrapment.
2. Constrained sintering resulted in non-uniform shrinkage and variations in dimension of a batch of components sintered under the same sintering conditions.

The first issue was rectified by changing the sintering environment to vacuum. Sintering of the Ti-6Al-4V tensile components were conducted in a high vacuum furnace with a vacuum level of 10^{-6} mTorr. The details on the microstructures of the sintered Ti-6Al-4V components are discussed in Section 4.2.4.

For the second issue, the ceramic sintering plate was replaced with molybdenum (Mo) sintering plate. Mo is one of the recommended materials used for the sintering of Ti components. However, bonding of the components to the Mo sintering plate still occurred despite the change. This was due to the diffusion of Mo atoms from the sintering plate to the Ti-6Al-4V components at high temperature. Therefore, this resulted in partial bonding of the component to the sintering plate. The graph in Figure 4.13 shows the diffusivity data of some of the elements in Ti. The dashed line in the graph indicates β to α transformation temperature. As referenced from the graph, diffusivity of Mo atoms in β-Ti is quite fast and its rate of diffusion increases with increasing temperature. A sintering temperature above 1200 ^{o}C would raise the diffusivity of Mo to more than 10^{-14} m^2/sec. The sintering temperatures selected for Ti-6Al-4V fall within the temperature range where Mo diffusion is active in Ti, therefore, the possibility that bonding between the Mo sintering plate and Ti can occur.

To prevent the reaction between Mo and Ti, the Mo plate was coated with a layer of ceramic. The ceramic coating acts as a barrier between the Mo sintering plate and the Ti component during the sintering process. Figure 4.14 shows the image of a Mo plate coated with the ceramic mixture. The coating was fabricated by first mixing the ceramic powder in IPA. IPA acts as a wetting agent to allow easy application of the powder particles onto the plate. This was followed by applying multiple layers of the mixture evenly over the surface of the Mo plate. After the IPA has evaporated, the sintering plate was sintered at 1400 ^{o}C in vacuum. The ceramic coating remained intact and bonded to the Mo sintering plate after the sintering process. Also, no visible cracks were observed on the coating after sintering. The debound Ti-6Al-4V components were placed on the ceramic coated

sintering plate and sintered at temperatures between 1200 to 1300 ^{o}C in vacuum atmosphere. No bonding was observed between the Ti-6Al-4V component and the sintering plate after sintering. In addition, the coating also remained intact after multiple uses. Therefore, the ceramic coating has successfully rectified the bonding issue.

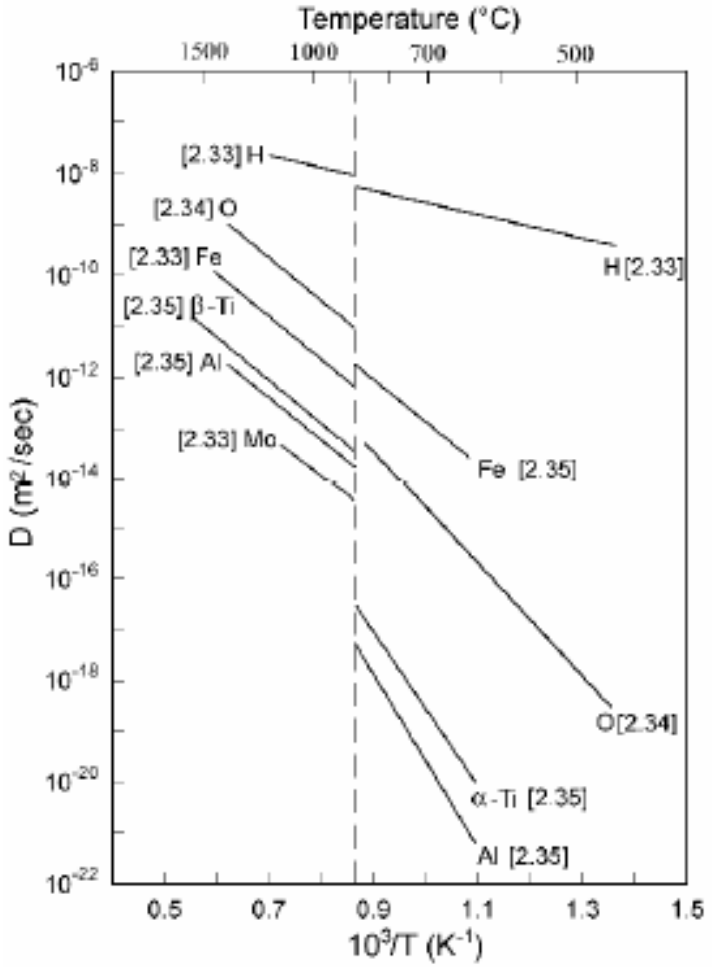

Figure 4.13 Diffusivity data of the different interstitial elements in Ti [38].

Figure 4.15 shows the outcome of Ti-6Al-4V components sintered using the different plates: 1) uncoated and 2) coated. As observed in Figure 4.15, an uneven and rough surface was observed on the contact surface of the Ti-6Al-4V component when sintered using uncoated Mo plate. This was due to the bonding between the Mo sintering plate and the component contact surface. A thin layer of the Ti-6Al-4V was peeled off from the contact surface when the component was removed

from the plate. Such surface finishing is not desirable as it destroys the aesthetics of the component and also introduces defects, which will affect its mechanical properties. Whereas, for Ti-6Al-4V component sintered using coated Mo sintering plate, a smooth surface was observed on the contact surface of the component.

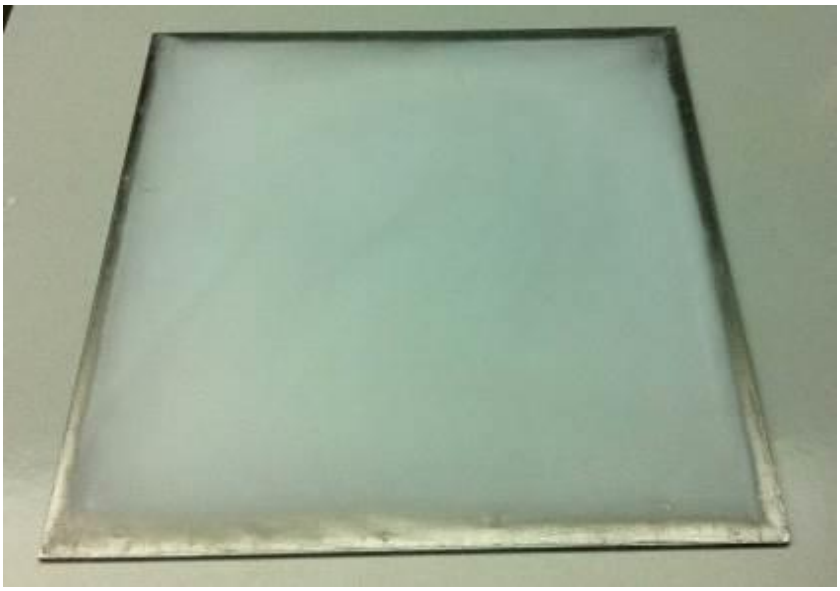

Figure 4.14 Mo plate coated with ceramic.

(i) Uncoated Mo Plate

(ii) Coated Mo Plate

Figure 4.15 Surface finish Ti-6Al-4V components on different sintering plates.

The bonding of the Ti-6Al-4V components to uncoated Mo sintering plate has also resulted in non-uniform shrinkage in the transverse and lateral directions of the component. This phenomenon was similar to the one observed in Section 4.1.4, when ceramic sintering plate was used to sinter CP-Ti components. Non-uniform shrinkage was not observed when the Ti-6Al-4V components were sintered using coated Mo plate.

The shrinkages of the Ti-6Al-4V components sintered using coated and uncoated Mo sintering plates were measured and compared. Shrinkage in the lateral direction was obtained from percentage difference between the length of sintered and green Ti-6Al-4V components, while the shrinkage in the transverse direction was referenced from their diameter measurements. Figure 4.16 presents the shrinkage values of Ti-6Al-4V components in the lateral and transverse direction. From Figure 4.16, a larger difference was observed between the lateral and transverse shrinkage for Ti-6Al-4V components using the uncoated Mo plate as compared those sintered on coated Mo plate. Shrinkage up to 6.38 % was observed in length, while shrinkage of 15.05 % was noted along the diameter for Ti-6Al-4V components sintered on uncoated Mo plate. On the other hand, a smaller difference in the shrinkage between the diameter (11.46 %) and the length (10.23 %) was observed in components sintered using ceramic coated Mo plate. This small difference was believed to be attributed by the effect of gravity. Therefore, this indicates that constrained sintering has an effect on the shrinkage uniformity of Ti-6Al-4V components. With the elimination of constrained sintering, variation in shrinkage values has also been reduced.

The microstructures of the components sintered using different sintering plates were also examined. Figure 4.17 shows the SEIs of the cross section of the Ti-6Al-4V components sintered using coated and uncoated Mo sintering plates at 1250 ^{o}C in vacuum atmosphere. It can be inferred from the images, that Ti-6Al-4V component sintered on uncoated plate has higher porosity as compared to component sintered using coated plate. This was also evident in the porosity and relative density measurements of the components conducted by Archimedes' method tabulated in Table 4.8. A porosity percentage of 1.08 % and relative density of 94.5 % was obtained for Ti-6Al-4V component sintered on uncoated Mo plate, while a porosity of 0.80 % and relative density of 96.1 % was achieved for component sintered on coated Mo plate.

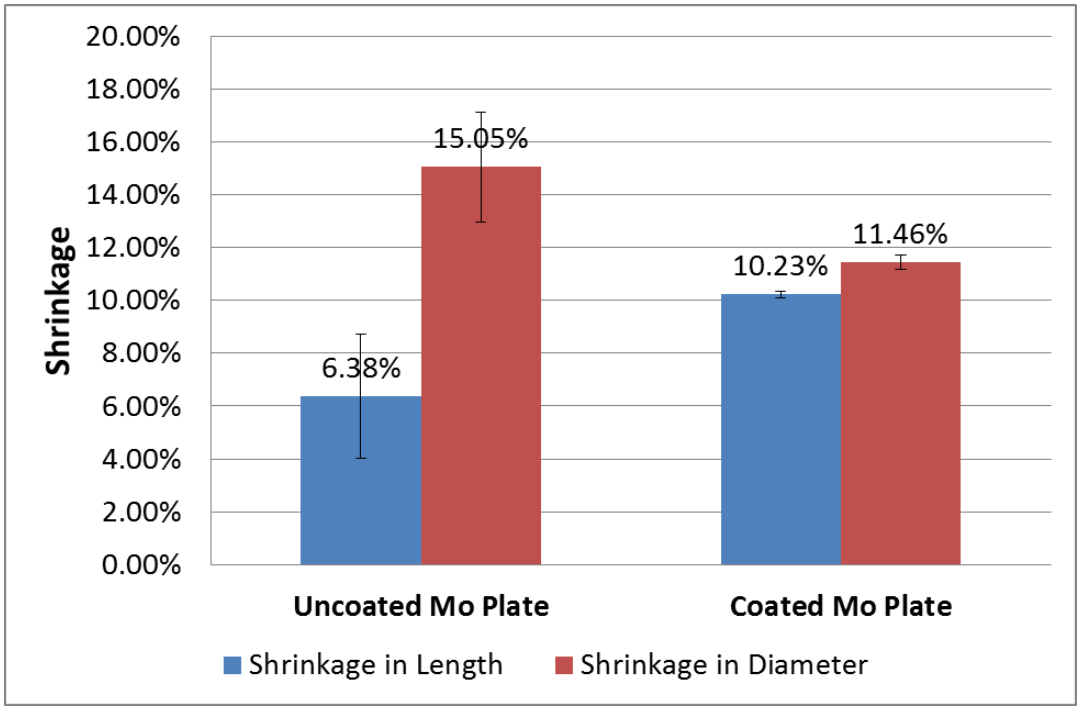

Figure 4.16 Shrinkage of components sintered on different Mo plates.

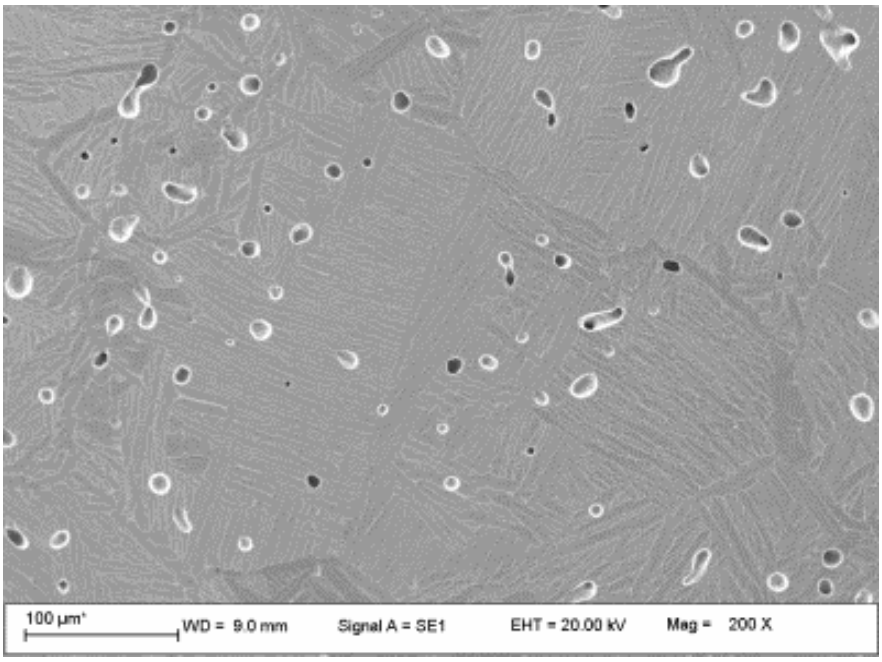

(i) Ti-6Al-4V on uncoated Mo Plate

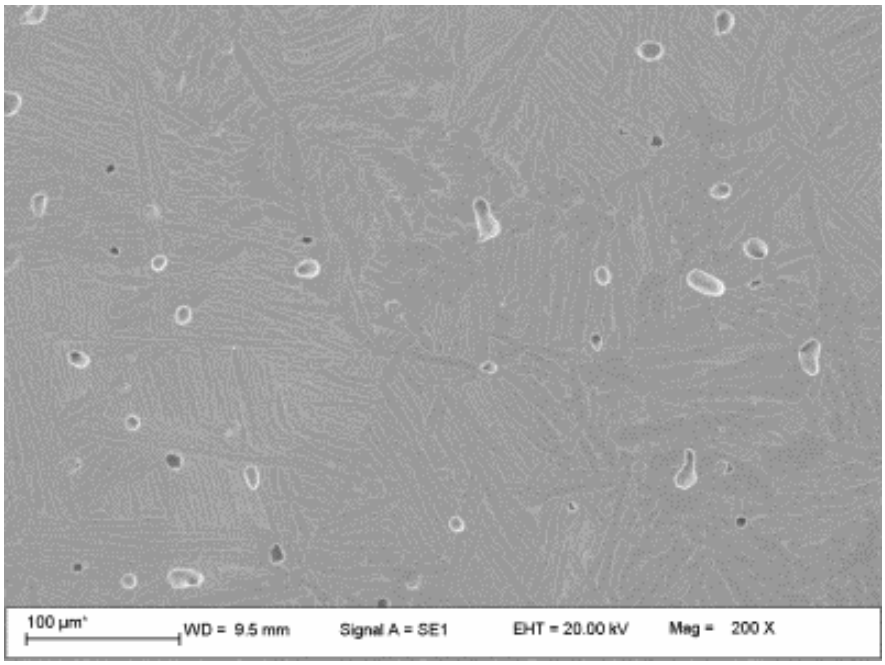

(ii) Ti-6Al-4V on coated Mo Plate

Figure 4.17 SEI of components sintered using different Mo sintering plate.

Table 4.8 Porosity and density of Ti-6Al-4V sintered using different Mo plates.

Sintering plate	Porosity (%)	Relative Density (%)
Uncoated Mo	1.08	94.5
Coated Mo	0.80	96.1

High porosity and low relative density are not desirable as they deteriorate the mechanical properties of the sintered component. This is because pores act as potential stress concentration sites. This can be inferred from the measured UTS and elongation measured from a set of Ti-6Al-4V components sintered using the different Mo plates. As seen in Figure 4.18, components sintered on uncoated Mo plate, have poorer tensile properties, in particular elongation, as compared to those sintered on coated Mo plate. From the figure, an elongation of only 5.62 % was obtained for Ti-6Al-4V components sintered using uncoated Mo plate, while an elongation of 13.74% was achieved for those sintered on coated plate. As mentioned earlier, rough and uneven patches were observed on the contact surfaces of the components sintered on uncoated Mo plate (see Figure 4.15 (i)). These patches can be detrimental to the tensile properties as they are potential points for crack initiation, hence, they can also be one of the contributing factors to the poor tensile properties.

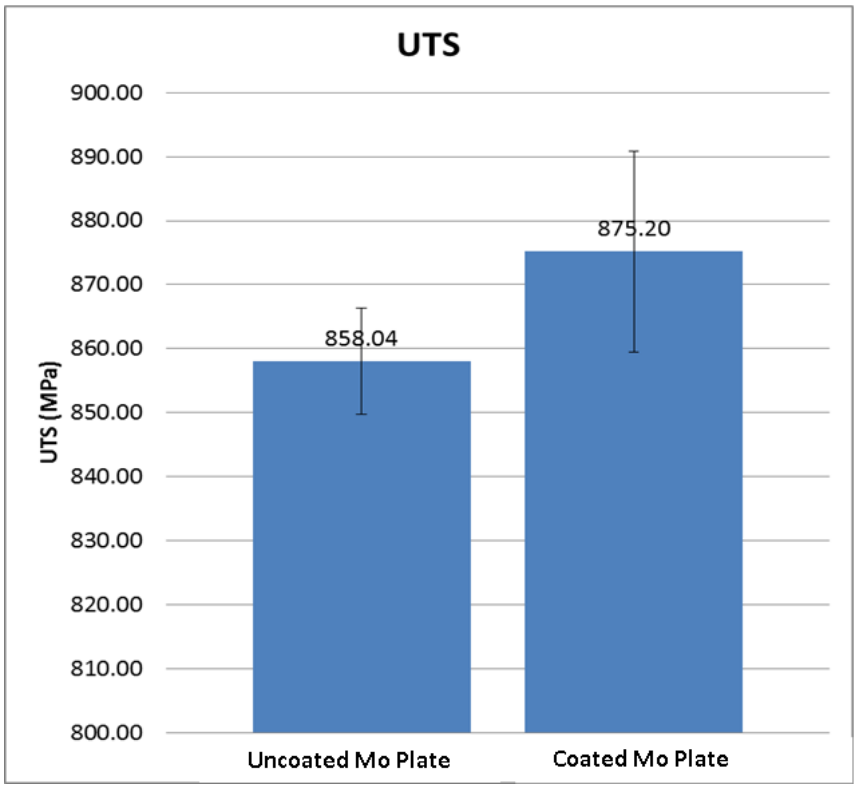

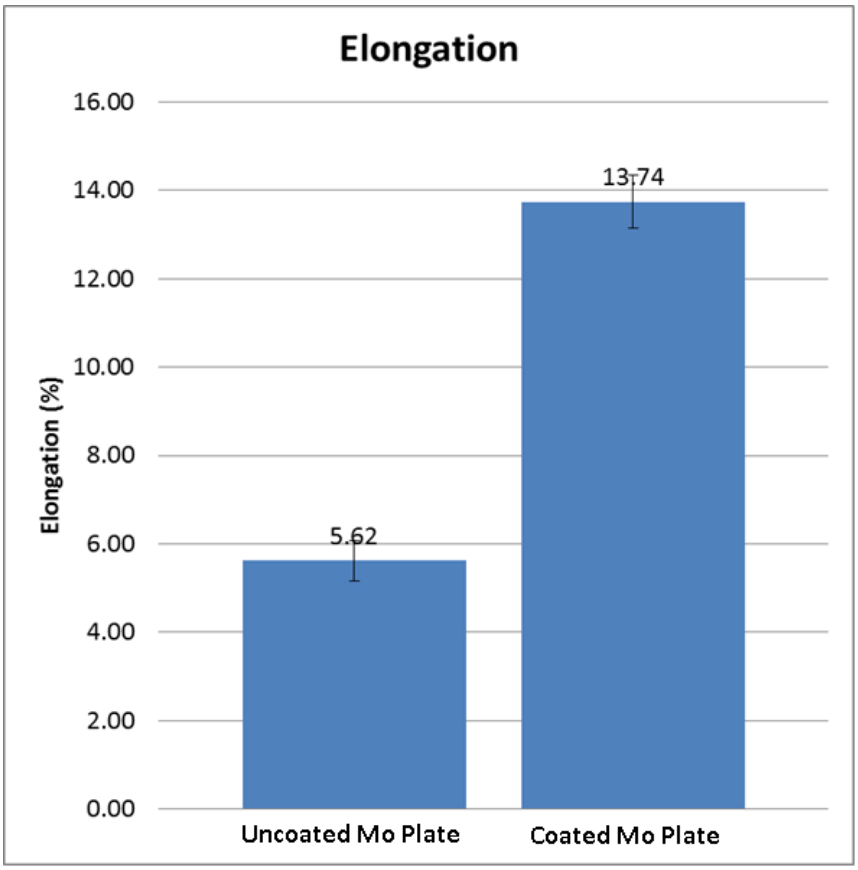

Figure 4.18 UTS and elongation of Ti-6Al-4V sintered on different Mo plates.

4.2.2 Design of Experiment on Sintering

Sintering is an important step in powder metallurgy as it determines the microstructures, physical and mechanical properties of the component. However, it is a complex process which involves several parameters such as temperature, dwell time, ramp rate, cooling rate, sintering environment and supporting plates. Most research work conducted on the sintering of PIM Ti components mainly involved studying the effects of temperatures and impurity intake on the final properties of Ti. However, detailed studies on the influence of the various sintering parameters on Ti properties have not been widely reported.

In the second phase of research, DOE was performed to study the effects of sintering parameters on the tensile properties of Ti-6Al-4V tensile components. The tensile properties studied in this work are the UTS and elongation. The microstructures of Ti-6Al-4V components sintered under the different DOE run parameters were also examined to understand their effects on the tensile properties.

Before the values of the sintering parameters for the DOE were determined, literature review and preliminary DOE were conducted to examine the suitable range of values to be used for the design. In the preliminary DOE, the responses (UTS and elongation) obtained were relatively close. Thus, it was difficult to conclude which parameters have significant effect on the responses. The cause for this was that the values selected for the parameters at the different levels were too close to cause significant effects on the responses. In DOE, the value chosen at each level for the individual parameters needs to be significantly different such that it results in a contrasting response for each run. However, care should be taken to ensure that the values selected will not affect the integrity of the components. For example, a wider difference of sintering temperature should be selected but at the same time ensure successful sintering.

For this DOE study, a fractional factorial design of 2^{4-1} was chosen. The advantage of using fractional factorial design is that the number of runs required can be reduced. For this design the number of runs was reduced from a total of 16 to 8 (refer to Table 4.9). Table 4.10 summaries the number of levels, replications, observations and generation used for the DOE design.

Table 4.9 Comparison of full factorial and fractional factorial design.

K	Full design	Original no. of runs	One-half fractional design	Reduced no. of runs
4	2^4	16	2^{4-1}	8

Table 4.10 Fractional design of 2^{4-1}

No. of levels	2
No. of replications, n	1
Total no. of observations, N	8
Generator	ABCD

The selected values for each parameter are listed in Table 4.11. They are (A) sintering temperature, (B) dwell time, (C) cooling rate and (D) ramp rate. The effects of the sintering parameters were analysed against the average elongation and UTS values obtained from the eight different sintering runs.

Table 4.11 Sintering factors used in DOE.

	Parameters	Low (-)	High (+)
A	Temperature / ^oC	1200	1300
B	Dwell Time / h	1	3
C	Cooling rate / ^oC/min	1	10
D	Ramp rate / ^oC/min	1	10

The run pattern for the 2^{4-1} design needs to be constructed from a full 2^4 design. This was done by selecting eight run out of the 16 runs from the full design. To plot the run patterns for this fractional design, the highest interaction for the design needs to be sacrificed in order to preserve the information from the main effect. The term generator (I) is used to address the highest interaction. The generator for this case is ABCD as indicated in Table 4.12. Table 4.12 also shows the alias structure for the design.

Table 4.12 Generator and alias structure

Generator (I) = ABCD	
Alias structure:	A = AI = A(ABCD) = BCD
	B = BI = B(ABCD) = ACD
	C = CI = C(ABCD) = ABD
	D = DI = D(ABCD) = ABC

The full design of 2^4 is plotted in Table 4.13. To select eight run patterns for the 2^{4-1} design, the selected fraction must have identical signs under the generator column. In this study, run patterns with generator having "+" signs were chosen. Sintering tests were then conducted based on the selected run patterns and their responses are plotted in Table 4.14 and Figure 4.19. The values reported for UTS and elongation responses are the average reading of three components for each run. The measurements for the responses were done randomly.

Table 4.13 Run pattern for 2^4 design.

Run	A Sintering Temp	B Dwell Time	C Cooling Rate	D Ramp Rate	ABCD
(1)	-	-	-	-	+
ad	+	-	-	+	+
bd	-	+	-	+	+
cd	-	-	+	+	+
ab	+	+	-	-	+
bc	-	+	+	-	+
ac	+	-	+	-	+
abcd	+	+	+	+	+
a	+	-	-	-	-
b	+	-	-	-	-
c	+	-	-	-	-
d	+	-	-	-	-
abc	+	+	+	-	-
abd	+	+	-	+	-
acd	+	-	+	+	-
bcd	-	+	+	+	-

Table 4.14 2^{4-1} Design matrix and their response

Factor						Response			
Run	**A Sinter-ing Temp**	**B Dwell Time**	**C Cool-ing Rate**	**D Ramp Rate**	**ABCD**	**Average Elongation (%)**	**Std Dev**	**Average UTS (MPa)**	**Std Dev**
(1)	-	-	-	-	+	13.80	4.22	833.64	1.22
ad	+	-	-	+	+	7.89	3.81	826.57	0.23
bd	-	+	-	+	+	11.42	3.94	838.55	2.86
cd	-	-	+	+	+	6.95	7.49	821.84	1.34
ab	+	+	-	-	+	17.15	4.71	882.77	2.00
bc	-	+	+	-	+	14.86	2.67	894.21	1.16
ac	+	-	+	-	+	13.29	8.42	904.49	2.60
abcd	+	+	+	+	+	14.44	1.76	900.40	2.78

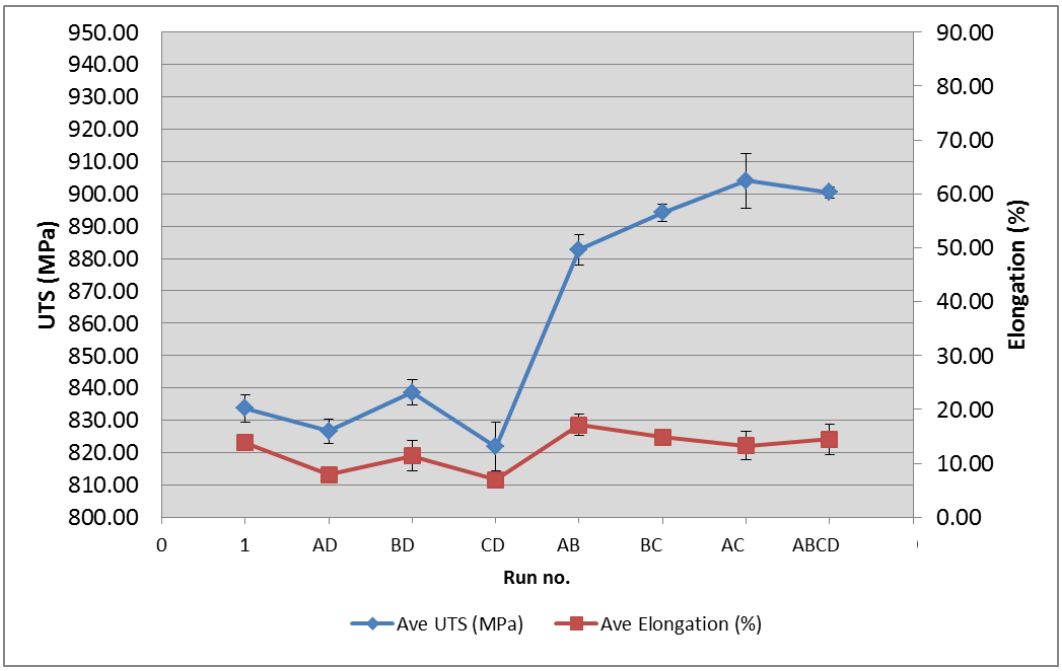

Figure 4.19 Plot of UTS and elongation against the different sintering runs.

X-ray inspections were conducted on the sintered Ti-6Al-4V components prior to tensile testing. This is to ensure that the components are free from cracks and voids before tensile testing was performed. Such defects affect the tensile properties and this can confuse the analysis on the effect of sintering parameters on the mechanical properties. Therefore, sintered components with obvious defects will not be used for any mechanical testing. In this research, the FEINFOCUS X-ray imaging instrument was used to carry out the inspection. The advantage of x-ray

inspection is that it can detect surface or embedded cracks and voids in the component. X-ray imaging is performed by scanning a heterogeneous x-ray beam over the area of interest. The amount of x-ray absorbed by the component depends on the density of each area. Areas which are denser appeared darker as they absorbed a higher intensity of x-ray, while the less dense area appeared brighter. Therefore, cracks and voids can be distinguished by spotting bright features in the x-ray images of the component. X-ray imaging was performed on both the clamping and gauge area of the sintered Ti-6Al-4V components. Figure 4.20, showed the x-ray images of the clamping and gauge area of a sintered Ti-6Al-4V component. Based on the x-ray inspection, no visible cracks or voids were detected in this batch of sintered Ti-6Al-4V components. This also indicates that the processing parameters used for the fabrication of Ti-6Al-4V components were suitable.

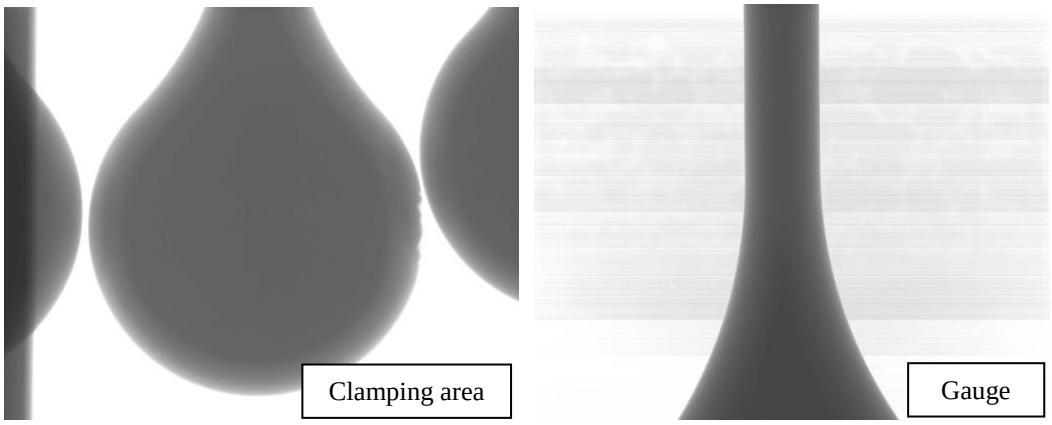

Figure 4.20. X-ray images of clamping and gauge area.

Once the response for each run was tabulated, analysis of variance (ANOVA) was performed to evaluate the effects and the significance each parameter had on the UTS and elongation. ANOVA is an important statistical tool for DOE as it is used to determine which factors or interactions have significant effect on the response. Details of ANOVA analysis for UTS and elongation are discussed in Section 4.2.2.1 and 4.2.2.2., respectively.

4.2.2.1 ANOVA Analysis for UTS

The first step in ANOVA is to determine which of the parameters in the fractional design has effect on the response, in this case, the UTS. Initial deduction on which parameters or their interactions has effect on the response can be deduced based on the calculated effect, 1. In order for the parameter or its interaction to be considered significant to the design, the calculated effect must be significantly large from the rest of the effect value. The calculated effect for each sintering parameters and their interactions are tabulated in Table 4.15.

Table 4.15 Calculated Effects for DOE response – UTS.

Effects	$\mathbf{l_A}$	$\mathbf{l_B}$	$\mathbf{l_C}$	$\mathbf{l_D}$	$\mathbf{l_{AB}}$	$\mathbf{l_{BC}}$	$\mathbf{l_{AC}}$
UTS	**31.50**	**32.35**	**34.85**	**-31.94**	-6.29	1.79	12.92

Based on the calculated effects, parameters (A) sintering temperature, (B) dwell time, (C) cooling rate and (D) ramp rate have effect on the UTS of Ti-6Al-4V. The initial calculation on the effect only indicates if they have any influence on the response. As to whether the parameters are significant to the response, an F test needs to be done. In order to determine which parameter has effect to the response, the calculated F value for each parameter (F_0) needs to be more than the F value obtained from the F distribution table according to the confidence level selected and calculated degree of freedom based on the design. The degree of freedom for numerator (v_1) and degree of freedom for denominator (v_2) obtained from the degree of freedom for the main parameter and degree of freedom for Total, respectively. Table 4.16 summaries the F test for UTS. A confidence level of 99 % was used for this F test.

Table 4.16 ANOVA on UTS.

Source of variation	Sum of Square	Degree of Freedom	Mean Square	F_0	F_0>F	
A	1984.19	1	1984.19	17.16	Significant	For α = 0.01 $F_{0.01,1,7}$ = 12.25
B	2092.72	1	2092.72	18.10	Significant	
C	2429.39	1	2429.39	21.01	Significant	
D	2040.01	1	2040.01	17.65	Significant	
AB	6.43	1	6.43	0.06	Not significant	
BC	6.43	1	6.43	0.06	Not significant	
AC	333.98	1	333.9	2.89	Not significant	
Error	346.83	3	115.61			
Total	8893.14	7				

From the ANOVA analysis, it can be concluded that all four parameters, (A) sintering temperature, (B) dwell time, (C) cooling rate and (D) ramp rate, have significant effect on UTS. Their interactions however, do not have any significant effect on UTS. Also from the effect calculated in Table 4.16, it can be deduced if a positive or negative trend on the parameters has significance on the selected response. In the case of UTS, higher sintering temperature, longer dwell time, faster cooling rate and slower ramp rate will result in higher UTS.

Residual analysis and model check were performed to ascertain if the observations obtained from this DOE are normally and independently distributed. The criteria for the check consist of the following:

1. Check for normal distribution
   This is done by plotting the residues on the normal probability paper. If the points plotted are in a straight line, it means that the residual distribution is close to normal.

2. Check independent distribution
   This is done by plotting the residuals against the run order in which the observations was measured. The distribution is only independent if the points are of a random pattern.

3. Check zero mean value
   This is satisfied automatically if criteria 1 and 2 are satisfied.

4. Check constant variance, σ^2, at all levels.
   This is done by plotting the residues against the levels and comparing the spreads of the residues. The criterion is satisfied if the range for all the levels are identical.

Based on the plots in Figure 4.21 to Figure 4.23, it can be deduced that the DOE model is valid and has satisfy all the four criteria. The linear regression, R^2, calculated in Figure 4.21, for each parameter have value close to 1, therefore, indicating that the model is normally distributed and satisfying criterion 1. An independent distribution and also similar constant variance were also observed for all the parameters, hence, also satisfying criteria 2 and 4. Criterion 3 will be satisfied when the remaining three conditions are fulfilled.

(1) Normal distribution

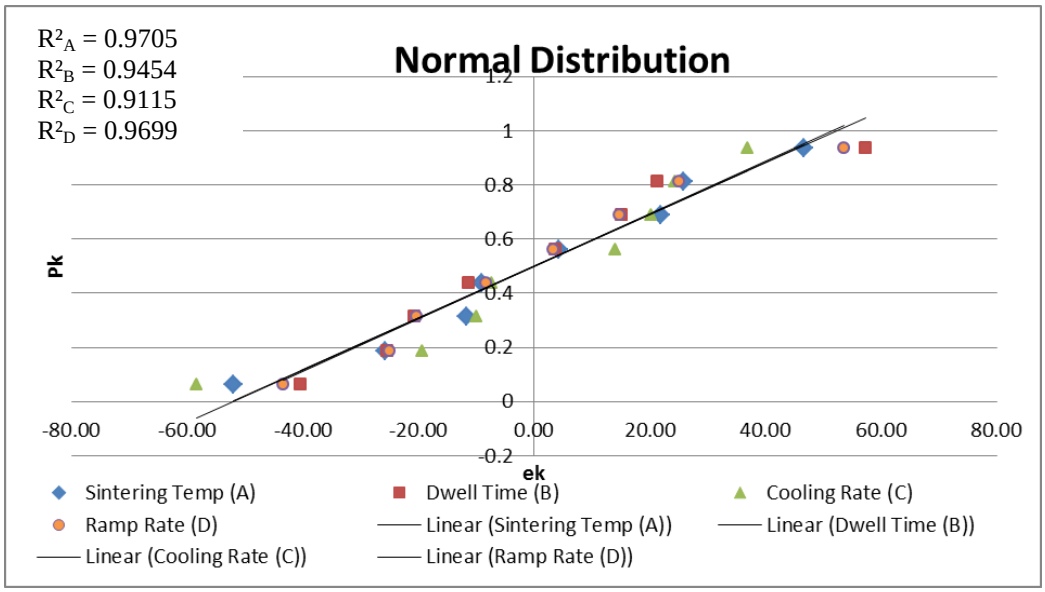

Figure 4.21 Plot of residual distribution for each factors on UTS.

(2) Independent distribution

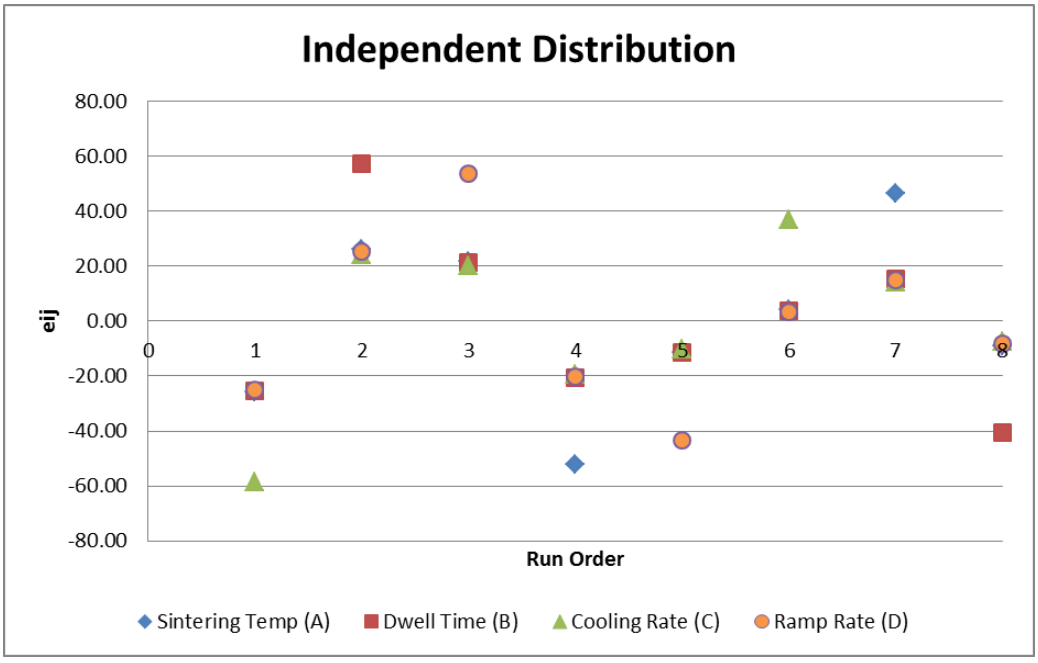

Figure 4.22 Independent distribution plot for each factors on UTS.

(4) Constant variance σ^2

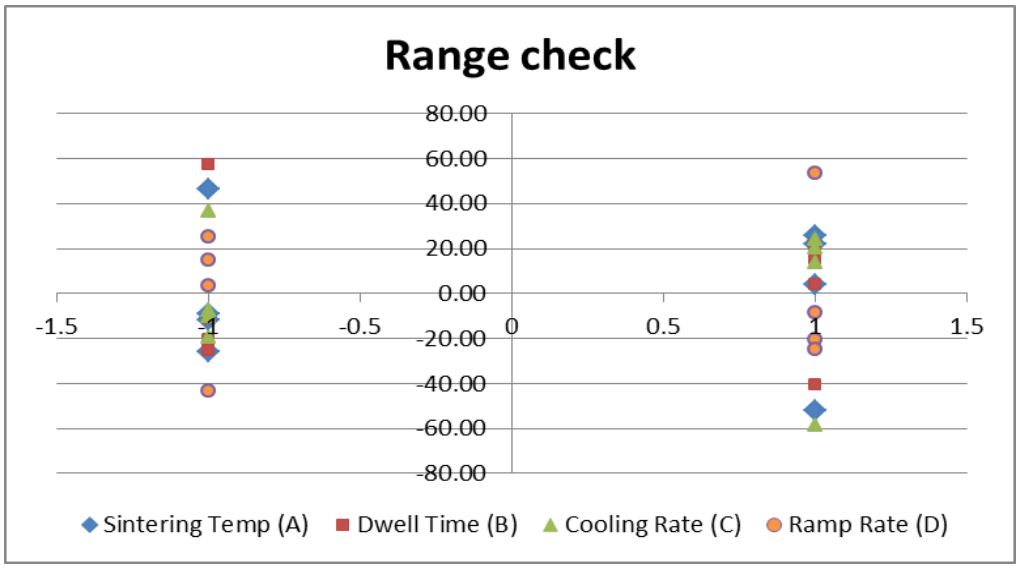

Figure 4.23 Plot of residuals vs. runs for each factors.

4.2.2.2 ANOVA Analysis for Elongation

The same procedure in Section 4.2.2.1 was applied for the DOE analysis on elongation.

Table 4.17 Calculated effect for DOE response - Elongation

Effects	l_A	l_B	l_C	l_D	l_{AB}	l_{BC}	l_{AC}
Elongation	0.57	**4.85**	0.69	**-5.47**	2.09	-0.32	2.39

From the calculated effects of the fractional factorial design shown in Table 4.17, the dwell time (B) and ramp rate (D) has effect on the elongation. The remaining two parameters, sintering temperature (A) and cooling rate (C) can be dropped from the design as their effects on elongation are not as significant as dwell time (B) and ramp rate (D). Hence, the design matrix is converted to a 2^2 design, as shown in Table 4.18, to evaluate the significance of these two parameters.

Similar to the DOE on UTS, the F test, with a confidence level of 99 %, was performed. The ANOVA for this design is summarized in Table 4.19. Based on the ANOVA in Table 4.19, both dwell time and ramp rate have significant effect on

the elongation. On the other hand, their interactions were found to have no significant effect on the elongation. Also from the ANOVA it can be deduced that longer dwell time and lower ramp rate are desirable for achieving better elongation. This is evident in run AB and BC, where a combination of high dwell time and lower ramp rate resulted in better elongation as compared to other runs.

Table 4.18 2^2 design matrix.

Run	B	D	BD	Average Elongation		Total
1	-	-	+	13.8	13.29	27.09
b	+	-	-	17.15	14.86	32.01
d	-	+	-	4.42	6.95	11.37
bd	+	+	+	11.42	14.44	25.86

Table 4.19 ANOVA on elongation.

Source of variation	**Sum of Sq**	**DOF**	**Mean Sq**	**F_0**		
B	31.72	1	31.72	16.35	Significant	For α = 0.01 $F_{0.01,1,7}$ = 12.25
D	42.27	1	42.27	21.79	Significant	
BD	4.64	1	4.64	2.39	Not Significant	
Error	7.76	4	1.94			
Total	86.39	7				

Lastly, the residue and model check was conducted to determine the validity of the design. The graphs for each model are plotted in Figure 4.24 to Figure 4.26. From Figure 4.24, the linear regression for parameter B and D are close to a value of 1, hence, they have fulfilled the criteria of being normally distributed. A random distribution and similar constant variance were also observed, as indicated in Figure 4.25 and Figure 4.26, respectively. Therefore, proving the design to be valid.

(1) Normal distribution

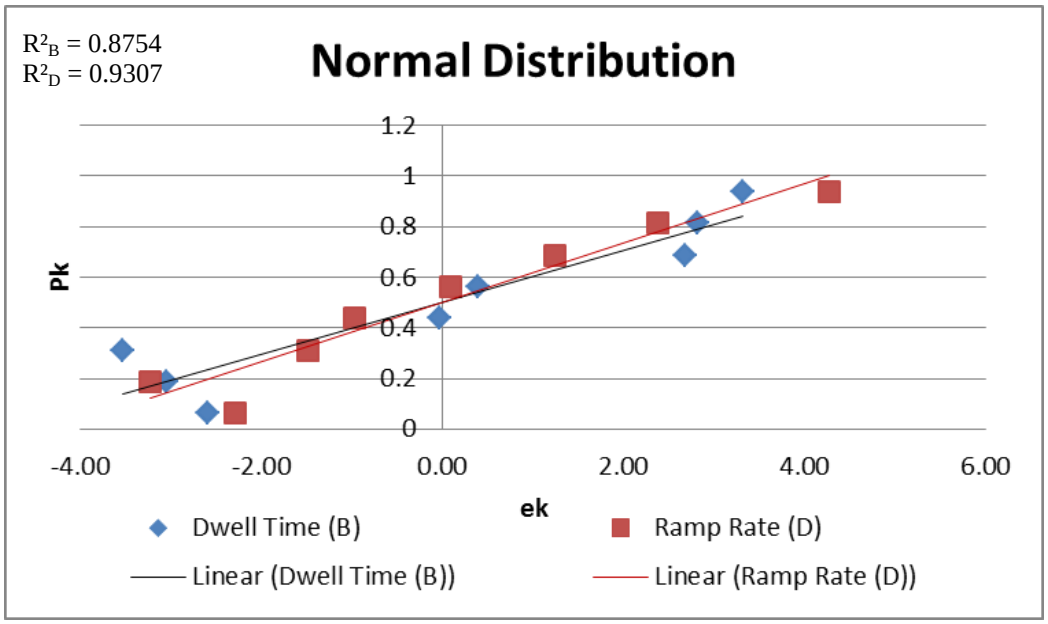

Figure 4.24 Plot of residual distribution for each factors on elongation.

(2) Independent distribution

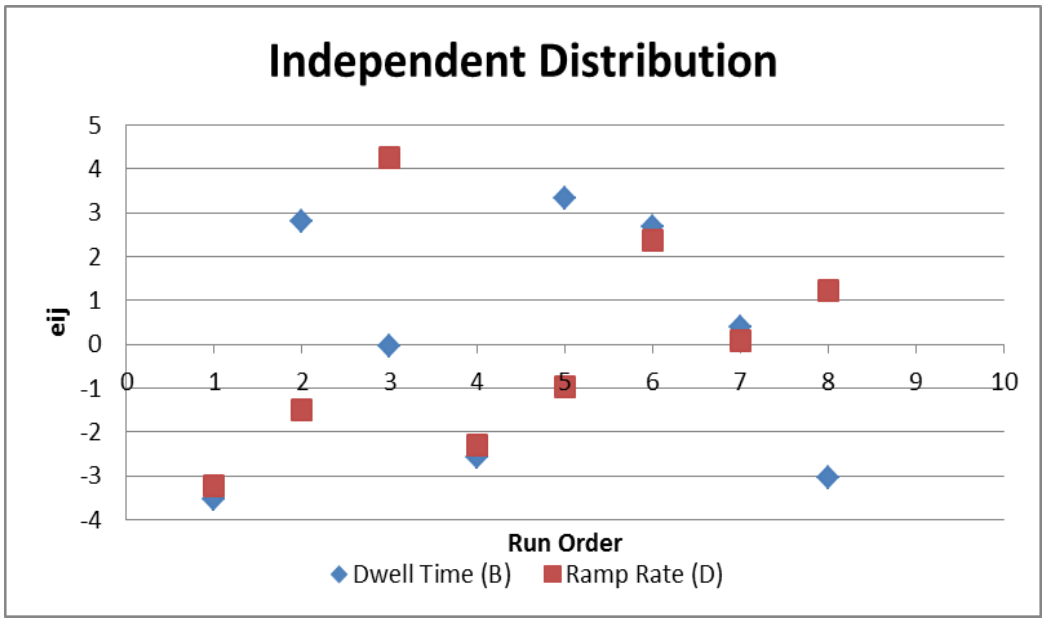

Figure 4.25 Independent distribution plot for each factors on elongation.

(4) Constant variance σ^2

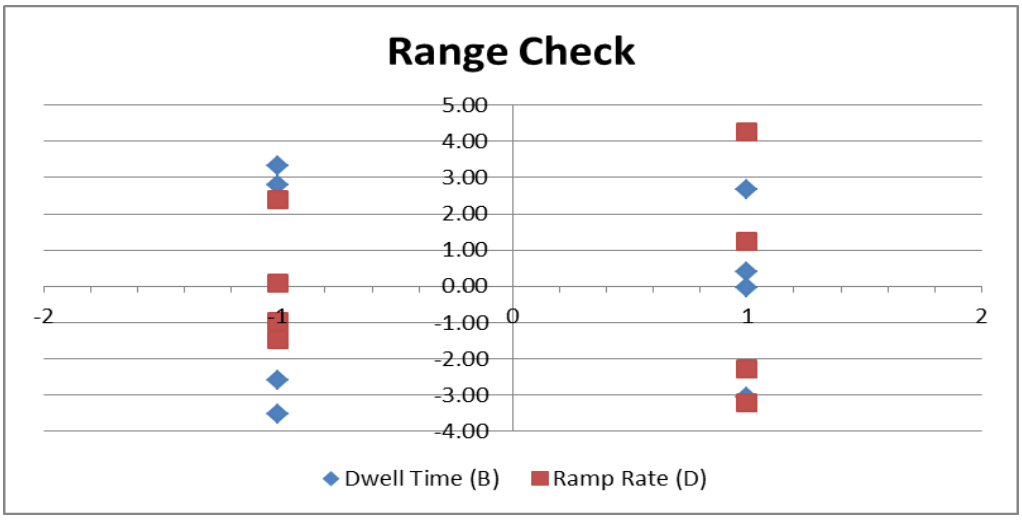

Figure 4.26 Plot of residuals vs. runs for each factors.

4.2.3 Porosity and Density of Sintered Ti-6Al-4V Tensile Components

The porosity of the sintered Ti-6Al-4V tensile components was measured using AnalySIS pro software. Measurements were taken from three different areas on the polished cross-section of the sintered components. The density was measured using the Archimedes' method. The average porosity, apparent solid density and relative density of the components are tabulated in Table 4.20.

Table 4.20 Density and porosity measurement of Ti-6Al-4V components.

Run	Parameter				Average Porosity (%)	Average Apparent Solid Density (g/cm^3)	Average Relative Density (%)
	Temp (^oC)	Dwell Time (h)	Cool (^oC/min)	Ramp (^oC/min)			
1	1200	1	1	1	3.60	4.27	96.4
AD	1300	1	1	10	3.92	4.30	97.2
BD	1200	3	1	10	2.39	4.33	97.7
CD	1200	1	10	10	4.46	4.19	94.5
AB	1300	3	1	1	2.28	4.39	99.0
BC	1200	3	10	1	3.03	4.31	97.3
AC	1300	1	10	1	2.33	4.35	98.2
ABCD	1300	3	10	10	2.34	4.33	97.8

From Table 4.20, it was noted that components sintered under run CD have the highest porosity (4.46 %), lowest apparent solid density (4.19 g/cm^3) and lowest relative density (94.5 %) as compared to the other runs. This was believed to be attributed by the lower sintering temperature (1200 ^oC) and shorter dwell time (1 hour) selected for this run. Higher relative density and lower porosity were observed in Ti-6Al-4V components sintered under higher temperatures (1300 ^oC) or at lower temperatures with prolonged dwell time (1200 ^oC with 3 hours dwell time). This is evident when the results for run CD were compared to run BD and BC, where a prolong dwell time was applied under the same sintering temperature, and in run AC and AD, where a higher sintering temperature for used while maintaining the same dwell time. In general, the sintering or densification rate usually increases with increasing sintering temperature and longer dwell time [17]. The trend on the relative density verses sintering temperature and time is presented in Figure 4.27.

High porosity and lower density are not desirable for PIM components as they degrade the component's mechanical properties. Taking the components sintered under run CD as an example, they have an UTS and elongation of 821.84 MPa and 6.95 %, respectively, which is the lowest compared to the other runs. Its elongation was also lower than the targeted value of more than 10 %. This is because high porosity and lower density may indicate incomplete sintering hence, affecting the strength of the component. In addition, pores are also potential stress concentration points hence, reducing the mechanical properties of the material. The rest of the components sintered under the remaining runs have achieved an average relative density of 96 % and above. The trend for the average porosity is in line with the average relative density measured. The higher the relative density, the lower the porosity level in the component.

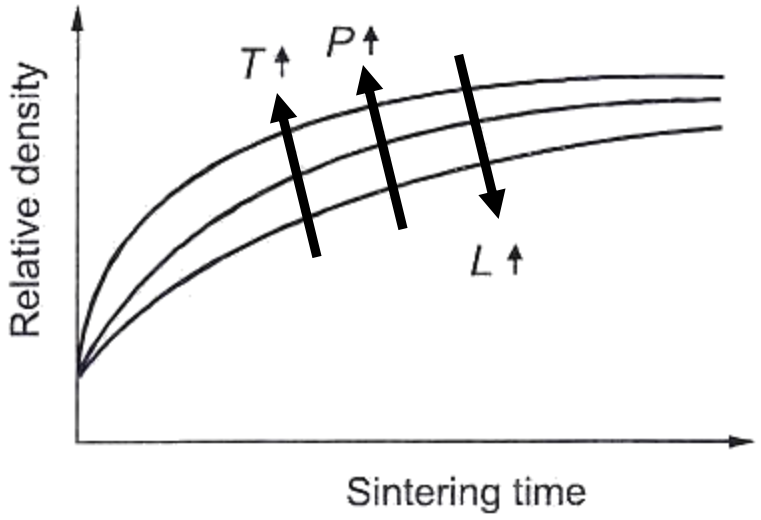

Figure 4.27 Effects of sintering parameters on density [17].

Besides sintering temperature and dwell time, another factor which affects the porosity and density is ramp rate. Comparing run CD and run 1, both runs have the same sintering temperature and dwell time. The only difference was the ramp rate and the cooling rate used. When the ramp rate was decreased from 10 ^{o}C per minute for run CD to 1 ^{o}C per minute for run 1, the relative density of the component increased from 94.5 to 96.4 %, which is a significant increase. Similar observations were also seen when comparing run AD with AC and run AB with ABCD. In both scenarios, an increased in density and decrease in porosity were observed when lower ramp rate was applied. The phenomena can be explained by grain boundary mobility, M and interaction with pores. As illustrated in Equation 3, grain boundary mobility is dependent on the temperature, which in turn depends on the ramp rate. Low ramp rate induced lower temperature increment, which reduced the grain boundary mobility. The pores are dragged by the slow moving grain boundaries and collated at the grain boundaries where they will shrink with further sintering and densification. High ramp rate increases the temperature increment, hence, leading to faster grain boundary mobility. The pores are broken away from the fast moving gain boundary and engulfed within the grains [46]. Therefore, lower grain boundary mobility is desirable as it decreases the risk of pore entrapment in the grains, leading to higher density and lower porosity. The

phenomenon is illustrated in Figure 4.28. In Figure 4.28 (i), most of the pores are located at the grain boundary, while in case (ii) pores are trapped within the grains, which makes them difficult to be removed by additional sintering process.

$$M = M_0 \exp(-Q/RT) \qquad (3)$$

where,

M_0 is a constant.

Q is the activation energy.

R is the gas constant.

T is temperature.

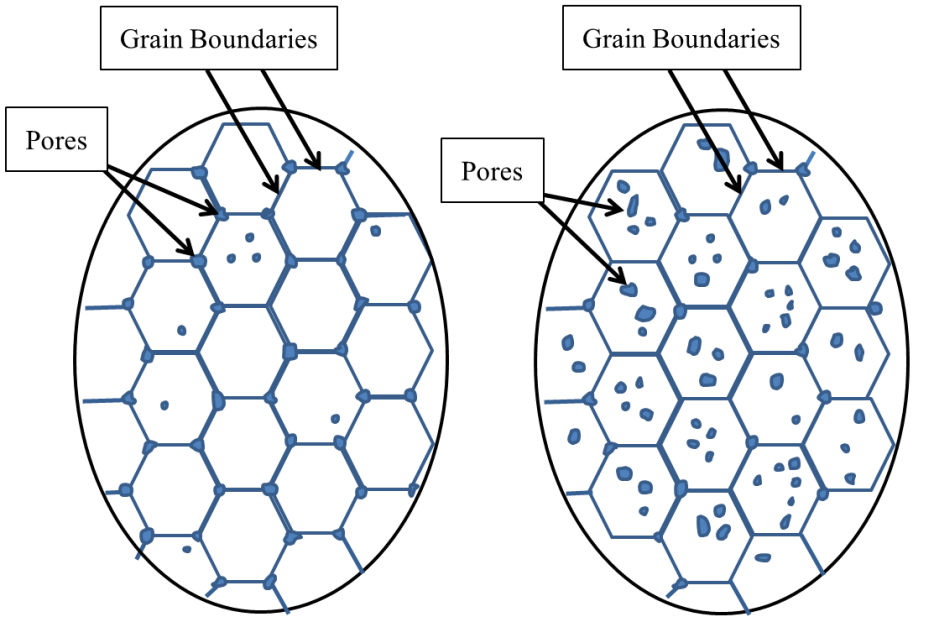

Figure 4.28 (i) Ideal and (ii) undesirable position for pores during sintering.

Another scenario which supports that lower ramp rate enhance the relative density of the component is the comparison between run AC and ABCD. In this case, both runs have similar sintering temperate and cooling rate but different dwell time and ramp rate. Generally, Ti-6Al-4V tensile components sintered in run ABCD should have better relative density due to its longer dwell time. However, the comparison between run AC and ABCD has proven that lower ramp rate has a stronger impact on the relative density of the component. This is because even through a longer dwell time was applied in run ABCD, its grain boundary mobility is enhanced by the fast ramp rate used. Hence, there is a possibility that a high percentage of pores are trapped in the grains. In addition, prolong dwell time did not aid in eliminating the porosity too.

However, there must be a balance in the ramp rate and the total sintering time. Too long a sintering time is not desirable as it reduces efficiency and also increases production cost. Zhang et al. [33] has explored the use of multiple steps sintering profile to achieve high density Ti-6Al-4V components. The multiple steps sintering cycle has similar effect to using low ramp rate to control the motion of grain boundaries. Therefore, Zhang et al. work can be applied to the future study of this research work by further modifying the current sintering profile to achieve high density Ti-6Al-4V components and also to reduce processing cost. Additional steps can be added to the sintering profile (see Figure 3.15) after the dwell step at 1050 ^{o}C. The ramp rate can be varied between 1050 ^{o}C to the peak temperature, where $\alpha+\beta$ to β phase transformation takes place, to control the grain boundary mobility and grain growth. It is crucial to study the effects of ramp in this region as it determines the microstructures of the component, which in turn affects the physical and mechanical properties.

In conclusion, the three sintering parameters which affect the porosity and density of Ti-6Al-4V tensile components are sintering temperature, dwell time and ramp rate. On the other hand, cooling rate has little effect on the density and porosity.

4.2.4 Effects of Sintering Parameters on Ti-6Al-4V Microstructures

The microstructures of the components sintered under the different runs in DOE were evaluated. The gauge section of the Ti-6Al-4V tensile components were sectioned and mounted for microstructure analysis. The polished samples were then etched in hydrofluoric nitric solution via immersion method to reveal the grain structures. A typical microstructure of sintered Ti-6Al-4V is shown in Figure 4.29. The laminar structure consists of colonies of hexagonal closed packed (hcp) α lamella within the large body center cubic (bcc) β phase grains. This β phase grain is known as prior β grain.

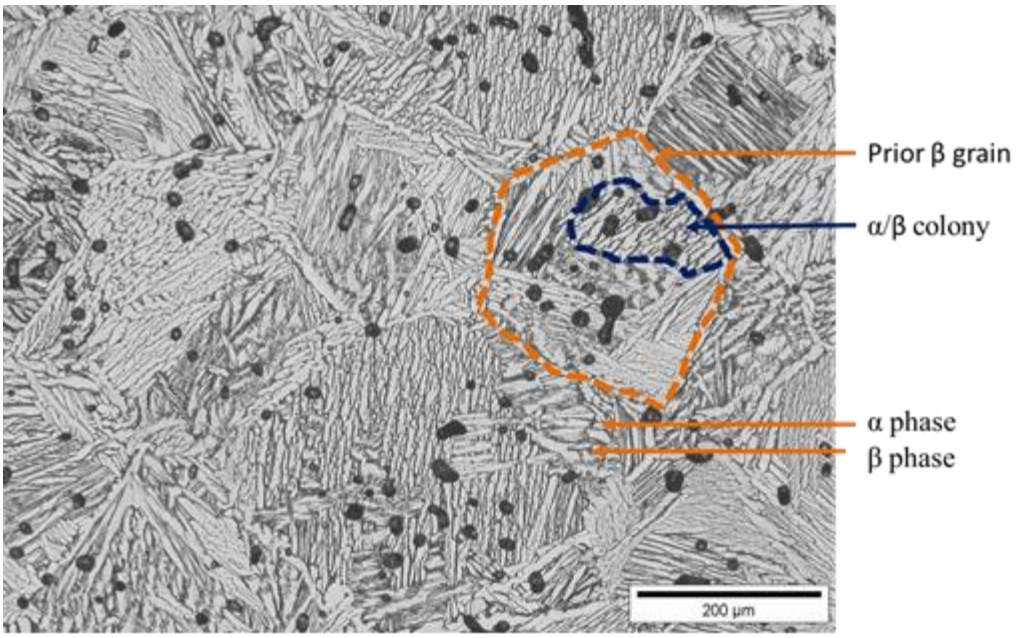

Figure 4.29 Typical microstructure for sintered Ti-6Al-4V.

The etched microstructures of the Ti-6Al-4V components sintered under the different DOE runs are shown in Figure 4.30. Two different types of microstructures were revealed from the etched Ti-6Al-4V components. From Figure 4.30 the microstructures for Ti-6Al-4V components sintered under run CD, AB, BC, AC and ABCD revealed a typical fully laminar structure. As for Ti-6Al-4V components sintered under run 1, AD, and BD, though laminar structures were observed, they contained lower volume fraction of α/β colony and the α plates are also much thicker and broader.

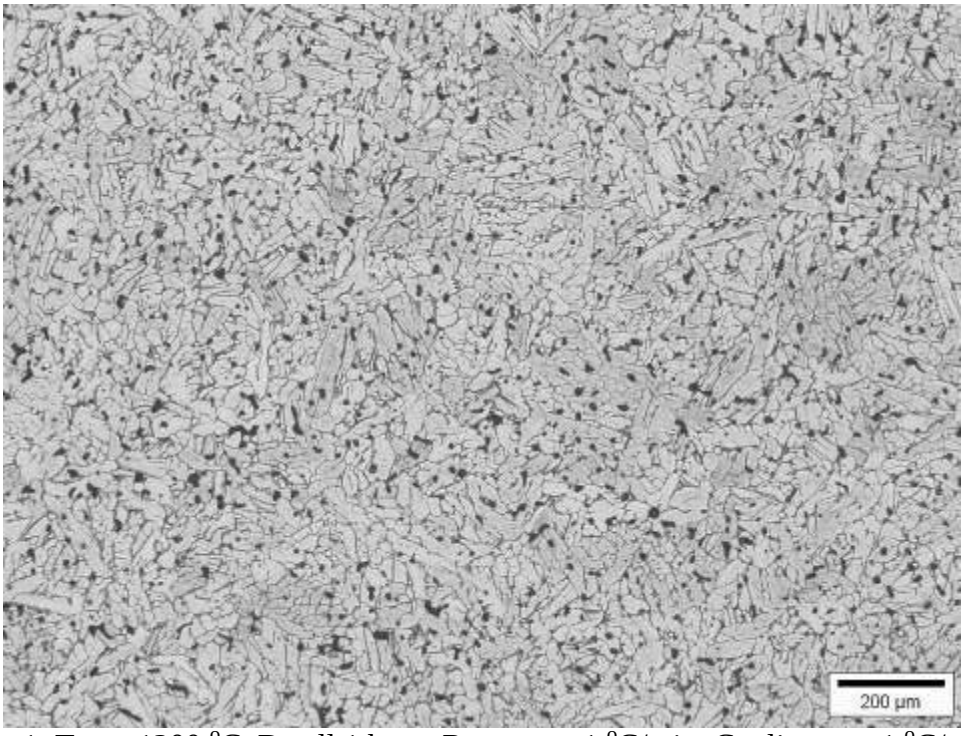

Run 1: Temp 1200 ^{o}C, Dwell 1 hour, Ramp rate 1 ^{o}C/min, Cooling rate 1 ^{o}C/min.

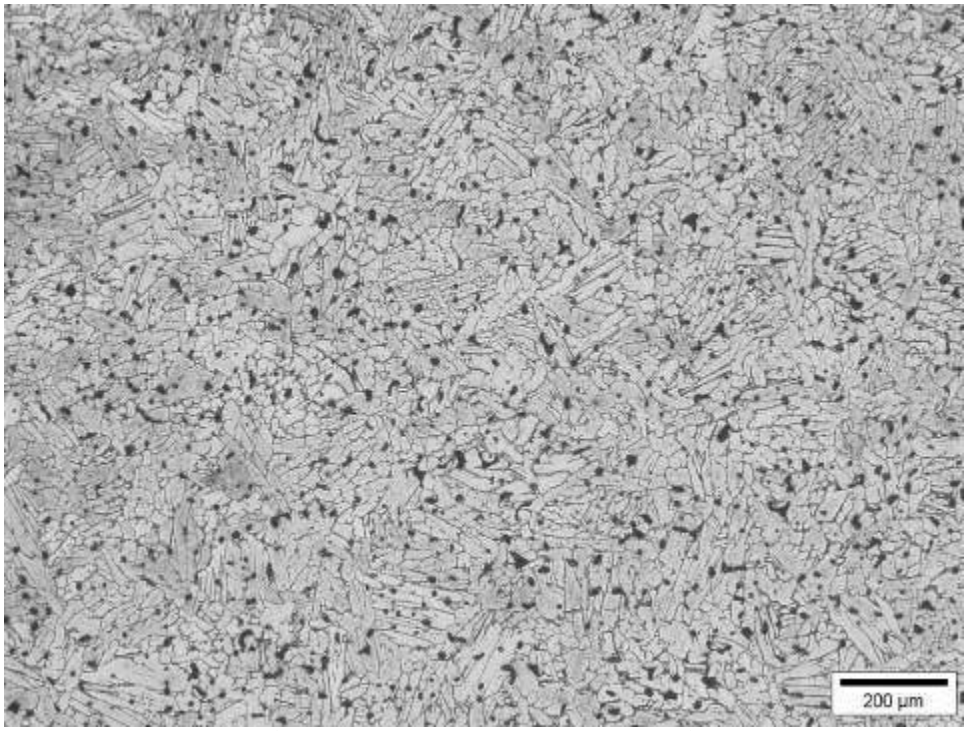

Run AD: Temp 1300 ^{o}C, Dwell 1 hour, Ramp rate 10 ^{o}C/min, Cooling rate 1 ^{o}C/min.

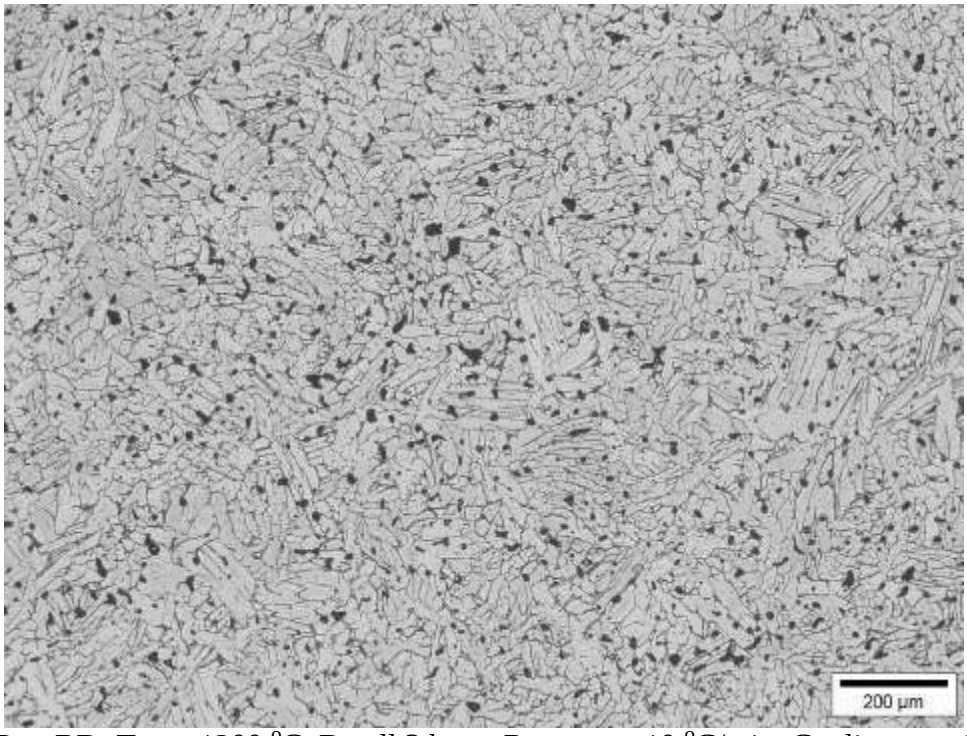

Run BD: Temp 1200 ^{o}C, Dwell 3 hour, Ramp rate 10 ^{o}C/min, Cooling rate 1 ^{o}C/min.

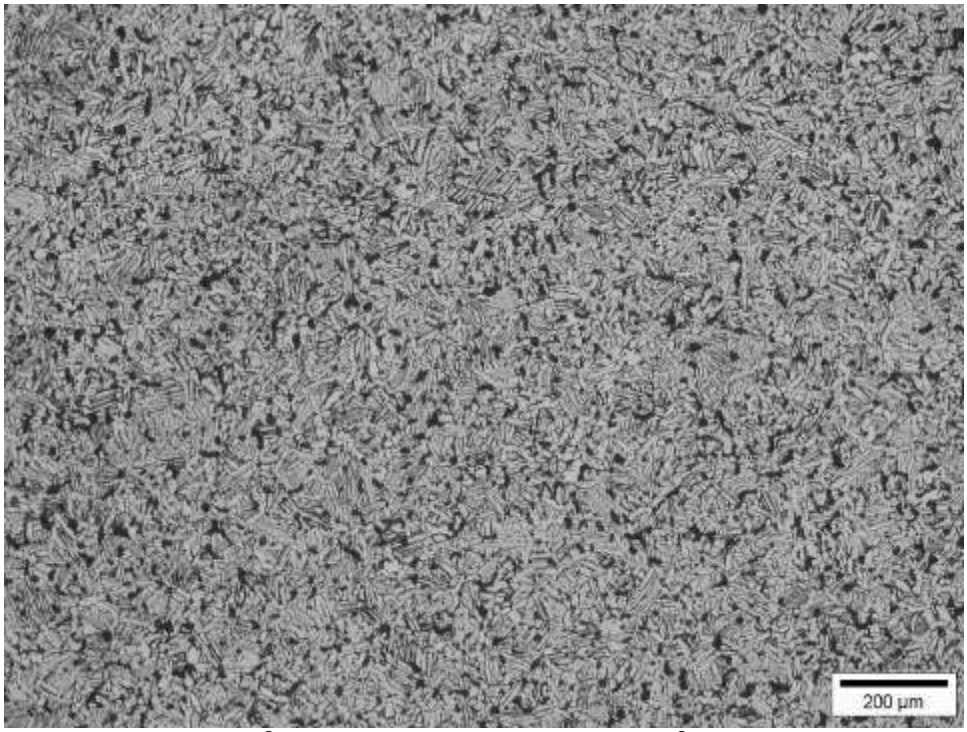

Run CD: Temp 1200 ^{o}C, Dwell 1 hour, Ramp rate 10 ^{o}C/min, Cooling rate 10 ^{o}C/min.

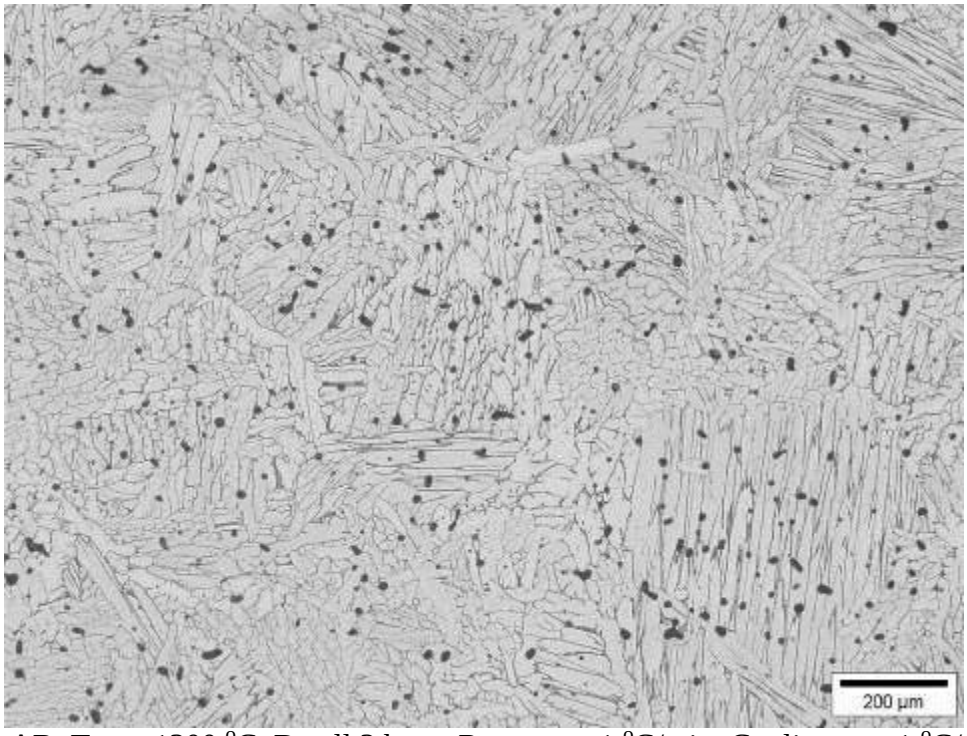

Run AB: Temp 1300 ^{o}C, Dwell 3 hour, Ramp rate 1 ^{o}C/min, Cooling rate 1 ^{o}C/min.

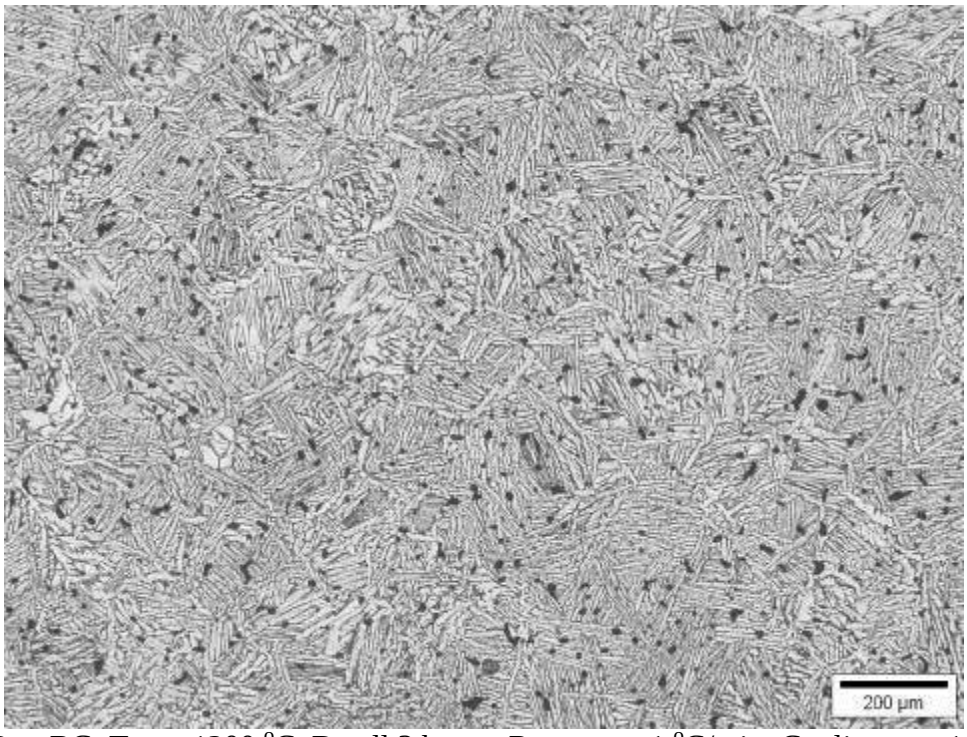

Run BC: Temp 1200 ^{o}C, Dwell 3 hours, Ramp rate 1 ^{o}C/min, Cooling rate 10 ^{o}C/min.

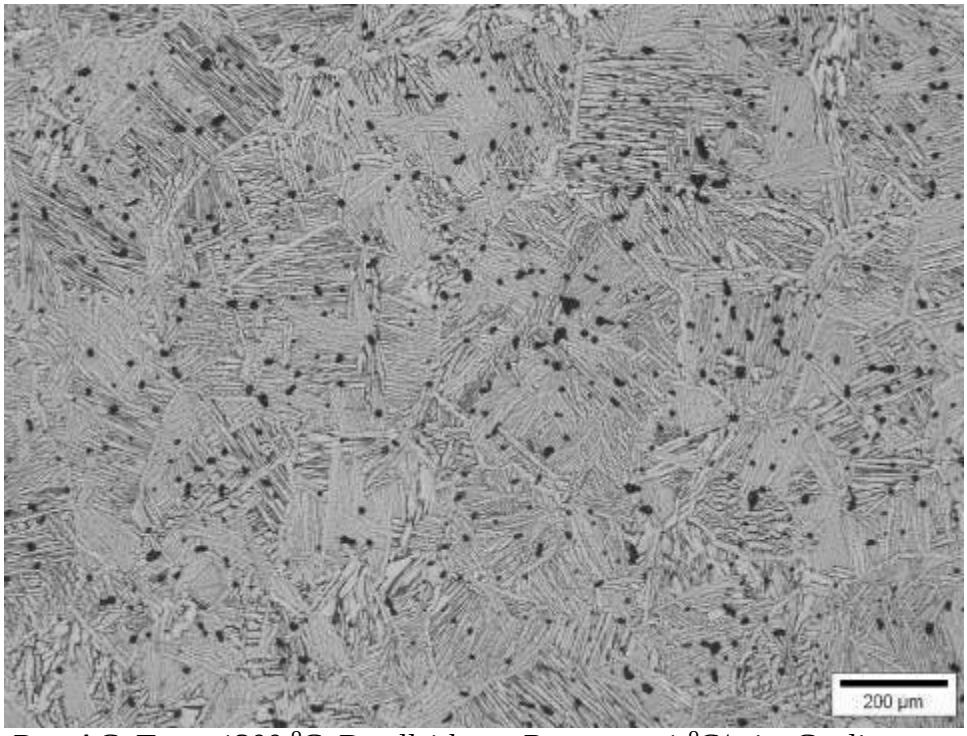

Run AC: Temp 1300 ^{o}C, Dwell 1 hour, Ramp rate 1 ^{o}C/min, Cooling rate 10 ^{o}C/min.

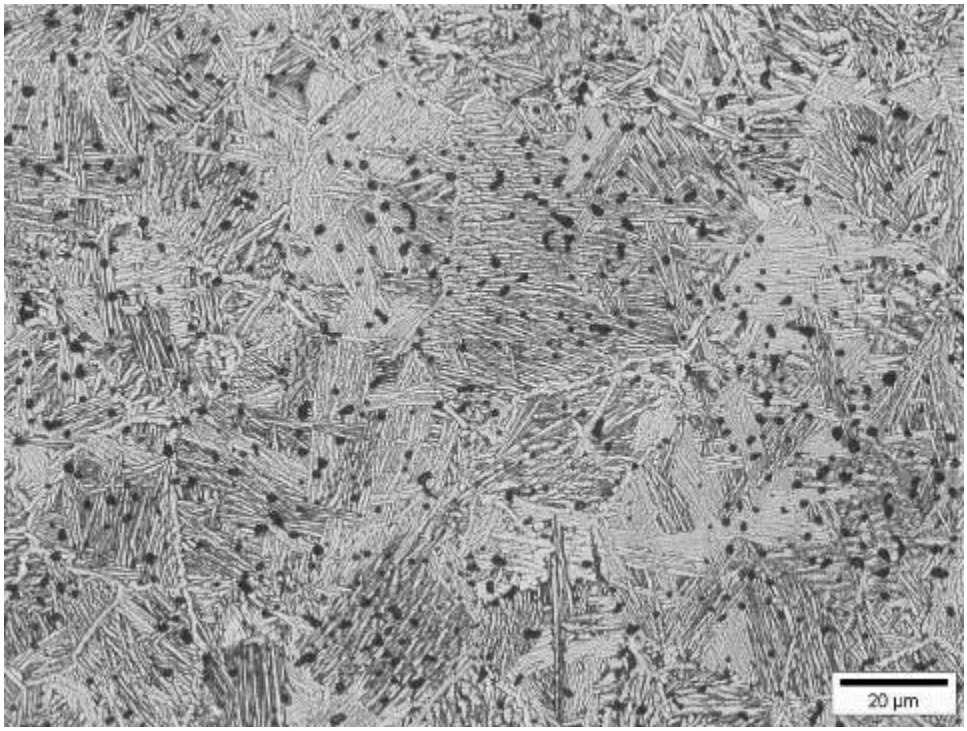

Run ABCD: Temp 1300 ^{o}C, Dwell 3 hour, Ramp rate 10 ^{o}C/min, Cooling rate 10 ^{o}C/min.

Figure 4.30 Microstructures of sintered Ti-6Al-4V under different runs.

Prior β grains were also observed in Ti-6Al-4V components sintered in runs AB, BC, AC and ABCD. The phase diagram of Ti-6Al-4V is presented in Figure 4.31. Based on the phase diagram, β grains formation starts when Ti-6Al-4V is sintered to temperature 990 ^{o}C and above. Since the sintering temperatures selected for this research are above 990 ^{o}C, it favored the formation of prior β grains and hence, they can be observed in some of the microstructures. No distinguishable prior β grains can be identified in the components sintered under runs 1, AD, BD and CD. For component sintered in run CD, the absence of the prior β grains in the structure was due to its incomplete sintering. As for components sintered in runs 1, AD and BD, the reason was probably due to the slower cooling rate used. As illustrated in Figure 4.31, when Ti-6Al-4V was cooled from β to α+β phase, α phase starts to nucleate in and around the prior β grains. With further decrease in temperature into the α+β phase field, α phase starts to grow and forms α/β colonies in the β grains, while a continuous layer of α phase forms around the β grains. The slow cooling process causes the continuous α phase around the β phase to grow to a thickness big enough till they almost "consumed" the β grains. Therefore, very few laminate α grains are induced and the prior β grains cannot be easily identified from the microstructures of the components sintered under these runs. On the other hand, the growth rate of α phase is reduced with increasing cooling rate, hence, reducing the thickness of the continuous α phase around the β grains. More laminate α grains are induced inside of β grains. This makes the prior β grains more distinguishable from the microstructures, as observed in runs AB, BC, AC and ABCD.

The size of α plates, α/β colony and prior β grains were also observed to be different for components sintered under the different sintering parameters. The size of α plate, α/β colony and prior β grain are dependent on the sintering temperature, dwell time, ramp rate and cooling rate. The thickness of α plates and prior β grains size were measured and tabulated in Table 4.21.

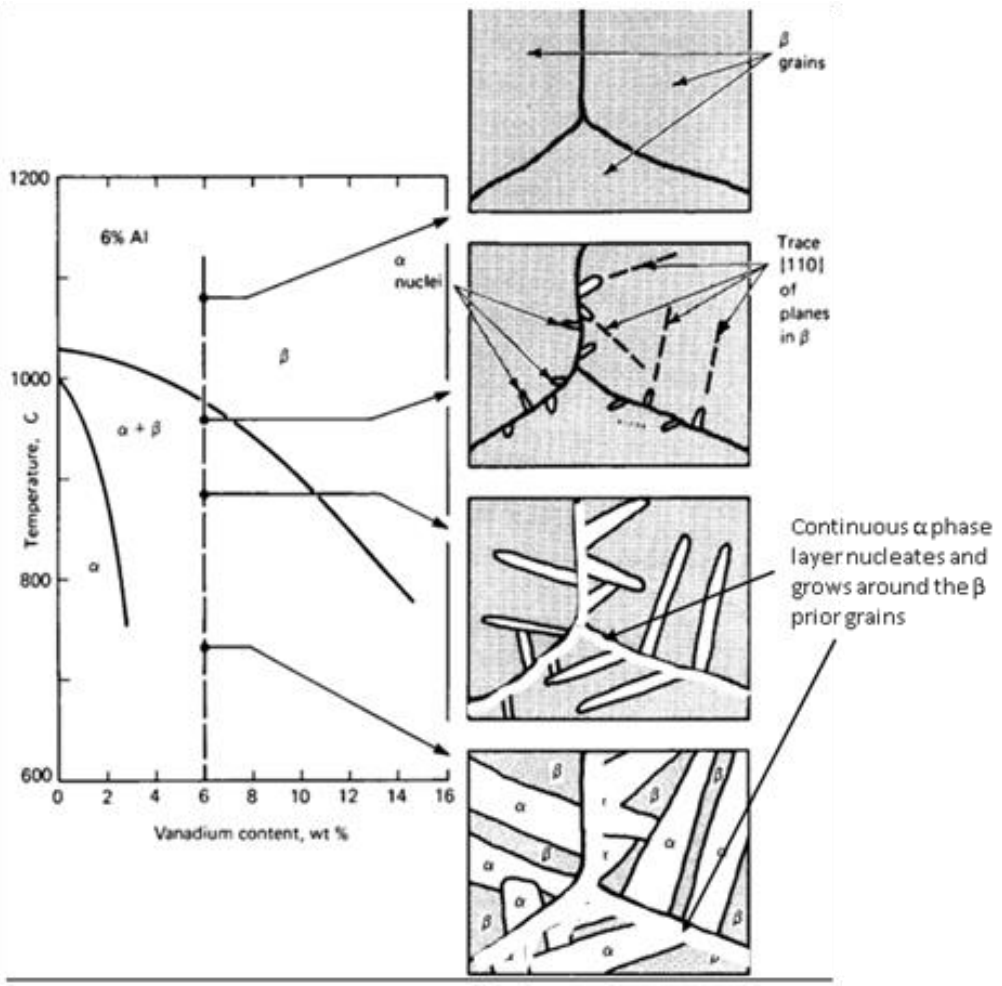

Figure 4.31 Phase diagram of Ti-6Al-4V [37].

Table 4.21 Prior β grain size and α phase thickness of sintered Ti-6Al-4V.

Run	Parameter				Average Prior β Grain Size (μm)	α phase thickness (μm)
	Temp (^oC)	Dwell Time (h)	Cool (^oC/min)	Ramp (^oC/min)		
1	1200	1	1	1	Nil	24.0
AD	1300	1	1	10	Nil	28.0
BD	1200	3	1	10	Nil	24.9
CD	1200	1	10	10	Nil	8.3
AB	1300	3	1	1	>400	19.5
BC	1200	3	10	1	247	11.1
AC	1300	1	10	1	353	9.3
ABCD	1300	3	10	10	271	8.1

Nil – unable to measure

It can be observed from Table 4.21 and Figure 4.30 that components sintered under runs 1, AD, BD and AB, have coarser α plates and larger α/β colonies, as compared to those sintered under run CD, BC, AC and ABCD. This was due to the cooling rate used in these run parameters. As indicated in Table 4.21, a lower cooling rate of 1 ^{o}C per minute was used for runs 1, AB, BD and AB as compared to runs CD, BC, AC and ABCD, which have cooling rates of 10 ^{o}C per minute. Based on Figure 4.31, when Ti-6Al-4V was cooled from β to α+β phase field, from the peak sintering temperature of 1200 ^{o}C or 1300 ^{o}C, nucleation of α phase occurs in the β grain boundaries. Slower cooling rate lowers the rate of nucleation of α phase and increases the rate of diffusion process (enhanced growth rate). Therefore, coarser α plates and larger α/β colonies were observed in components cooled using lower cooling rate. This phenomenon can also be further explained using the nucleation rate and grain growth rate equations shown in equations 4 and 5, respectively. As presented in equations 4 and 5, at slower cooling rate the overall temperature of the system remains higher as compared to one with a higher cooling rate. Therefore, by substituting T, with a high value, the overall rate of nucleation, I, decreases while growth rate, U, increases.

$$I = \beta\,[N \exp(-\Delta G^*/kT)] \qquad (4)$$

where,

I is the nucleation rate.

β is the is the rate at which atoms join critical nuclei (s-1), thereby making them stable.

G is critical free energy.

k is Boltzmann constant.

T is temperature.

$$U = n v_0 \lambda exp\left(-\frac{q}{RT}\right)[\,1 - \exp(-\frac{\Delta G}{RT})] \quad (5)$$

where,

U is the grain growth rate.

n is grain growth exponent.

v_0 is the velocity of the grain boundary.

q is the activation energy for boundary mobility

G is critical free energy.

T is the temperature.

R is the gas constant.

In addition, slower cooling rate also tend to form α phase with less laminar typed structures, which is evident in the microstructures for runs 1, AC and BD, where a small percentage of the α phase appeared broader and slightly roundish. However, with increasing cooling rate, the rate of nucleation of α phase increases. The α/β colonies nucleating in the β grains are not able to fill the whole grain interior, hence, other colonies start to nucleate at the boundary of the initial colonies [38]. In order to minimise the elastic strain, new α plates nucleate by "point" contact on the broad face of existing α plates and new α/β colonies are then formed nearly perpendicular to the initial colonies [40]. Faster cooling rate also decreases the rate of diffusion hence leading to finer α plate. This eventually led to the formation of Widmanstätten microstructure in the components, which are evident in the microstructures of the components sintered under run BC, AC and ABCD, as shown in Figure 4.30.

The prior β grains size presented in Table 4.21 were measured using ASTM E112-10 linear intercept method. This method involves the counting of the number of grains or grain boundary being intercepted by the test lines, per unit length of line, to calculate the lineal intercept length, l. This is then used to determine the ASTM grain size number, G. It was observed from Table 4.21, the average grain size of

the prior β grains ranges from 247 to above 400 μm with different sintering conditions, which are much bigger than the initial Ti-6Al-4V powders (D_{50} approximately 24.70 μm). Another observation made was Ti-6Al-4V components sintered at 1200 ^{o}C have smaller prior β grains than those sintered at 1300 ^{o}C. This is because the driving force for grain growth is to lower the total boundary energy and this is achieved with increasing temperature as the rate of grain growth increases with temperature. The mobility of the grain boundary also increases with increasing temperature. Hence, the tendency for larger grains to grow at the expense of the smaller ones is higher with increasing temperature. Therefore, components sintered under higher sintering temperatures tend to have larger grains than those sintered at lower temperatures.

Besides the grain structures, the pore characteristic can also be inferred from the etched microstructures. In general, spherical and isolated pores were noted in most of the sintered Ti-6Al-4V components. This indicates that the sintering combinations selected were suitable in producing fully sintered Ti-6Al-4V components. High percentage of interconnected porosity was however, observed in Ti-6Al-4V sintered under run CD, which indicates incomplete sintering. This was due to the combination of low sintering temperature and dwell time used. Therefore, the sintering parameters used in this run is not suitable for achieving fully sintered components, which will have a detrimental effect on the integrity and mechanical properties of the component.Pores were also observed to be within the grains of the components sintered under all the run combinations. As mentioned earlier, this is not desirable as it reduces the density of the components and they cannot be removed with additional sintering process. Therefore, even though some of the sintering parameters selected were able to produce a fully sintered structures, improvements to the sintering profile and parameters is required to prevent pore entrapment within the grains.

4.2.5 Effects of Ti-6Al-4V Microstructures on Mechanical Properties

The UTS and elongation of the sintered Ti-6Al-4V components were measured by tensile testing. Table 4.22 lists the average UTS and elongation for the Ti-6Al-4V components sintered under the different sintering parameter tabulated the DOE design. Average readings of three measurements were taken for each run.

From Table 4.22, it can be observed that Ti-6Al-4V components sintered under runs AB, BC, AC and ABCD overall have better UTS (~882 – 904 MPa) and elongation (~13 – 17%) as compared the rest of the runs. Run AB, which has the highest elongation (~ 17 %), coincided with our DOE conclusion in the earlier section whereby elongation is enhance with longer dwell time and lower ramp rate. The difference in the mechanical properties between components sintered in runs AB, BC, AC and ABCD and runs 1, AD, BD and AC was believed to be due to their microstructures. Elongated and finer α plates were observed in Ti-6Al-4V components sintered in runs AB, BC, AC and ABCD. On the other hand, Ti-6Al-4V components sintered in runs 1, AD and BD have broader and thicker α plates. The differences in the shape of the α plates were believed to be the cause for the dissimilarities in the mechanical properties. Broad and less elongated α phase lowers the strength within the platelet region as compared to fully laminar structure. Therefore, this caused the mechanical properties for Ti-6Al-4V components sintered in runs 1, AD and BD to be less superior to those in runs AB, BC, AC and ABCD. As for Ti-6Al-4V components sintered in run CD, their inferior mechanical properties, were attributed by the relatively high porosity and low relative density, which was a resultant of incomplete sintering. This is evident in its microstructure displayed in Figure 4.30, which showed a relatively large quantity of interconnected porosity.

Table 4.22 Mechanical properties of Ti-6Al-4V sintered under different runs.

Run	Parameter				Average Elongation (%)	Average UTS (MPa)
	Temp (^oC)	Dwell Time (h)	Cool (^oC/min)	Ramp (^oC/min)		
1	1200	1	1	1	13.80	833.64
AD	1300	1	1	10	7.89	826.57
BD	1200	3	1	10	11.42	838.55
CD	1200	1	10	10	6.95	821.84
AB	1300	3	1	1	17.15	882.77
BC	1200	3	10	1	14.86	894.21
AC	1300	1	10	1	13.29	904.49
ABCD	1300	3	10	10	14.44	900.40

The mechanical properties of Ti-6Al-4V components with lamellar microstructures are also dependent on the size of the α/β colonies [38]. This is because α/β colonies determine the effective slip length in the lamellar microstructures [38]. Smaller α/β colonies improve yield strength, ductility and crack propagation resistance [36]. As the α/β colony size was not measured in this study, α plate thickness was used as a comparison instead. The UTS and elongation of the sintered Ti-6Al-4V components were plotted against α plate thickness and are presented in Figure 4.32 and Figure 4.33, respectively. From the plot of UTS verse α plate thickness, Ti-6Al-4V components with smaller α plate thickness (runs AC, BC and ABCD) had better UTS as compared to those with thicker α plates (runs AB, 1, BD and AC). Similar trend was also observed for the plot of elongation verse α plate thickness in Figure 4.33. A decreasing elongation value was noted when α plate thickness was more than 20 μm. Therefore, the earlier discussion on the α/β colonies size against the mechanical properties holds. In general, sintered Ti-6Al-4V components with smaller α plate thickness have better elongation and UTS as compared to those with bigger α plate thickness. Based on the plots in Figure 4.32 and Figure 4.33, smaller α plate thickness was observed in Ti-6Al-4V components cooled at faster cooling rate (10 ^oC / minute). As explained earlier, faster cooling rate induces faster rate of nucleation and lower diffusion rate of α phase.

In the case of run CD, lower UTS and elongation were observed even through the α plate thickness was relatively small. The cause for this was incomplete sintering of the components.

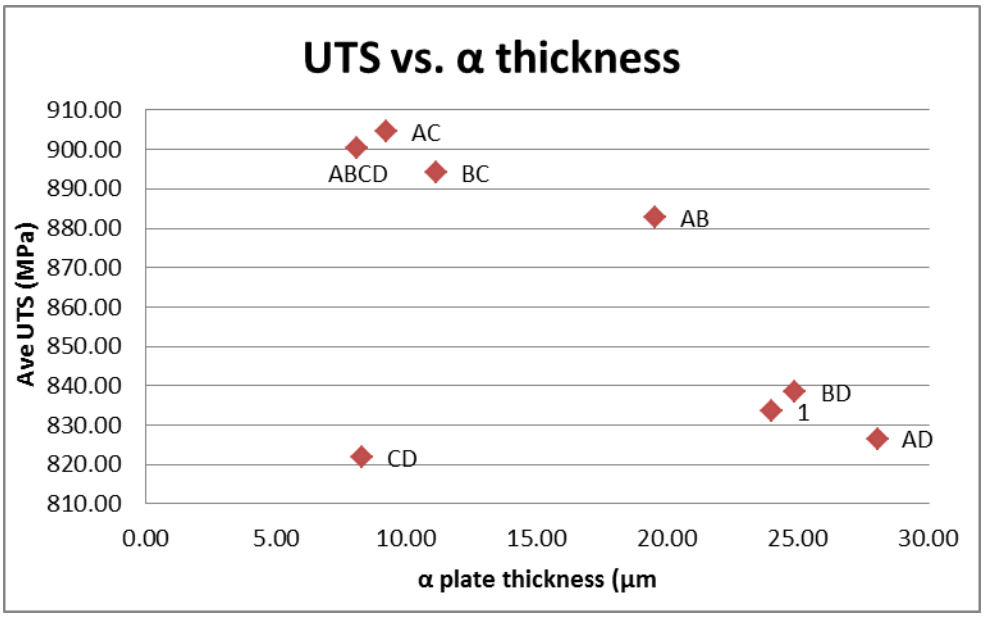

Figure 4.32 Plot of UTS vs. α plate thickness.

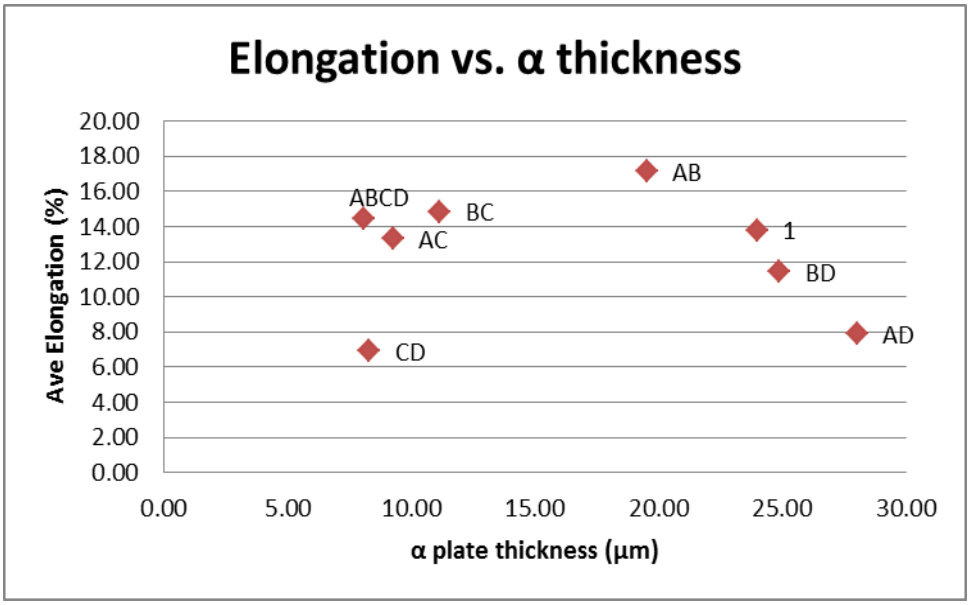

Figure 4.33 Plot of elongation vs. α plate thickness.

The trend on the sintered Ti-6Al-4V components UTS and elongation verse their relative densities are plotted in Figure 4.34 and Figure 4.35, respectively. From the plot of UTS verse relative density in Figure 4.34, higher UTS were generally observed in Ti-6Al-4V components with higher relative density (> 97 %). Exceptions were noted for Ti-6Al-4V components sintered in run AD and BD. This is because in addition to the relative density, UTS is also affected by the type of microstructures formed and also the size of their grain structures. Therefore, even though Ti-6Al-4V components sintered in run AD and AB achieved relative densities above 97 %, the size and shape of the α plates in the microstructures had affected their UTS and elongation values.

A similar trend was observed for the plot of elongation verse α plate thickness in Figure 4.35. An increased in elongation was observed with increasing relative density. This is because higher relative density translates to lower porosities. Pores are potential stress concentration sites, hence, they degrade the mechanical properties. Therefore, to achieve sintered component with good mechanical properties a relative high density and low porosity is desirable. An exception was noted for Ti-6Al-4V components sintered in run AD, where an elongation of only 7.89 % was measured. Again, cause for the poor elongation was due to the size of α plates. Ti-6Al-4V components sintered in run AD had α plates measuring up to 28 μm, which is the largest among all the other runs.

Another observation made from Figure 4.35 was the increment in elongation becomes less obvious at relative density above 96 %. Therefore, the effect on relative density on elongation becomes less significant when the relative density is more than 96 %.

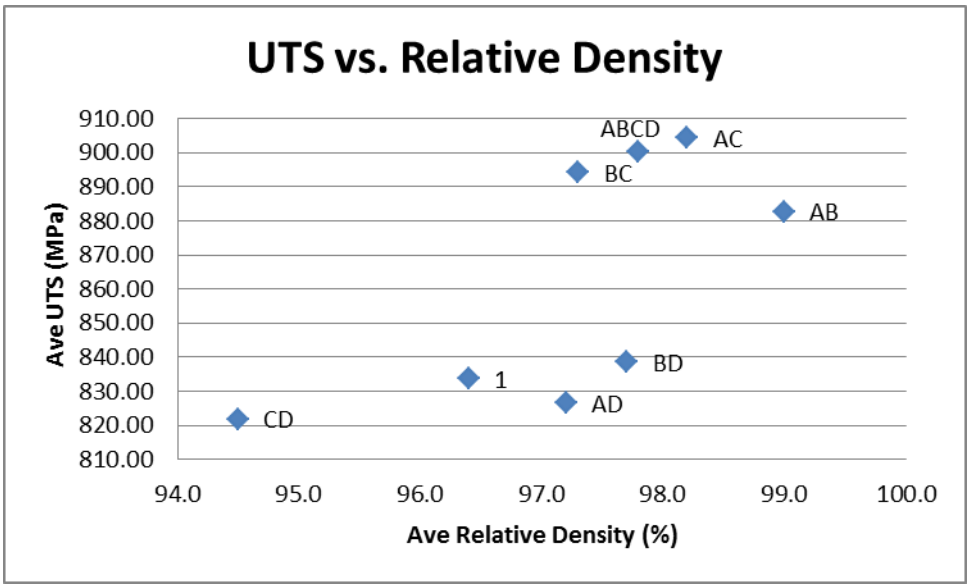

Figure 4.34 Plot of UTS vs. relative density.

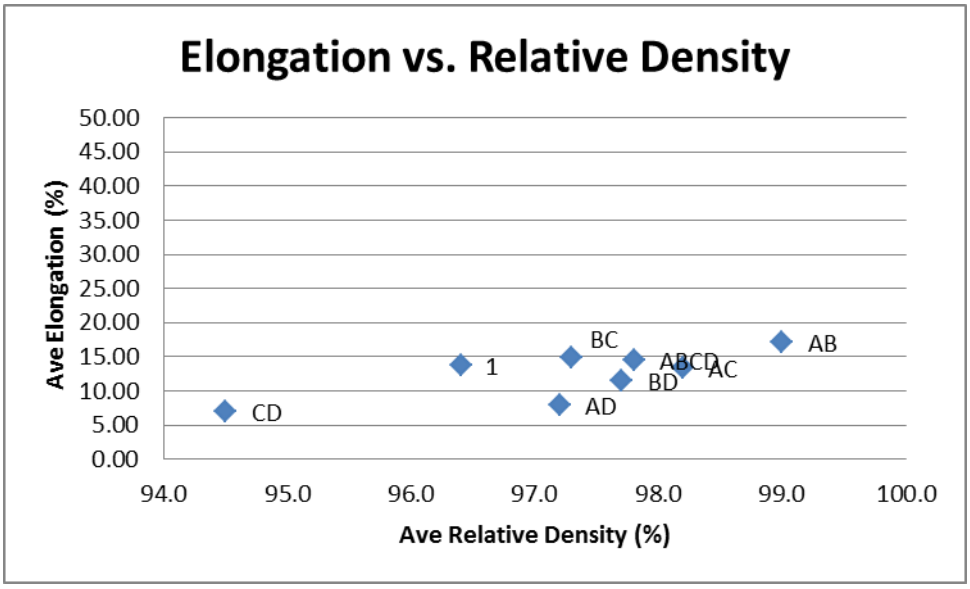

Figure 4.35 Plot of elongation vs. relative density.

Lastly, based on the UTS and elongation results from Table 4.22, it can be concluded that the sintering parameters selected are able to produce components that meets the tensile properties of Grade 5 Ti-6Al-4V. The ASTM standard for tensile properties of Grade 5 Ti-6Al-4V is tabulated in Figure 4.23. Ti-6Al-4V tensile components sintered in run BC, AC and ABCD have achieved the tensile properties equivalent to or better than Grade 5 Ti-6Al-4V.

Table 4.23 ASTM B265 – Grade 5 Ti-6Al-4V.

	YS (MPa)	UTS (MPa)	E (GPa) (typical)	Elongation in 50mm, %	Chemical Composition (maximum in wt. %)				
					O	N	C	H	Fe
Grade 5 Ti-6Al-4V	>828	>895	114	>10	0.20	0.05	0.08	0.015	0.04

4.2.6 Comparison of Mechanical Properties to Other Research Work

Several research work have been conducted in the PIM of Ti-6Al-4V as discussed in Chapter 2. Table 4.24 tabulates the mechanical properties of PIM Ti-6Al-4V components gathered from the various research studies. According to the values in Table 4.24, the UTS and elongation of PIM Ti-6Al-4V components ranged from 541 – 880 MPa and 0.9 – 16.0 %, respectively. A wide range of mechanical data was observed as the mechanical values were dependent on the binder system, solid loading, debinding and sintering profiles, and final interstitial contents in the sintered component. German et al. [47] also found that the tensile strength of sintered Ti-6Al-4V varies with the type of powder used and the processing parameters, and generally the mechanical properties of PIM Ti-6Al-4V components are lower than wrought Ti-6Al-4V (UTS ~ 950 MPa, elongation ~ 14 %). For fully sintered PIM Ti-6Al-4V components with oxygen content less than 2000 ppm, they achieved an elongation of 12 % and tensile strength ranging from 710 – 850 MPa [47].

Based on the mechanical properties measured from the DOE studies in Table 4.22, the UTS and elongations obtained from some of the DOE runs in this research study fell within the range or better than those tabulated in Table 4.24.

Table 4.24 UTS and elongation values of sintered PIM Ti-6Al-4V obtained from various sources.

UTS (MPa)	Elongation (%)	Reference Number
826.57 - 904.49	7.89 - 17.15	Table 4.22
800	15.0	2
852 - 880	8.5 - 16.0	4
850	12.0	6
800	15.0	21
541.53	0.90	47
700 - 790	15.0	48
832 - 861	13.4 - 15.5	49
760	11.0	50

*Note: data presented are only for gas atomised Ti-6Al-4V powders.

CHAPTER 5 CONCLUSIONS

In the first phase of the research, CP-Ti tensile components were successfully fabricated via the PIM process. Mechanical results showed that CP-Ti components sintered under all three temperatures (1240 ^{o}C, 1260 ^{o}C and 1280 ^{o}C) in argon have met the targeted UTS of grade 3 CP-Ti (> 450 MPa) but still lacked in elongation. Elongation of less than 10 % was measured for all components. This was lower than the targeted value of >18 %. Variations in the mechanical results were also observed due to non-uniform shrinkage of the components. This was a resultant of partial bonding between the component and the sintering plate during sintering. The microstructures of sintered CP-Ti components revealed needle-liked structures containing small percentages of Fe. Oxides peaks were also detected in the XRD spectra of components sintered at 1240 ^{o}C and 1280 ^{o}C. This was related to interstitial elements contamination, which were picked up from the binder or during the processing steps. The relative densities of the sintered CP-Ti components were also less than the targeted value of 98 %. Components sintered under all three temperatures had relative densities of only 95 %. This was attributed by argon gas entrapment during sintering, which created large quantity of porosities in the microstructures.

In the second phase of the research, the problems encountered in the first phase were rectified to improve the fabrication process and mechanical properties of Ti-6Al-4V tensile components. The following modifications were made to the fabrication process of Ti-6Al-4V:

- Modification to the binder composition. CW was removed from the original binder formula as TGA studies showed it may cause C and O contaminations.
- Modification to the sintering plate. The sintering plate was replaced by ceramic coated Mo plate to eliminate bonding between the component and the sintering plate during sintering.

- Modification to the sintering environment. The sintering environment was switched to vacuum to inhibit argon gas entrapment in the component.

After the improvement works have been implemented, DOE on sintering was conducted to examine the effects of each sintering parameters on the UTS and elongation of Ti-6Al-4V components. The parameters studied were sintering temperature, dwell time, ramp rate and cooling rate. Base on the DOE studies, it was found that:

- Dwell time and ramp rate have significant effects on the elongation.
- Longer dwell time and slower ramp rate have positive influence on the elongation.
- Sintering temperature, dwell time, ramp rate and cooling rate have significant effects on the UTS.
- Higher UTS can be achieved with higher sintering temperature, longer dwell time, slower ramp rate and faster cooling rate.
- Some components sintered in the DOE experiment have achieved average UTS of up to 900 MPa and elongation up to 17 % and have met the targeted UTS (> 895 MPa) and elongation (> 10 %) for Grade 5 Ti-6Al-4V.

The porosity and the density of the sintered Ti-6Al-4V components were analysed. Most of the sintered Ti-6Al-4V components have relative densities of at least 97 %. A relative density of only 94 % was obtained for one run, which was attributed by incomplete sintering. Significant improvement on the relative density was observed as compared to the first phase of the research work. This is because sintering in a high vacuum environment eliminated the issue on gas entrapment hence, reducing the amount of porosity. In addition to the sintering environment, it was found that sintering parameters such as ramp rate, dwell time and sintering temperature also affected the porosity and relative density.

The tensile properties of the sintered Ti-6Al-4V components were also affected by the density and porosity values. In general, it was observed that Ti-6Al-4V tensile components with relatively high density and low porosity have better UTS and elongation and vice versa.

The microstructures of the sintered Ti-6Al-4V components were also examined and compared to the sintering parameters. The following deductions were from made based on the microstructure analysis:

- Size of α plate, α/β colony and β prior grain are dependent on the sintering temperature, dwell time, ramp rate and cooling rate.
- Coarser α plates and larger α/β colonies were observed in components cooled using lower cooling rate.
- α phase with broader and less elongated structures are formed with slower cooling rate.
- Sintered Ti-6Al-4V tensile components with smaller α plate thickness have better elongation and UTS as compared to those with bigger α plate thickness.
- β prior grains were observed in components cooled using higher cooling rate and its size increases with increasing sintering temperature.

CHAPTER 6 FUTURE WORK

Primary work on DOE studies on the sintering of Ti-6Al-4V only indicated which sintering parameters have significant effect on the UTS and elongation. Further work can be done to examine the value for each parameter which will yield the highest UTS and elongation. This can be done by general regression method to predict the response for the entire range of values used for each significant factor.

The microstructures of the sintered Ti-6Al-4V components showed porosity trapped within the grains. Therefore, future work will look into improving the sintering profiles (i.e. ramp rate) so as to prevent pore entrapment in the grains and also improve the relative density. Multiple steps sintering also can be applied to current sintering profile after 1050 ^{o}C to control grain boundary mobility. Mechanical properties are also dependent on the position of the pores in the grain structures hence, it is essential to reduce or eliminate pore entrapment. Current research work has also indicated that α plate affects the mechanical properties of Ti-6Al-4V. Therefore, further work can be done to examine how to control the size and shape of the α plate to improve the mechanical properties of Ti-6Al-4V.

After improvement works on the sintering profile has been completed, the fatigue strength of PIM Ti-6Al-4V components will also be examined in the future work. For this study, Ti-6Al-4V will need to be moulded into fatigue bars.

The current experimental work mainly focused on the physical and mechanical properties of the Ti-6Al-4V components. Therefore, for future work, minor elements analysis on the sintered components can be conducted to quantitatively examine the interstitial elements such as carbon, oxygen and nitrogen in the sintered components. A comparison in the minor elements content will also be made between components with and without CW in the binder. This is to examine if CW is a possible source of contamination.

References

1. F.H (Sam) Froes, “Getting better: big boost for Ti MIM prospects”, Metal Powder Report, 2009, Vol. 3, No. 4, pp 21-37.

2. O.M. Ferri, T.Ebel, R. Bormann, "High cycle fatigue behaviour of Ti-6Al-4V fabricated by metal injection moulding technology", Materials Science and Engineering A, 2009, Vol. 504, No, 1-2, pp 107-113.

3. E. Baril, "Titanium and titanium alloy Powder Injection Moulding: Matching application requirements", Powder Injection Moulding International, 2010, Vol. 4, No. 4, pp 22-32.

4. A.T. Sidambe, I.A Figueroa, H. Hamiltom, I. Todd, "Metal injection moulding of Ti-64 components using a water soluble binder", Powder Injection Moulding International, 2010, Vol. 4, No. 4, pp 56-62.

5. Brian E. Hurless, F.H. (Sam) Froes, “Lowering the Cost of Titanium”, AMPTIAC Quarterly, Vol. 6, No. 2, pp 1-23.

6. R.M German, “Titanium Powder Injection Moulding: A Review of the current status of materials, processing, properties and applications”, Powder Injection Moulding International, 2009, Vol. 3, No. 4, pp 21-37.

7. D. Whittaker, “Developments in the PIM of Ti”, Powder Injection Moulding International, 2007, Vol. 1, No. 1, pp 27-32.

8. Guo Shibo, Qu Xuanhui, He Xinbo, Zhou Ting, Duan Bohua “Powder injection molding of Ti-6Al-4V alloy”, Journal of Materials Processing Technology, 2006, Vol. 173, pp 310-314.

9. R.M. German (1991). "Metal Powder Injection Moulding". In I. Jenkins and J.V. Wood (EDs), Powder Metallurgy - An Overview, pp 102-113. Great Britain: The Institute of Metals.

10. R.M German, Animesh Bose, "Injection Molding of Metals And Ceramics", Metal Powder Industries Federation, Princeton, New Jersey, 1997.

11. R.M. German, "Powder metallurgy and particulate materials processing: the processes, materials, products, properties and applications", Metal Powder Industries Federation, Princeton, New Jersey, 2005.

12. C.H Ji, "Mechanical Properties of Metal Injection Molding (MIM) Parts", 1998, M.Eng. Thesis, Nanyang Technological University, Singapore.

13. Mannschatz A, Axel Muller, Tassilo Moritz, "Influence of powder morphology on properties of ceramic injection mouding feedstocks", Journal of the European Ceramic Society, 2011, Vol. unknown, pp. unknown.

14. Pavan Suri, Sunfar V. Atre, Randall M. German, Jupiter P. de Souza, "Effect of mixing on the rheolgoy and particle characteristics of tungsten-based powder injection molding feedstock", Materials Science and Engineering A356, 2003, Vol. 356, No. 1-2, pp 337-344.

15. SHS IBDT Guide to Manufacturing Processes. Shaping Processes. Retrieved on 28th June 2011 from http://www.schenectady.k12.ny.us/users/pattersont/IBDT%20website/Page_Generators/Shaping%20Processes.html.

16. O.M. Ferri, "Optimisation of Fatigue Behaviour of Ti-6Al-4V Alloy Components Fabricated by Metal Injection Moulding", 2010, Ph.D. Thesis, Technischen Universität Hamburg-Harburg, Germany.

17. Suk-Joong L. Kang, "Sintering: Densification, Grain Growth, and Microstructure", Elsevier Butterworth-Heinemann, Oxford, 2005.

18. J.M Benson, H.K Chikwanda, "The challenges of Ti Metal Injection Moulding", Transportation weight reduction: 8th Annual International RAPDASA Conference, Tshwane University of Technology and Pilanesburg, South Africa, 7-9th November 2007, pp 11.

19. Mimest SpA, "Mimest: Developing a market in Italy for MIM titanium and performance products", Powder Injection Moulding International, 2010, Vol. 4, No. 3, pp. 35-37.

20. Osaka Yakin Kogyo: Investments reflect optimistic outlook for MIM of titanium, Powder Injection Moulding International, 2008, Vol. 2, No, 2, pp 33-36.

21. TiJet (2010). Innovative Injection Molding of Titanium. Retrieved on 12th November 2010 from http://www.tijet.de/en/?Downloads.

22. TiJet (2011). Examples. Retrieved on 16th July 2011 from http://www.tijet.de/en/?Examples.

23. Colin McCracken, Dan Barbis, "Production of fine titanium powders via the Hydride Dehydride (HDH) process", PIM International, 2008, Vol. 2, No. 2, pp 55-57.

24. K. Kusaka, T. Kono, A. Horata, "Tensile behavior of Sintered Ti and Ti-6Al-4V Alloy by MIM Process", Advances in Powder Metallurgy and Particulate Materials, 1996, Vol. 5, pp 127-131.

25. Powder Injection Moulding International (2011). Binders and Binder Removal Technique. Retrieved on 20th May 2011 from http://www.pim-international.com/aboutpim/mim_materials.

26. E. Carreño-Morelli, W. Krstev, B. Romeira, M. Rodriguez-Arbaizar, H. Girard, J.-E. Bidaux, S. Zachmann, "Titanium parts by PIM of TiH2 - based feedstocks", Powder Injection Moulding International, 2009, Vol. 4, No. 3, pp 60-63.

27. Guo Shibo, Duan Bohua, He Xinbo, Qu Xuanhui, "Powder injection molding of pure titanium", Rare Metals, 2009, Vol. 28, No. 3, pp 261.

28. Eric Nyberg, Megan Miller, Kevin Simmons, K. Scott Weil, "Microstructure and mechanical properties of Ti components fabricated by a new powder injection molding technique", Materials Science & Engineering C, 2005, Vol. 25, No. 3, pp 336-342.

29. F.H (Sam) Froes, "Advances In Titanium Metal Injection Molding", 2007, Powder Metallurgy and Metal Ceramic, Vol. 46, No. 5-6, pp 303-310.

30. A.F. Galio, L. Schaeffer, "Characteristics of titanium parts produced by powder injection moulding", Journal of Engineering Manufacture, 2006, Volume 220, No. 5, pp 783-786.

31. "Research efforts highlight trends in PIM titanium implants", Powder Injection Moulding International, 2010, Vol. 4, No. 3, pp 26-27.

32. L.P. Lefebvre, E. Baril, "Effects of Oxygen Concentration and Distribution opn the Compression Properties of Titanium Foams", Advance Engineering Materials, 2008, Vol. 10, No. 9, pp 868-876.

33. R. Zhang, J. Kruszewski, J. Lo, "A study of the effect of sintering parameters on microstructure and properties of Ti6Al4V", 2008, Powder Injection Moulding International, Vol. 2, No. 3, pp 74-78.

34. E. Baril, L.P. Lefebvre, Y Thomas, "Interstitial sources and control in titanium P/M processes", PM2010 World Congress, October 10-14, Florence, Italy, 2010.

35. D. F. Heaney, R.M. German, "Advances in the Sintering of Titanium Powders", PM Lightweight and Porous Materials, 2004, Vol. unknown, No. unknown, pp unknown.

36. Robert Pederson, "*Microstructure and Phase Transformation of Ti-6Al-4V*", Licentiate Thesis, Lulea University of Technology, 2002.

37. Donachie, Jr., Matthew J, "Titanium - A Technical Guide", ASM International (2nd Edition), 2002.

38. G. Lutjering, J. C. Williams, "Titanium", Springer, 2007.

39. G. Lutjering, "Influence of processing on microstructure and mechanical properties of (α+β) titanium alloys", 1998, Materials Science Engineering, Vol. A243, pp. 32-45.

40. Edgar Javier Rodriguez Robles, "*Effect of Boron on the Microstructure and Properties of Ti-6Al-4V*", 2010, Master Thesis, Lulea University of Technology,

41. Wikipedia (2011). Laser Diffraction Analysis. Retrieved on the 19th July 2011 from http://en.wikipedia.org/wiki/Laser_diffraction_analysis.

42. Wikipedia (2013). Carnauba wax. Retrieved on the 15th September 2013 from http://en.wikipedia.org/wiki/Carnauba_wax.

43. British Standard. Advanced technical ceramics - Monolithic ceramics – General and textural properties - Part 2: Determination of density and porosity. UK: BS, 1993 (BS EN 623-2:1993).

44. D.C. Montgomery, "Design and Analysis of Experiments", John Wiley, New York, 2001.

45. R. Gunawidjaja, T. Myint, H. Eilers, "A factorial design approach for pressureless sintering in air of (Pb,La)(Zr,Ti)O3 synthesized via coprecipitation of oxide-alkoxides", Ceramics International, 2012, Vol 38, pp 775-786.

46. R.M German, "Sintering Theory and Practice", John Wiley & Sons, Inc, 1996.

47. R.M. German, "Progress in Titanium Metal Powder Injection Molding", 2013, Materials, pp. 3641-3662

48. R. Ibrahim, M Azmirruddin, M. Jabir, M.R. Ismail, M. Muhanmad, "Injection Molding of Titanium Alloy Implant For Biomedical Application Using Novel Binder System Based on Palm Oil Derivative", American Journal of Applied Sciences, 2010, vol 7, no. 6, pp 811 – 814.

49. O.M. Ferri, T. Ebel, R. Bormann, "Fatigue Property of Ti-6Al-4V Components Fabricated by Metal Injection Moulding", 2008, Euro PM2008, pp 209-214.

50. G.C. Obasi, O.M Ferri, T. Ebel, R. Bormann, "Influence of processing parameters on mechanical properties of Ti-6Al-4V alloy fabricated by MIM", 2010, Materials Science and Engineering A, Vol. 527, pp 3929-3935.

51. M. Hideshi, I. Yoshinori, U. Toshiaki, S. Kenji, "The influence of density and oxygen content on the mechanical properties of injection molded Ti-6Al-4V alloys", 2010, pp.446 – 453.

APPENDIX

Table 7.1 Mechanical data for CP-Ti sintered in Ar.

Temp (°C)	UTS (MPa)	Average UTS (MPa)	Std Dev	Li_{25} (mm)	Lf_{25} (mm)	Strain @ 25 mm (%)	Average Strain @ 25 mm (%)	Std Dev	YS (MPa)	Average YS (MPa)	Std Dev
1240	426.89	466.37	26.62	25.06	26.03	3.87	8.31	4.26	376.20	398.74	37.19
	494.00			25.22	28.95	14.79			388.70		
	470.20			24.95	26.78	7.33			390.50		
	455.13			25.01	27.49	9.92			374.30		
	485.63			25.28	26.70	5.62			464.00		
1260	440.45	455.47	21.17	25.57	29.93	17.05	14.28	8.02	356.02	378.86	35.47
	432.58			25.47	30.78	20.85			332.80		
	484.95			25.22	26.28	4.20			423.60		
	468.00			25.19	26.27	4.29			397.90		
	451.35			25.18	26.47	5.12			384.00		
1280	522.60	484.57	23.73	24.99	26.04	4.20	9.31	7.31	447.09	402.95	34.7
	489.62			25.41	26.93	5.98			410.53		
	480.57			25.30	25.92	2.45			421.41		
	464.41			25.19	30.09	19.45			369.40		
	465.65			24.91	28.51	14.45			366.30		

Table 7.2 Mechanical data for sintered Ti-6A-4V.

Sample ID	UTS (MPa)	Average UTS (MPa)	Std Dev	Strain @ 25 mm (%)	Average Strain @ 25 mm (%)	Std Dev
1	829.06	833.64	4.220	13.42	13.80	1.217
	834.47			15.16		
	837.38			12.82		
AD	827.02	826.57	3.810	14.83	7.89	0.233
	830.13			4.59		
	822.55			4.26		
BD	839.10	838.55	3.942	9.54	11.42	2.858
	842.18			10.00		
	834.36			14.71		
CD	827.14	821.84	7.493	7.90	6.95	1.339
	816.54			6.01		
AB	880.02	882.77	4.707	15.67	17.15	2.000
	880.07			16.35		
	888.20			19.42		
BC	891.15	894.21	2.669	14.60	14.86	1.161
	896.04			16.13		
	895.44			13.85		
AC	896.11	904.01	8.420	10.76	13.29	2.599
	903.04			15.95		
	912.87			13.14		
ABCD	900.10	900.40	1.761	14.42	14.44	2.777
	898.81			17.23		
	902.29			11.68		